AD-A065 064 POLITECNICO DI MILANO (ITALY) IST DI MACCHINE F/G 19/1
THE DYNAMICS OF SOLID PROPELLANT COMBUSTION.(U)
SEP 78 L DE LUCA, A COGHE, A REGGIORI DAERO-78-G-029

UNCLASSIFIED NL

1 OF 2 ADA 065064

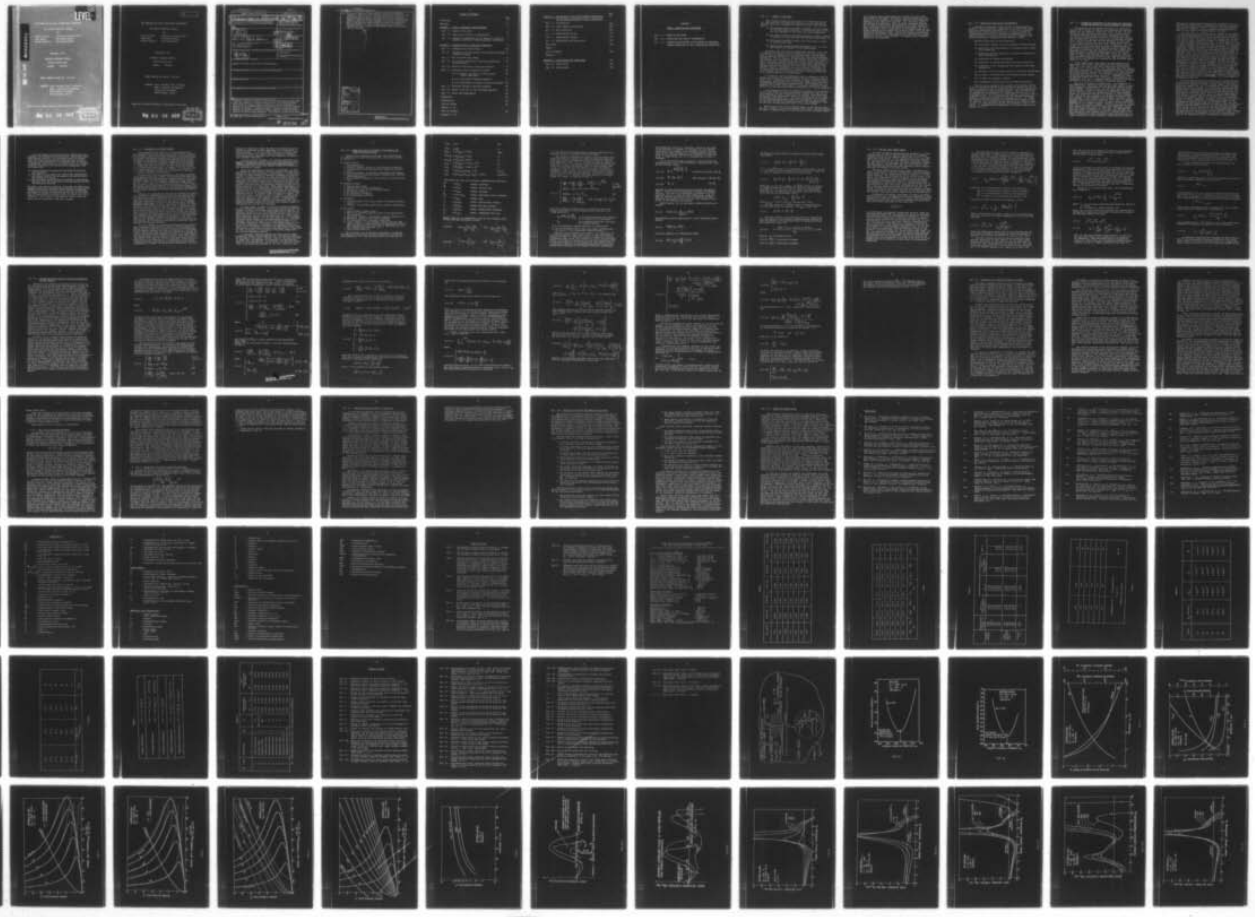

LEVEL II

THE DYNAMICS OF SOLID PROPELLANT COMBUSTION

1st Annual Technical Report

by

Luigi De Luca (Principal Investigator)
Aldo Coghe (Co-Investigator)
Adolfo Reggiori (Co-Investigator)

September 1978

EUROPEAN RESEARCH OFFICE
United States Army
London England

AD A065064

DDC FILE COPY

GRANT NUMBER DA-ERO No. 78-G-029

GRANTEE Prof. Corrado Casci, Director
CNPM - Istituto di Macchine
Politecnico di Milano
20133 Milano, Italy.

Approved for Public Release; distribution unlimited

79 02 26 057

DDC RECEIVED FEB 26 1979

AD

THE DYNAMICS OF SOLID PROPELLANT COMBUSTION

1st Annual Technical Report

by

Luigi De Luca (Principal Investigator)
Aldo Coghe (Co-Investigator)
Adolfo Reggiori (Co-Investigator)

September 1978

EUROPEAN RESEARCH OFFICE
United States Army
London England

GRANT NUMBER DA-ERO No. 78-G-029

GRANTEE Prof. Corrado Casci, Director
CNPM - Istituto di Macchine
Politecnico di Milano
20133 Milano, Italy.

Approved for Public Release; distribution unlimited

79 02 26 057

DDC
RECEIVED
FEB 28 1979
E

UNCLASSIFIED

SECURITY CLASSIFICATION OF THIS PAGE (When Data Entered)

R&D 2401

REPORT DOCUMENTATION PAGE	READ INSTRUCTIONS BEFORE COMPLETING FORM
(9) 1. REPORT NUMBER: Technical rept. no. 1 (Annual) 2. GOVT ACCESSION NO. 3. RECIPIENT'S CATALOG NUMBER: Sep 77-Sep 78,	
(6) 4. TITLE (and Subtitle): The Dynamics of Solid Propellant Combustion.	5. TYPE OF REPORT & PERIOD COVERED: First Annual Technical Report Sep 77-Sep 78
	6. PERFORMING ORG. REPORT NUMBER
(10) 7. AUTHOR(s): Luigi De Luca, Aldo Coghe, Adolfo Reggiori	8. CONTRACT OR GRANT NUMBER(s): (15) DAERO-78-G-029 NW
9. PERFORMING ORGANIZATION NAME AND ADDRESS: Politecnico di Milano ~~Milano~~, (Italy) Ist. di Macchine	10. PROGRAM ELEMENT, PROJECT, TASK AREA & WORK UNIT NUMBERS: (16) 6.11.02A 1T161102BH57-06 (17) 00-709
11. CONTROLLING OFFICE NAME AND ADDRESS: U.S. Army R&S Gp (Eur) Box 65 FPO NY 09510	12. REPORT DATE: (11) Sep~~tember~~ 1978
	13. NUMBER OF PAGES: 150
14. MONITORING AGENCY NAME & ADDRESS (if different from Controlling Office): (12) 156p.	15. SECURITY CLASS. (of this report): Unclassified
	15a. DECLASSIFICATION/DOWNGRADING SCHEDULE

16. DISTRIBUTION STATEMENT (of this Report)

Approved for Public Release Distribution unlimited

17. DISTRIBUTION STATEMENT (of the abstract entered in Block 20, if different from Report)

18. SUPPLEMENTARY NOTES

19. KEY WORDS (Continue on reverse side if necessary and identify by block number)

20. ABSTRACT (Continue on reverse side if necessary and identify by block number)

A nonlinear stability analysis of solid propellant burning was carried out, within the framework of a thermal theory and for quasi-steady gas phase. This required an integral method in reducing the partial differential equation for the condensed phase heat conduction to an approximate ordinary differential equation. A nonlinear algebraic function, called restoring function, was found that contains all basic properties of equilibrium and stability of burning solid propellants. This function depends on the nature

→ over

DD FORM 1 JAN 73 1473 EDITION OF 1 NOV 65 IS OBSOLETE

UNCLASSIFIED

SECURITY CLASSIFICATION OF THIS PAGE (When Data Entered)

28545p S/N 393706

20. of the solid propellant (including its flame) and the operating conditions. Analysis of the restoring function revealed the existence of lower and upper static as well as dynamic burning instability. Nonlinear static and dynamic stability boundaries were determined and stability properties of several unsteady flame models were compared. Most of the predictions were verified by computer simulated tests. The experimental part of this research program is in progress; preliminary results obtained by laser doppler velocimetry and shock tube are discussed.

ACCESSION for
NTIS White Section X
DDC Buff Section ☐
UNANNOUNCED ☐
JUSTIFICATION
BY
DISTRIBUTION/AVAILABILITY CODES
Dist. AVAIL. and/or SPECIAL
A

TABLE OF CONTENTS

CHAPTER 1

SCOPE, OBJECTIVES AND BACKGROUND

Sec. 1.1 - SCOPE OF THIS WORK

Sec. 1.2 - OBJECTIVES AND PLAN OF PRESENTATION

Sec. 1.3 - HISTORICAL BACKGROUND ON THE THEORY OF NONLINEAR DYNAMIC STABILITY OF SOLID PROPELLANTS COMBUSTION.

Sec. 1.1 - SCOPE OF THIS WORK

The ultimate purpose of this work is to formulate the basic laws governing the nonlinear dynamics of solid propellant burning within the framework of a thermal theory. This implies that :

(1) the findings should be readily extended to other cases of heterogeneous combustion ; in particular the results are not dependent on the nature of solid propellant.

(2) new flame models are not being proposed, rather a method is offered to judge how good any unsteady flame model is.

(3) information regarding steady state solutions is found as a particular case.

(4) interactions combustion/fluidodynamics (e.g., in a rocket combustion chamber) are not considered.

By making the usual set of assumptions (see Sec. 2.1), one is reduced to study the stability properties of the nonlinear heat conduction equation in the condensed phase (the standard Fourier partial differential equation with time-varying boundary conditions). This is done by an approximate analytical technique, but keeping the nonlinearity of the problem. It will be shown that a nonlinear algebraic function, called static restoring function, can be determined defining nonlinear static and dynamic burning stability boundaries for finite size disturbances. The dynamic stability boundaries are, in principle, restricted to forcing functions monotonically changing in time (a common case in actuality), but are valid for any kind of transient burning (e.g., depressurization or deradiation).

It should be explicetely observed that no attempt is made to explain or predict the steady flame structure of burning propellants. This is supposed to be assigned in terms of burning rate vs pressure (experimental data) and flame temperature vs pressure (thermochemical equilibrium computations). This information, in addition to a proper flame model, is enough to define the fundamental nonlinear burning stability properties of a given propellant.

It is emphasized that this stability analysis can be applied to any flame model and solid propellant composition, but the actual numerical values do depend on the specific flame model and solid propellant composition chosen. The results can be verified by computer simulation (i.e., by direct integration of the basic set of governing equations) and/or by experiments. While plenty of computer results are already available, the experimental part of this work is entering just now in its crucial phase.

Since this is the first detailed report on the subject after the Ph.D. thesis of one of the authors (see below), the opportunity is taken to summarize most of the findings of the nonlinear stabi-

lity analysis under examination and to make the point about the status of the theory. To avoid a too long discussion, the review will be limited to the common case of static restoring function of the type A-B-C (see Sec. 2.5). The less common, but specially interesting, case of static restoring function of the type A-B-C-D-E will be reviewed in the next annual report; only some hints will be given in this report. The complete literature so far published by this working group on the topics treated in this report is listed as Refs. 1-10; the most exhaustive reference is Ref. 3 which was recently distributed. Reading of this report, complemented with some portions (later specified) of Ref. 3 and with Ref. 10, should give a complete picture of the situation.

Sec. 1.2 - OBJECTIVES AND PLAN OF PRESENTATION

Consider the physical system of Fig. 1a representing a strand of solid propellant, subjected to a radiant flux impinging with istantaneous intensity $(1-r)\cdot I_o(t)$ at its surface, burning with instantaneous rate $R(t)$ in a closed vessel at instantaneous pressure $P(t)$ and ambient temperature T_a. The overall problem of transient solid propellant combustion consists of predicting the burning rate history in time.

Specific objectives of this study are :

(1) distinction between static and dynamic burning regimes.

(2) definition and determination of nonlinear static stability boundaries.

(3) definition and determination of nonlinear dynamic stability boundaries.

(4) prediction of dynamic extinction.

(5) prediction of number and nature of static solutions.

(6) influence of the implemented flame model on the above predictions.

(7) influence of the integral method on the above predictions.

(8) is there a self-sustained oscillating burning regime?

(9) is there an ignition boundary?

(10) experimental verification of the above predictions.

Most of these questions will be dealt with in what follows. First, a literature survey of the problem is offered in Sec.1.3 (this literature survey is taken from Ref. 3 and is reported for the convenience of the interested reader). Then, the basic set of assumptions and equations is illustrated in Sec. 2.2 ; the transformation of the PDE into an approximately equivalent ODE is performed in Sec. 2.4 ; properties of the resulting nonlinear algebraic restoring function are discussed in Sec. 2.5. Static and dynamic burning stability are respectively treated in Sec. 2.6 and Sec. 2.7. The point on the status of the theory is made in Sec. 2.8. Experimental problems are discussed in Sec. 2.9 and Ch. 3. Conclusions and suggestions for future work are collected in Ch. 4.

Sec. 1.3 - HISTORICAL BACKGROUND ON THE THEORY OF NONLINEAR DYNAMIC STABILITY OF SOLID PROPELLANT COMBUSTION

The question of the dynamic extinction by depressurization and in general of the burning stability has been well debated in the technical literature (Refs. 11-19), but few works have been really constructive. The erroneous application of the quasi-steady gas phase assumption (Ref.20), the strong limitations due to the use of linearized theories and the empirical nature of several of the proposed criteria (Refs. 12-13) are the most serious drawbacks in this area. For a critical review, the interested reader might wish to consult the work by Merkle (Ref. 21b). A paper by T'ien (see below) is the only one aiming directly at establishing an extinction criterion for fast depressurization. Merkle himself did not formulate any criterion, but just picked up an empirical value of surface temperature (θ_s =0.43) below which chemical reactions are considered to be too weak in order to sustain the deflagration wave. Likewise, no criterion has been formulated so far for the case of dynamic extinction by fast deradiation reported by the Princeton group (Refs. 3, 22, 23b).

T'ien argues that "heat losses are the mechanism for both static and dynamic extinctions of solid propellants" (Ref. 24); this view is not fully shared in this instance (see Sec. 2.7). In any event T'ien concludes that "for depressurization transients, if the instantaneous burning rate drops below the unstable burning rate solution at the final pressure, extinction will occur". T'ien derives his quantitative criterion from another study by him of flammability limits of premixed flames under the influence of environmental disturbances (Ref. 25). A somewhat similar result will be obtained here by following a completely different approach.

The line of research evolved within the framework of the mechanistic (Zeldovich) approach has been unable to reach truly meaningful conclusions so far about the dynamic stability boundary. Istratov et al. in 1964 (Ref. 26) used an integral method in order to determine an approximate solution to the unsteady nonlinear energy equation in the condensed phase of a propellant burning with constant surface temperature. Extinction was assumed to occur when the surface thermal gradient on the condensed side exceeds a critical value corresponding to the static stability line. This is a <u>serious mistake</u>, since nothing can really be said a priori about the possibility of a dynamic burning regime in a range of burning rate that is statically unstable. In this study also an integral method has been used, but completely different results have been found. Novozhilov in 1967 (Ref. 27) improved the previous model by considering a variable surface temperature and recognizing that dynamic burning is allowed also in the range of parameters where statically stable solutions are not found. Extinction is then assumed to occur when the burning

rate at the final pressure drops below a limiting value experimentally established in nonstationary burning conditions. This criterion heavily relies in very delicate experimental results and, moreover, fails to assign any premonitory signal, if any, about the approaching of the limit.

This question of a possible early warning of extinction during a depressurization transient evaluated via the Zeldovich method was examined in a paper by the Princeton group (Ref. 28) in 1972. The possibility was checked that the crossing of the static stability boundary is sufficient to subsequently produce dynamic extinction. No clear answer to this question was given. The position taken here is that the static stability boundary has only secondary relevance in a dynamic situation. Indeed, according to the same Princeton reference, "the dynamic conditions of extinguishement tend to shift the stability line" (p. 257 of Ref. 28). More extensive work in this area (Ref. 29) also failed to reach any significant conclusion. In any event, Novozhilov (p. 216 of Ref. 30) in 1973 observes that this "question requires certain information about the properties of the system outside the area of smooth burning. Such information cannot be obtained from experiments on steady state combustion. For the calculation of unsteady conditions in the unstable region it is necessary to draw on certain schemes of combustion, which make it possible to predict the properties of propellants beyond the (static) stability limit". In other words the author admits the failure of the mechanistic approach in this respect and recognizes that burning in the statically unstable region can only be treated with a flame model. However, the need for more advanced treatments in the framework of flame models is advocated in Ref. 31.

In this work, quantitative criteria for dynamic stability of burning propellants (and in particular for dynamic extinction) are defined by means of flame models. The integral method of Goodman (Ref. 32) is implemented in order to apply known mathematical methods to the resulting approximate ODE formulation of the problem. The same method has already been applied (Ref. 33) to droplet burning; somewhat simpler use has been made at Princeton (Refs. 34-35) in solid propellant rocket engines. The concept of using the simpler ODE formulation of the problem, instead of the PDE one, is relatively common in Soviet literature. However, the method of transformation is rather different; an interesting review of the mathematical problem was made by Gostintsev (Ref. 36). The approach has been applied mainly to ignition (Refs. 37-38, e.g.), unsteady burning (Refs. 26-39, e.g.) and stability problems (Refs. 30,40, e.g.). Remark that the Soviet approach (Refs. 26,30,36-40) differs not only in the mathematical details but especially in the structure of the physical model. Indeed, instead of using a flame model, the Soviet investigators resort to the Zeldovich method, consisting of constructing

the thermal gradient at the condensed phase side of the burning surface from experimental steady state data (see Ref. 28, e.g.). However, it was already mentioned that the Zeldovich method, requiring steady state experiments, is useful in establishing intrinsic stability boundaries but, at least in principle, cannot be extended to obtain dynamic stability boundaries.

CHAPTER 2

NONLINEAR SOLID PROPELLANT COMBUSTION

In this chapter an overview of the theoretical developments, both analytical and numerical, concerning nonlinear burning stability of solid propellants is offered. First the basic assumptions and equations are revised, then the transformation of the governing PDE into an ODE is performed. This allows us to define static and dynamic stability properties of a burning solid propellant. For the first time:

(a) results obtained by using MTS and KTSS flame models are compared;
(b) the effect of the power law, chosen for implementing an integral method, on the shape of the static restoring function is shown;
(c) the nonlinear static stability boundary is determined directly from the flame model and also through the static restoring function.

Moreover, some detailed analyses of the MTS and KTSS (both linearized and full versions) flame models are offered. Numerical computations verifying the analytical predictions are shown. A section on the state of the art of the nonlinear burning stability analysis ends the theoretical developments of this chapter. Experimental results from the shock tube are reported in the last section.

Sec. 2.1 - BACKGROUND AND NOMENCLATURE

The physical system dealt with is presented in its most general form in the schematic of Fig. 1a. The pressure of the vessel, the radiant flux impinging on the surface of the strand (originating exclusively from some external energy source), the ambient temperature measured at the cold boundary of the propellant sample (supposed to be infinitely long), and any other parameter which can be controlled in a known way from the outside of the vessel are designated as controlling parameters. A change of one or more of these controlling parameters will affect, in some way, the state of the physical system and, consequently, they are also called external perturbations.

On the other side, we designate as intrinsic perturbations sources all those "small" (in a sense to be specified) irregularities and imperfections always present in the real world but which are nevertheless neglected in the idealized picture of Fig. 1a. For example, nonuniform composition of the strand, impurities variuosly scattered in the condensed phase, complicated geometry of the burning surface, etc., all contribute to hopefully small but persistent differences of the actual phenomena from those described by mathematical models.

Whether the perturbation sources are external or intrinsic, the prior, supposedly unperturbed steady state profile of temperature in the combustion wave will be modified to some new perturbed unsteady profile. Let us define the disturbance temperature profile as the profile of the point-by-point difference between the perturbed profile and the original, unperturbed profile. The general problem of static stability may be stated as follows: given a stationary state of the physical system, the system is forced to a close but nonstationary state and it is asked whether the system, after a long enough period of time, will go back to its initial state or will move away from it. In the specific physical configuration considered in this study, it is asked whether the disturbance temperature profile will die out in time or not. Mathematically, the problem is an initial value problem and is usually described by a parabolic type of partial differential equation.

It is of concern to distinguish between static and dynamic stability. The general problem of dynamic stability may be stated as follows: given an initial stationary state of the physical system, the system is forced to a different (final) stationary state by means of appropriate changes in time of pressure and/or radiant flux and it is asked whether the system, after a long enough period of time, will reach the wanted final state or another (unwanted) final state. In other words, the stability of a system where intrinsic perturbation sources exclusively are considered to be acting (stability of a state) is called static.Conversely, the sta-

bility of a system in which the external controlling parameters are changing in time (stability of a transition) is called dynamic. It will be shown that in the latter case, the rate of change in time of the pressure, for example, is of fundamental importance and this explains the expression "dynamic stability".

In this research program, the ultimate objective is to establish boundaries separating regions of stability from those of instability on some convenient graphical plot . It will be shown that static and dynamic stability boundaries are different in nature.

Since the mathematical problem is formidable, no general method has been found so far for solving the stability problem in its various aspects. Historically, a large amount of work has been devoted to stability problems in fluid dynamics. A standard treatment in this and related fields is the linearized approach, which is based on two essential assumptions: disturbance quantities infinitesimally small and a mathematical model (differential equations, boundary conditions, and any other relationship) containing only disturbance quantities of first order. Under these hypotheses, the problem reduces to an eigenvalue formulation whose mathematical theory is very well developed. Besides this standard approach ,several other approximate and often ad hoc methods have been set up in various fields of applied sciences. The reason for such a confusing state of affairs is essentially one: the behavior of most physical system is described by nonlinear equations and nowadays not only a mathematical theory encompassing all types of nonlinearities, but even analytical methods capable of dealing with specific types of nonlinearities, are not yet available.

In this study, in order to avoid the serious drawbacks of any linearized treatment, a nonlinear combustion stability analysis by means of an approximate approach is offered. Basically, the problem will be transformed from a PDE into an ODE formulation via an integral method. Notice that the proposed approach requires the implementation of a flame model, since Zeldovich method is of no help (see Sec. 1.3). However, any flame model capable to describe quantitatively the heat feedback from the gas phase to the burning surface is in principle acceptable. The choice of the flame model is a duty of the investigator. Obviously, the proposed stability theory can only extract the stability properties (both static and dynamic) implicitely buried in any flame model. This fact, in turn, might help in the choice of the best flame model for a given combustion problem.

A composite, ammonium perchlorate based solid rocket propellant, denoted as AP/PBAA No. 941, is taken as datum case throughout this report. However, this by no means is meant to imply that the approach is restricted to some specific class of solid propellants. The physical and chemical properties of the propellant AP/PBAA No. 941 are listed in Tab.1.

THIS PAGE IS BEST QUALITY PRACTICABLE
FROM COPY FURNISHED TO DDC

Sec. 2.2 - FORMULATION OF THE GENERAL QUASI-STEADY GAS PHASE TRANSIENT PROBLEM

Except where explicitely excluded, the following set of assumptions is valid throughout this work. With reference to Fig. 1:

a) Entire Strand.

1. Monodimensional.
2. Constant thermal, physical, and chemical properties.
3. Condensed phase and gas phase have identical specific heats.
4. At cold boundary, in thermal equilibrium with ambient.
5. Subjected to no external forces (acceleration, gravity, electromagnetism).
6. No emission of radiation (only external radiation sources).

b) Condensed Phase.

1. Semi-infinite slab.
2. Uniform and isotropic composition.
3. Adiabatic, except at the burning surface.
4. No chemical activity.
5. No radiation scattering.
6. No photochemical effects.

c) Interface.

1. Infinitesimally thin plane surface (collapsed reacting layer).
2. One-way, irreversible gasification process (pyrolysis).

d) Gas Phase.

1. Semi-infinite column of gas.
2. Mixture of thermally perfect gases of average molecular weight $\overline{m}$.
3. One-phase, laminar, nonviscous, strongly subsonic flow.
4. Adiabatic, except at the burning surface.
5. No interaction with (external) radiation.
6. Lewis number = 1, each chemical species has the same specific heat C_g, mass diffusion is expressed by Fick's law; therefore the gas phase can be described by a simple thermal model (see Sec. 2.3).
7. Quasi-steady behavior.

The following set of reference parameters is used for nondimensionalizing (with specific reference to the propellant AP/PBAA No. 941 taken as datum case; see also Tab. 1):

P_{ref}	$\equiv 68$	atm
T_{ref}	$\equiv 300$	K
R_{ref}	$\equiv R(P_{ref}) = 0.837$	cm/s
$T_{s,ref}$	$\equiv T_s(P_{ref}) = 1,000$	K
$T_{f,ref}$	$\equiv T_f(P_{ref}) = 2,430$	K
x_{ref}	$\equiv \alpha_c/R_{ref} = 1.673 \times 10^{-3}$	cm
t_{ref}	$\equiv \alpha_c/R_{ref}^2 = 1.998 \times 10^{-3}$	s
Q_{ref}	$\equiv C_c(T_{s,ref}-T_{ref}) = 231$	cal/g
I_{ref}	$\equiv \rho_c C_c R_{ref}(T_{s,ref}-T_{ref}) = 297.8$	cal/cm^2-s

from which one gets the following nondimensional variables:

$\mathcal{P}$	$= P/P_{ref}$	nondim. pressure
$\mathcal{R}$	$= R/R_{ref}$	nondim. burning rate
X	$= x/x_{ref}$	nondim. distance
δ_a	$= (1/a)/x_{ref}$	nondim. absorption layer thickness
τ	$= t/t_{ref}$	nondim. time
H	$= Q_s/Q_{ref}$	nondim. surface heat release
Q	$= Q_f/Q_{ref}$	nondim. gas heat release
F_o	$= I_o/I_{ref}$	nondim. radiant flux intensity
$\dot{q}$	$= \dot{q}/I_{ref}$	nondim. conductive heat flux.

Notice that for the temperature, both of the following definitions are used according to need:

$$\text{(2.2.1a)} \qquad \theta \equiv \frac{T_{(\,)} - T_{ref}}{T_{s,ref} - T_{ref}} \quad , \text{e.g.} \quad \theta_f = \frac{T_f - T_{ref}}{T_{s,ref} - T_{ref}}$$

$$\text{(2.2.1b)} \qquad \mathcal{T}_{(\,)} \equiv \frac{T_{(\,)}}{T_{(\,),ref}} \quad , \text{e.g.} \quad \mathcal{T}_f = \frac{T_f}{T_{f,ref}}$$

And the choice of the particular definition depends on the specific physical phenomenon being considered.

The general nondimensional quasi-steady gas phase transient formulation includes the unsteady condensed phase problem (Eq. 2.2.2), relationships accounting for the surface mass production (Eqs. 2.2.3), the quasi-steady gas phase problem (Eqs. 2.2.4 - 2.2.8), some auxiliary relationships assigning the gas phase and burning surface heat releases (Eqs. 2.2.9 - 2.2.10) and the time history of the controlling parameters (Eqs. 2.2.11 - 2.2.12). Obviously, the gas phase treatment is not complete without the energy equation whose first integral gives the heat feedback law; this is discussed in Sec. 2.3. For details about the writing of the equations, the reader is referred to Ref. 3.

$$
(2.2.2)\quad
\begin{cases}
\dfrac{\partial\theta}{\partial\tau} + \mathcal{R}\dfrac{\partial\theta}{\partial X} = \dfrac{\partial^2\theta}{\partial X^2} + \dfrac{N_t(1-r)}{\delta_a} F\, e^{X/\delta_a} & \text{II PDE} \quad \tau \geq 0, X \leq 0 \\
\theta(X, \tau = 0) = \text{some given function} & \text{IC} \\
\theta(X \to -\infty, \tau) = \theta_{-\infty} & \text{BC2} \\
\left(\dfrac{\partial\theta}{\partial X}\right)_{c,s} = \dfrac{\lambda_g}{\lambda_c}\left(\dfrac{\partial\theta}{\partial X}\right)_{g,s} - H\,\mathcal{R} + (1-N_t)(1-r)F_o - \dot{q}_\ell & \text{BC1}
\end{cases}
$$

where the boundary condition BC1 at X=0 merely states the energy conservation at the burning surface (see Fig. 1b). In the above BC1:

$\dot{q}_{g,s}(\mathcal{P},\mathcal{R}) \equiv \dfrac{\lambda_g}{\lambda_c}\left(\dfrac{d\theta}{dX}\right)_{g,s}$ is the nondimensional heat feedback to be defined by a flame model;

$\dot{q}_\ell$ is a nondimensional heat loss from the burning surface;

H is conventionally supposed positive if endothermic;

N_t is a trasparency factor (N_t=0 for opaque condensed phase and N_t = 1 for transparent condensed phase).

The last point deserves some comment. The hypothesis of a collapsed reacting layer might imply in some cases that a certain thickness of condensed phase is shrunken to an infinitesimally small value. For consistency, then, the (external) radiant flux should be separated in a portion deposited directly at the surface (as if the propellant were opaque) and in a (remaining) portion distributed volumetrically in the condensed phase according to the proper extinction coefficient.

The trasparency factor N_t, therefore, should be set equal to the fraction of radiant flux absorbed in the reacting layer when it is thought of as extended. However, the extent and the very existence of a condensed phase reacting layer is an extremely controversial question. In this study N_t is taken either as 0 or 1, although this is not a necessity.

As to the surface mass production, the following combined pyrolysis law is used according to need both for steady and unsteady states:

(2.2.3a) $$\mathcal{R} = e^{\frac{-E_s}{\mathcal{R}\, T_{s,ref}}\left(\frac{1}{T_s}-1\right)}$$ Arrhenius pyrolysis, $\theta_s \geq \theta_k$

(2.2.3b) $$\mathcal{R} = \left(\theta_s - \theta_m\right)^w$$ KTSS pyrolysis, $\theta_k \geq \theta_s \geq \theta_m$

(2.2.3c) $$\mathcal{R} = 0$$ $\theta_s < \theta_m$

where θ_m is some empirically defined minimum temperature under which the solid propellant undergoes no chemical activity. The power w is determined by matching the two pyrolysis laws at a given surface temperature, say $\theta_s = \theta_k$, near the ambient temperature. This formulation of the pyrolysis law allows us to avoid the "cold boundary difficulty" of the Arrhenius expression.

Relationships for the gas phase include the mass continuity

(2.2.4) $$u\left(X,\tau\right) = \frac{\rho_c}{\rho_g\left(X,\tau\right)}\,\mathcal{R}\left(\tau\right) \quad ;$$

the momentum equation describing a trivial pressure distribution.

(2.2.5) $$P\left(X,\tau\right) = P\left(\tau\right) \quad ;$$

the state equation (in dimensional terms)

(2.2.6) $$P(t) = \rho_g\left(x,t\right)\frac{\mathcal{R}}{\overline{m}}\,T\left(x,t\right) \quad ;$$

the integral energy balance assigning the quasi-steady flame temperature

$$\theta_f(\tau) = \theta_f + \frac{c_g}{c_c}\left(Q - \frac{\dot{q}_{g,s}}{\mathcal{R}}\right) \tag{2.2.7}$$

where $\dot{q}_{g,s}(\mathcal{P},\mathcal{R})$ has to be defined by a flame model; and the integral energy balance assigning the steady state flame temperature in presence of an external radiant flux

$$\overline{\theta}_f(\mathcal{P},F_o) = \overline{\theta}_f(\mathcal{P},F_o=0) + \frac{(1-r)F_o - \dot{q}_l}{\mathcal{R}(\mathcal{P},F_o)} \tag{2.2.8}$$

where $c_g/c_c = 1$ has been assumed and $\overline{\theta}_f(\mathcal{P},F_o=0)$ is the adiabatic flame temperature furnished by standard thermochemical computations. For example, for the datum case considered (see Tab. 1), the following relationship was found to hold up to 100 atm: in dimensional terms

$$T_f(p) = T_{f,ref} - \frac{50}{68}(p_{ref} - p)$$

where $T_{f,ref}$ = 2430 K and p_{ref} = 68 atm (Ref. 21b).

The heat release in the gas phase is considered to be uniquely defined by the pressure: for $c_g/c_c = 1$ one finds

$$Q(\mathcal{P}) = H + \overline{\theta}_s + \overline{\theta}_f \quad . \tag{2.2.9}$$

The heat release at the burning surface is considered strictly depend on the original condensed phase composition only; for example, for the broad class of composite, AP based propellants (Ref. 43c)

$$H = \frac{p(Q_{cr} + Q_{v,AP} - Q_{A/PA}) + (1-p)Q_{v,B}}{Q_{ref}} = \text{const} \quad . \tag{2.2.10}$$

Finally, it is understood that

$$\mathcal{P}(\tau) = \text{externally assigned} \tag{2.2.11}$$

$$F_o(\tau) = \text{externally assigned.} \tag{2.2.12}$$

Sec. 2.3 - MTS and KTSS FLAME MODELS

In order to define explicitely the function $\dot{q}_{g,s}(\mathcal{P}, \mathcal{R})$ required for the BC1 of the PDE describing the transient thermal profile in the condensed phase (Eq. 2.2.2), a flame model has to be chosen. It is emphasized that any flame model can be picked up. For the composite propellant AP/PBAA No. 941 taken as a datum case, two flame models were tested: the MTS (Ref.21) and the KTSS (Ref.42) flame models. Both were developed by Summerfield and coworkers; other flame models will be tested in the near future.

The model worked out by Merkle, Turk, and Summerfield (MTS) is basically a judicious combination, based on experimental data, of the diffusive and kinetic aspects of the gas phase reactions. The model worked out by Krier, T'ien, Sirignano, and Summerfield (KTSS) can be see as a particular case of the previous one when the flame is purely diffusion controlled. Both models are thermal in nature and invoke the assumptions mentioned in Sec. 2.2. The MTS model will be used for most of the theoretical developments of this report. For a detailed knowledge of how the model is derived, the reader is referred to the original Ref. 21b and also to Refs. 43-44, treating the GDF theory from which the MTS flame model has evolved. Only qualitative comments will be offered here.

Any pattern of chemical reactions, no matter how complicated, involves the two physically distinct phenomena of mass diffusion and chemical kinetics. It is known from homogeneous combustion theory that quite often diffusion processes dominate the kinetic processes in the sense that

$$\tau_{di}/\tau_{ki} \gg 1 \quad .$$

or, conversely, the opposite extreme may be true. These two limiting configurations are respectively known as diffusion and premixed flames. For heterogeneous combustion, in particular of solid propellants, there are instances in which the gas phase portions of the deflagration wave may be treated according to one of the above limiting configurations. But, in principle, especially for transients connected to large excursions of the controlling parameters, the gas phase treatment of a heterogeneous combustion wave has to account for both processes. This was originally done by Summerfield in his GDF theory for the AP steady flame model. Later, an extension was made for the AP quasi-steady flame model accounting for variable flame and surface temperatures. Although derived for the specific case of the AP class of propellants, the formulation of the MTS flame model is quite general and may be adapted to other cases of heterogeneous combustion.

For the specific case of an AP composite propellants, the MTS flame model accounts not only for the granular diffusion flame (GDF) of the oxidizer with the binder (Ref.21) but also for a distended premixed flame corresponding to the AP decomposition products burning. In this study, the simplified version with the premixed flame collapsed at the burning surface has been adopted. This assumption is acceptable (p. 28 of Ref. 21b) for pressure values not lower than say, 1 atm. The most important parameter characterizing the gas phase during a quasi-steady transient is the heat feedback to the burning surface. According to the (collapsed) MTS flame model, the nondimensional heat feedback is

$$(2.3.1) \qquad \dot{q}_{g,s}(P,R) = Q R \left[\frac{\sqrt{\tau'_{ki}}}{\sqrt{\tau'_{re}}} e^{-R^2 \tau'_{re}} + \frac{\sqrt{\tau'_{di}}}{\sqrt{\tau'_{re}}} \frac{1 - e^{-R^2 \tau'_{re}}}{R^2 \tau'_{re}} \right]$$

where τ'_{ki} is a nondimensional kinetic time parameter;
τ'_{di} is a nondimensional diffusion time parameter;
τ'_{re} is a nondimensional reaction time parameter;
R is given by an Arrehenius-type pyrolis law.

Following the MTS flame model development, we put

$$(2.3.2) \qquad \sqrt{\tau'_{ki}} = A_M \frac{T_f}{P} e^{\frac{E_f}{2R T_{f,ref}} \left[\frac{1}{T_f} - 1 \right]}$$

where a second order gas phase reaction has been postulated to occur wholly at the highest temperature T_f (p.29 of Ref. 43a) and

$$(2.3.3) \qquad \sqrt{\tau'_{di}} = B_M \frac{(T_f)^{5/6}}{(T_s)^{7/8} (P)^{1/3}}$$

where the diffusional mixing rate of fuel pockets with the surrounding atmosphere of oxygen-rich gases is assumed to depend on the surface temperature T_s (p.31 of Ref. 43a).

The two constants A_M and B_M are determined for each specific propellant by "the best fit of the steady state burning rate theory to the measured burning rate data" (p. 38 of Ref. 21b). An application is shown in Fig. 2 for the propellant AP/PBAA No. 941. In the spirit of the GDF theory, it is further assumed (e.g., see p. 33 of Ref. 21b)

that the overall solid propellant reaction time parameter can be expressed as the following simple combination of the two above limiting cases:

$$\sqrt{\tau'_{re}} = \sqrt{\tau'_{di}} + \sqrt{\tau'_{ki}} \qquad (2.3.4)$$

This relationship has been shown to represent the pressure dependence of the burning rate quite accurately for a wide range of composite solid propellants (Ref.43) and also to describe the depressurization extinction correctly for both composite and double-base solid propellants (Ref.21). However, it should be recognized that the whole MTS approach depends on the arbitrary assumption of Eq. 2.3.4 and the choice of the A_M constants. How this choice is affected by the fitting procedure mentioned above is illustrated in Fig. 2 (different pressure interval) and Fig. 3 (different low end of the pressure interval).

According to the KTSS flame model, the nondimensional heat feedback is

$$\dot{q}_{g,s}(\mathcal{P}, \mathcal{R}) = \frac{Q}{\mathcal{R}} \frac{1 - e^{-\mathcal{R}^2 \bar{\tau}'_{di}}}{\bar{\tau}'_{di}} \qquad (2.3.5.)$$

where $\bar{\tau}'_{di}$ is an average nondimensional diffusion time parameter;
$\mathcal{R}$ is given by a power pyrolysis law.

Notice that the above KTSS heat feedback law, derived for a diffusionally controlled AP flame, is a particular case of the MTS heat feedback law where

$$\sqrt{\tau'_{re}} \simeq \sqrt{\tau'_{di}} \gg \sqrt{\tau'_{ki}} \qquad (2.3.6)$$

$$\tau'_{di} = \frac{B_M^2}{(\mathcal{P})^{2/3}} \frac{(T_f)^{5/3}}{(T_s)^{7/4}} \simeq \frac{\text{const}}{(\mathcal{P})^{2/3}} \equiv \bar{\tau}_{di} \qquad (2.3.7)$$

That is, when the diffusion time parameter is much larger than the kinetic time parameter and is temperatu - re independent. Extensive experimental investigation (Ref. 43) shows that for AP propellant flames the diffusional mixing is, indeed, sensibly slower than the

chemical kinetics as long as the pressure is larger than say, 5 atm. It is also expected (Ref.21) that flame temperature undershoots during decelerated transients slow down the chemical kinetics much more effectively than the diffusional mixing (compare Eq. 2.3.2 vs Eq. 2.3.3).

In its linearized version, the nondimensional KTSS heat feedback law is given by

$$\dot{q}_{g,s}(\mathcal{P}, \mathcal{R}) = \frac{Q}{\mathcal{R}\,\bar{\tau}_{di}} \tag{2.3.8}$$

which is a particular case of the full expression (Eq.2.3.5), when the further assumption is made that

$$e^{-\mathcal{R}^2 \bar{\tau}'_{di}} \ll 1 \tag{2.3.9}$$

corresponding to $\bar{\tau}'_{di}$ very large but finite burning rate.The constraint of Eq. 2.3.9 is usually valid for steady burning, but is not acceptable in extinction transients, since under this circumstance $\mathcal{R} \to 0$ while $\bar{\tau}'_{di}$ remains finite and, therefore,

$$e^{-\mathcal{R}^2 \tau'_{di}} \to 1.0$$

Note:in the linearized version commonly used, the nondimensional KTSS heat feedback law is written as

$$\dot{q}_{g,s}(\mathcal{P}, \mathcal{R}) = \frac{\mathcal{P}^{2n}\left(\mathcal{P}^{n/w} - H\right)}{\mathcal{R}} \tag{2.3.9}$$

Then,by comparing Eq. 2.3.8 with Eq. 2.3.9, the average nondimensional diffusion time parameter can be evaluated

$$\bar{\tau}'_{di} = \frac{Q}{\mathcal{P}^{2n}\left(\mathcal{P}^{n/w} - H\right)} \tag{2.3.10}$$

An essential ingredient for both MTS and KTSS flame models is the experimental stationary $\bar{\mathcal{R}}(\bar{\mathcal{P}})$curve. The steady state structure of the MTS and KTSS models are respectively shown in Fig. 4 and Fig. 5 for the propellant AP/PBAA No.941.

It is worthwhile to remark that even the linearized version of the KTSS model can accurately reproduce the experimental stationary $\bar{R}(\bar{P})$ curve. A comparison of the two plots shows no strong difference as to the steady state behavior of the flame models under examination. Consider now the quasi-steady behavior as plotted in Fig. 6 (MTS model) and Fig. 7 (KTSS model). It is obvious that the linearized KTSS model is physically unrealistic for low burning rate.

In summary:

(a) stationary or small perturbation solutions of the MTS and KTSS (even linearized) flame model are similar at high pressure, since in these instances only small changes in temperature and burning rate are considered;

(b) at low pressure and/or low burning rate, AP flame is kinetically controlled and therefore should not be described by the KTSS (even non linearized) model;

(c) the KTSS linearized model can never predict extinction because the heat feedback law is found to be inversely proportional to the burning rate.

A useful comparison for what follows is shown in Fig. 8, where the MTS heat feedback (often used in this study) and the linearized KTSS heat feedback (commonly used in the literature) are plotted together in the range 10 to 40 atm ($\dot{q}_{g,s}$ curves). From this graphical plot one observes that, for a given set of external conditions, two steady solutions (reacting configuration A and unreacting configuration C) are found for the MTS model, but only one for the linearized KTSS model (reacting configuration A).

The quasi-steady gas phase working map for the MTS flame is illustrated in Fig. 9. On this plot, besides the usual heat feedback lines at constant pressure, lines at constant ambient temperature (for adiabatic burning) or at constant radiant flux (at standard ambient temperature) are drawn measuring the stationary heat flux

$$\bar{\dot{q}}_{c,s}(\theta_a, F_o ; \bar{R}) = \bar{R}(\bar{\theta}_s - \theta_a) + \bar{R}H - F_o$$

absorbed in the condensed phase. Where $\dot{q}_{g,s}(\bar{P}, \bar{R})$ crosses $\dot{q}_{c,s}(\theta_a, F_o ; \bar{R})$, steady state solutions $\bar{R}(\bar{P}, \theta_a, F_o)$ vs $\dot{q}_{g,s}$ are singled out. Obviously, the curves $\dot{q}_{c,s}(\theta_a, F_o ; \bar{R})$ do not depend on the choice of the flame model, while the curves $\dot{q}_{g,s}(\bar{P}, \bar{R})$ do depend. Similar remarks hold true in Fig. 10, where a large fan of lines at constant ambient temperature are drawn on a MTS flame plot. Notice that even at zero degrees Kelvin (assuming the flame model still valid!) the steady solution is far from the lower static stability boundary (cf. Sec. 2.6).

It will be shown that the burning stability properties are strongly affected by the value of the surface heat release. For our datum case (see Tab. 1), the best value computed from the literature is Q_s = -158.2 cal/g (the exothermicity is

due to the primary ammonia/perchloric acid flame occurring in the ammonium perchlorate decomposition). Changing Q_s, while keeping $T_f(P)$ fixed, means to consider a family of solid propellants whose R (P) behavior is shown in Fig. 11 and Tab. 2.

Sec. 2.4 - AN ORDINARY DIFFERENTIAL EQUATION FORMULATION OF THE PROBLEM

Basically, the mathematical method is the one set up for the first time by Von Karman and Polhausen in the study of boundary layers and later generalized by Goodman, among others, to a large number of thermal problems. The method can be extended to any other problem described by nonlinear PDE of parabolic type. In our case, the approach consists in defining a parameter $\xi(\tau)$, called the penetration distance of the thermal wave in the condensed phase, "such that for $X \geq \xi(\tau)$ the propellant slab, for all practical purposes, is at an equilibrium temperature and there is no heat transferred beyond this point" (p.53 of Ref. 32). The evolution in time of the thermal profile in the condensed phase is obtained by following the time history of the penetration distance propagating into an initially uniform temperature field. Within this penetration layer, progressing in time, the qualitative space distribution of temperature is assumed known a priori; but we make sure that, in so doing, the integral balance of thermal energy in the condensed phase is preserved. In other words, the price to be paid for making the transformation from PDE to ODE formulation is an approximate solution of the local space distribution of temperature; this is not such a serious drawback because the interest is in the time evolution of the surface temperature. In any event, several investigations found an error of only some percents for various cases in which both the exact and the integral solutions were evaluated. For example, see Fig. 5 on p. 89 of Ref. 32 showing the temperature time history at the surface of a semi-infinite slab with triangular surface heat flux.

In order to get a deeper understanding of questions related to the integral method as applied to thermal problems, the interested reader might wish to consult the excellent review by Goodman (Ref.32) and the references given there. Before getting involved in mathematical details, the reader should be warned about the limits of the integral method. Any solution obtained by the integral method contains hopefully small but irrevocable errors in the final numerical results. The question of how to improve the accuracy then arises. It has been argued that "there is no a priori guarantee that increasing the order of the polynomial (used to represent the space distribution of the unsteady temperature profile) will improve the accuracy. Although the accuracy is frequently improved with this technique, it can be demonstrated, nonetheless, that there are cases for which it actually worsens" (p.96 of Ref. 32). In this same reference it is suggested that the method of weighted residuals provides a very efficient method for improving the accuracy of the results obtained by using the integral method.

The simple integral method implemented in this work can be considered a special case of the method of weighted residuals when just one parameter (the penetration distance ξ) and one weighting function are considered. Under these circumstances, the only equation to be considered is the heat balance integral (see below). Since the integral method assumes a uniform initial distribution of temperature, a new nondimensional variable is defined:

$$u(X,\tau) \equiv \overline{\Theta}_i(X) - \Theta(X,\tau) \tag{2.4.1}$$

where

$$\overline{\Theta}_i(X) = \overline{\Theta}_{-\infty} + (\overline{\Theta}_s - \overline{\Theta}_{-\infty})\, e^{X\overline{\mathcal{R}}_i} \tag{2.4.2}$$

is the initial steady state distribution of temperature and $\Theta(X,\tau)$ is the temperature distribution following some perturbation. The new variable $u(X,\tau)$ may therefore be conveniently interpreted as the finite temperature disturbance propagating inside the condensed phase and superimposed on the initial temperature distribution after the action of perturbation. At the initial instant $\tau = 0$, by definition $\Theta(X,\tau) = \overline{\Theta}_i(X)$ and $u(X,\tau) = 0$. Suppose now that, in the following instant, a perturbation starts acting on the system and makes $u(X,\tau) \neq 0$: the goal of the analysis is to determine the ultimate effect of such a temperature disturbance after waiting a period of time sufficiently long for the perturbation to disappear. No assumption whatsoever is made as to the size of the temperature disturbance.

The analysis will be restricted to the case of an optically opaque propellant (in the sense that $(\alpha_c/\mathcal{R})/(1/\alpha) \gg 1$) at constant (not necessarily reference) ambient temperature. The basic set of nondimensional equations for an optically opaque propellant ($N_t = 0$), initially burning with constant rate $\overline{\mathcal{R}}_i$ at constant pressure $\mathcal{P}_i$, while subjected to a radiant flux of constant intensity $F_{o,i}$, is

$$\begin{cases} \dfrac{\partial\Theta}{\partial\tau} + \mathcal{R}\dfrac{\partial\Theta}{\partial X} = \dfrac{\partial^2\Theta}{\partial X} & \text{II PDE} \quad \tau \geq 0,\ X \leq 0 \\ \Theta(X, \tau = 0) = \overline{\Theta}_i(X) & \text{IC} \\ \Theta(X = -\infty, \tau) = \overline{\Theta}_{-\infty} & \text{BC2} \\ \left(\dfrac{\partial\Theta}{\partial X}\right)_{c,s} = \dfrac{\lambda_g}{\lambda_c}\left(\dfrac{\partial\Theta}{\partial X}\right)_{g,s} - \mathcal{R}H + (1-r)F_o & \text{BC1} \end{cases} \tag{2.4.3}$$

where $\mathcal{R}(\tau)$ is the burning rate defined by any appropriate pyrolysis law and $(\lambda_c/\lambda_g)(\partial\Theta/\partial X)_{g,s}$ is the heat feedback law defined by any appropriate flame model. In terms of the disturbance temperature $u(x,\tau)$, the set of equations is:

$$
(2.4.4)\quad
\begin{cases}
\dfrac{\partial u}{\partial \tau} = \mathcal{R}\left(\dfrac{d\bar{\Theta}_i}{dX} - \dfrac{\partial u}{\partial X}\right) + \dfrac{\partial u^2}{\partial X^2} - \dfrac{d^2\bar{\Theta}_i}{dX^2} & \text{II PDE} \quad \tau \geq 0,\ x \leq 0 \\
u\left(X,\ \tau = 0\right) = 0 & \text{IC} \\
u\left(X \to -\infty,\ \tau\right) = 0 & \text{BC2} \\
\left(\dfrac{\partial u}{\partial X}\right)_{c,s} = \dfrac{\lambda_g}{\lambda_c}\left(\dfrac{\partial u}{\partial X}\right)_{g,s} - \dfrac{\lambda_g}{\lambda_c}\left(\dfrac{d\bar{\Theta}_i}{dX}\right)_{g,s} + \mathcal{R}\cdot H & \\
\qquad + \left(\dfrac{d\bar{\Theta}_i}{dX}\right)_{c,s} - (1-r)\ F_o & \text{BC1}
\end{cases}
$$

where

$$
(2.4.5)\quad
\begin{cases}
R(\tau) = e^{-\dfrac{E_s}{\mathcal{R}T_{s,ref}}\left[\dfrac{1}{(\bar{\Theta}_{i,s}-u_s)\left(1-\frac{T_{ref}}{T_{s,ref}}\right)+\frac{T_{ref}}{T_{s,ref}}} - 1\right]} & \text{for } (\bar{\Theta}_{i,s}-u_s) \geq \Theta_K \\
R(\tau) = \left[\bar{\Theta}_{i,s} - u_s(\tau)\right]^w & \text{for } (\bar{\Theta}_{i,s}-u_s) \leq \Theta_K
\end{cases}
$$

and $(\lambda_g/\lambda_c)(\partial u/\partial X)_{g,s}$ is again defined by any appropriate flame model.
Notice that at the initial instant $\tau = 0$, the surface energy balance is

$$
(2.4.6)\quad \left(\frac{d\bar{\Theta}_i}{dX}\right)_{c,s} - \frac{\lambda_g}{\lambda_c}\left(\frac{d\Theta_i}{dX}\right)_{g,s} - (1-r)\ F_{o,i} = -\mathcal{R}_i H
$$

where

$$
(2.4.7)\quad
\begin{cases}
\mathcal{R}_i = e^{-\dfrac{E_s}{\mathcal{R}T_{s,ref}}\left[\dfrac{1}{\bar{\Theta}_{i,s}\left(1-\frac{T_{ref}}{T_{s,ref}}\right)+\frac{T_{ref}}{T_{s,ref}}} - 1\right]} & \text{for } \bar{\Theta}_{i,s} \geq \Theta_K \\
\mathcal{R}_i = \bar{\Theta}_{i,s}^{w} & \text{for } \bar{\Theta}_{i,s} \leq \Theta_K
\end{cases}
$$

THIS PAGE IS BEST QUALITY PRACTICABLE
FROM COPY FURNISHED TO DDC

Therefore, BC1 of Eq. 2.4.4 can be written as

$$(2.4.8) \qquad \left(\frac{\partial u}{\partial X}\right)_{c,s} \equiv \left(u_X\right)_{c,s} = \frac{\lambda_g}{\lambda_c}\left(\frac{\partial u}{\partial X}\right)_{g,s} - H\left(\bar{\mathcal{R}}_i - \mathcal{R}\right) + (1-r)\left(F_{o,i} - F_o\right)$$

The transformation into an ODE of the PDE of Eq.2.4.4, with BC1 given by Eq. 2.4.8, can be performed by assuming a polynomial dependence of the disturbance temperature on the space variable:

$$(2.4.9) \qquad u\left(X,\tau\right) \simeq K_o(\tau) + K_1(\tau)\,X + K_2(\tau)\,X^2 + K_3(\tau)\,X^3 + \ldots K_n(\tau)\,X^n.$$

Comments about the implications of this particular thermal profile are given below. The above n+1 coefficients $K_i(\tau)$ are to be determined from the boundary conditions which express no disturbance (up to the (n-2)-th derivative) at the cold end of the penetration depth and the energy balance at the hot boundary of the penetration depth. With our formulation this implies:

$$(2.4.10) \qquad \begin{cases} 1.\ \dfrac{\partial u}{\partial X}\left(X=0,\tau\right) = \left(u_X\right)_{c,s} \\ 2.\ u\left(X=X_\xi,\tau\right) = 0 \\ 3.\ \dfrac{\partial u}{\partial X}\left(X=X_\xi,\tau\right) = 0 \\ \vdots \\ n.\ \dfrac{\partial^{n-2} u}{\partial X^{n-2}}\left(X=X_\xi,\tau\right) = 0 \end{cases}$$

where $X_\xi = -\xi(\tau)$ is the penetration distance to be obtained below. After algebric manipulations, one obtains for the unknown profile of the disturbance temperature

$$u\left(X,\tau\right) \simeq \left(u_X\right)_{c,s}\ \frac{\xi}{n}\left(1+\frac{X}{\xi}\right)^n$$

For X = 0 one obtains at the burning surface

$$u\left(X=0,\tau\right) \equiv u_s = \left(u_X\right)_{c,s}\ \frac{\xi}{n}$$

from which the unknown penetration depth can be expressed as

$$(2.4.11) \qquad \xi(\tau) = \frac{n\, u_s}{(u_X)_{c,s}}$$

The disturbance temperature profile is then given by

$$(2.4.12) \qquad u(X,\tau) \simeq u_s \left(1 + \frac{X}{\xi}\right)^n$$

where $u_s(\tau)$ is the unknown surface temperature disturbance to be determined. It is obvious from the above relationship that the time history of the disturbance temperature is restricted to disturbance thermal profiles monotonically decaying in space. Indeed, there is no way for a polynomial profile to accommodate an inflection point. This difficulty may be overcome by "allowing a new penetration depth to begin propagating at each maximum or minimum" (p.96 of Ref.32) of the heat input into the condensed phase. However, this procedure will not prove necessary here, since testing both the static and dynamic stability does not require a detailed knowledge of the structure of the thermal profile.

A space integration can now be performed over X from 0 to $-\xi(\tau)$ of the PDE:

$$(2.4.13) \qquad \frac{d}{d\tau}\int_0^{-\xi(\tau)} u(X,\tau)\,dX = \mathcal{R}\,u_s - (u_X)_{c,s} - \mathcal{R}\,\Delta(\bar{\Theta}_i) + \Delta\left(\frac{d\bar{\Theta}_i}{dX}\right)$$

where

$$(2.4.14) \qquad \begin{cases} \Delta(\bar{\Theta}_i) = \bar{\Theta}_i(X=0) - \bar{\Theta}_i(X=-\xi) \\ \Delta\left(\dfrac{d\bar{\Theta}_i}{dX}\right) \equiv \dfrac{d\bar{\Theta}_i}{dX}(X=0) - \dfrac{d\bar{\Theta}_i}{dX}(X=-\xi) \end{cases}$$

being $\xi(\tau)$ defined by Eq. 2.4.11. Upon substituting the approximate disturbance temperature profile described by Eq. 2.4.12, the following differential expression is obtained:

$$(2.4.15)\qquad \frac{d}{d\tau}\,\frac{u_s^2}{(u_x)_{c,s}} = -\frac{n+1}{n}\left[\mathcal{R}\,u_s - (u_x)_{c,s} - \mathcal{R}\,\Delta(\bar{\Theta}_i) + \Delta\left(\frac{d\bar{\Theta}_i}{dX}\right)\right]$$

Since $(u_x)_{c,s} = f\,(u_s\,(\tau);\ \mathcal{P}\,(\tau),\ F_o\,(\tau)\,)$, one obtains from Eq. 2.4.8.

$$(2.4.16)\qquad \frac{d(u_x)_{c,s}}{d\tau} = \frac{du_s}{d\tau}\left[\frac{\partial(u_x)_{c,s}}{\partial u_s}\right]_{\mathcal{P},F_o} + \frac{d\mathcal{P}}{d\tau}\left[\frac{\partial(u_x)_{c,s}}{\partial \mathcal{P}}\right]_{F_o,u_s} - (1-r)\frac{dF_o}{d\tau}$$

For example, the time derivative of the thermal gradient at the condensed phase side may be explicitely written, for $c_g/c_c = 1$, as

$$(2.4.17)\qquad \frac{d(u_x)_{c,s}}{d\tau} = \frac{du_s}{d\tau}\left[\frac{\lambda_g}{\lambda_c}\left(\frac{\partial(u_x)_{g,s}}{\partial u_s}\right)_{\mathcal{P}} + H\,\frac{d\mathcal{R}}{du_s}\right] + \frac{\lambda_g}{\lambda_c}\,\frac{d\mathcal{P}}{d\tau}\left(\frac{\partial(u_x)_{g,s}}{\partial \mathcal{P}}\right)_{u_s} - (1-r)\,\frac{dF_o}{d\tau}$$

which can be evaluated once a flame model has been chosen and the laws $\mathcal{P}(\tau)$ and $F_o(\tau)$ have been externally assigned. By derivating, one obtains from Eqs. 2.4.15 and 2.4.16

$$(2.4.18)\qquad \frac{1}{(u_x)_{c,s}^2}\left[2u_s\,\frac{du_s}{d\tau}(u_x)_{c,s} - u_s^2\left[\frac{du_s}{d\tau}\left(\frac{\partial(u_x)_{c,s}}{\partial u_s}\right)_{\mathcal{P},F_o} + \frac{\partial \mathcal{P}}{\partial \tau}\left[\frac{\partial(u_x)_{c,s}}{\partial \mathcal{P}}\right]_{F_o,u_s} - (1-r)\frac{dF}{d\tau}\right]\right] = -\frac{n+1}{n}\left[\mathcal{R}\,u_s - (u_x)_{c,s} - \mathcal{R}\,\Delta(\bar{\Theta}_i) + \Delta\left(\frac{d\bar{\Theta}_i}{dX}\right)\right]$$

Finally, the following nonlinear ODE for the time dependent surface temperature disturbance is obtained:

$$
(2.4.19)\quad
\begin{cases}
\dfrac{du_s}{d\tau} = -\dfrac{n+1}{2n}\dfrac{(u_x)_{c,s}}{u_s}\dfrac{\Re\, u_s - (u_x)_{c,s} - \Re\,\Delta(\bar{\theta}_i) + \Delta\left(\dfrac{d\bar{\theta}_i}{dX}\right)}{1 - 1/2\,\dfrac{u_s}{(u_x)_{c,s}}\left[\dfrac{\partial (u_x)_{c,s}}{\partial u_s}\right]_{\mathcal{P},F_o}} \\
\qquad + \dfrac{\dfrac{d\mathcal{P}}{d\tau}\left[\dfrac{\partial (u_x)_{c,s}}{\partial \mathcal{P}}\right]_{F_o,u_s} - (1-r)\dfrac{dF_o}{d\tau}}{2\dfrac{(u_x)_{c,s}}{u_s} - \left[\dfrac{\partial (u_x)_{c,s}}{\partial u_s}\right]_{\mathcal{P},F_o}} \\
u_s(\tau=0) = 0
\end{cases}
$$

which is approximately equivalent to the initial PDE+boundary conditions formulation. Notice that in the above equation $\bar{\theta}_i(X)$ is known (see Eq. 2.4.2) and that only the surface temperature appears.

The above nonlinear ODE in the unknown $u_s(\tau)$ describes the response of the system to a finite size departure of the surface temperature from the stationary value due not only to intrinsic perturbation sources acting on the system (static stability), but also to any arbitrary but externally assigned monotonical change in time of controlling parameters such as pressure and radiant flux (dynamic stability). If one wishes to know the whole temperature profile, he has only to substitute $u_s(\tau)$ in Eq. 2.4.12, evaluate $\xi(\tau)$ from Eq. 2.4.11 with the help of Eq. 2.4.8, and then use the $u_s(\tau)$ definition (Eq. 2.4.1) in order to determinate the resultant temperature profile.

Considerations of a general character on the static stability of the system described by Eq. 2.4.19 can now be made. According to the theory based on the Lyapunov theorems, a given equilibrium configuration of the system is asymptotically stable if

$$
\left.\begin{aligned} u_s(\tau) &\to 0 \\ \text{or} \qquad \theta(X,\tau) &\to \bar{\theta}_i(X) \end{aligned}\right\} \text{for} \qquad \tau \to \infty
$$

In other words, the system is (asymptotically) stable is the disturbance disappears at large time and the system returns to its initial configuration. Following Lyapunov (p. 216 of Ref. 45), Eq. 2.4.19 can be written, in a more concise way, as

$$(2.4.20)\qquad \begin{cases} \dfrac{du_s}{d\tau} = -f(u_s) + g(\tau, u_s) \\ u_s(\tau = 0) = 0 \end{cases}$$

where

$$(2.4.21)\qquad f(u_s) \equiv \frac{n+1}{2n}\,\frac{(u_x)_{c,s}}{u_s}\;\frac{\mathcal{R}\,u_s - (u_x)_{c,s} - \mathcal{R}\,\Delta(\bar{\theta}_i) + \Delta\left(\dfrac{d\bar{\theta}_i}{dx}\right)}{1 - 1/2\,\dfrac{u_s}{(u_x)_{c,s}}\left[\dfrac{\partial (u_x)_{c,s}}{\partial u_s}\right]_{\mathcal{P},F_o}}$$

is the autonomous (i.e., time independent) contribution, and

$$(2.4.22)\qquad g(\tau, u_s) = \frac{\dfrac{d\mathcal{P}}{d\tau}\left[\dfrac{\partial (u_x)_{c,s}}{\partial \mathcal{P}}\right]_{F_o,u_s} - (1-r)\dfrac{dF}{d\tau}}{2\dfrac{(u_x)_{c,s}}{u_s} - \left[\dfrac{\partial (u_x)_{c,s}}{\partial u_s}\right]_{\mathcal{P},F_o}}$$

is the nonautonomous (i.e., time dependent) contribution. If no forcing function is acting on the system, i.e.

$$\mathcal{P} = \text{cost} \qquad \text{and} \qquad F_o = \text{cost},$$

then Eq. 2.4.20 reduces to

$$(2.4.23)\qquad \frac{du_s}{d\tau} = -f(u_s)$$

by which the autonomous contribution assumes the meaning of a static restoring function. Indeed, under these circumstances, one can think of the chemically reacting system comprised of the deflagrating condensed material as analogous to a mass-spring type of mechanical system with the nonlinear characteristic $f(u_s)$. Considering the $u_s(\tau)$ definition of Eq. 2.4.1, Eq. 2.4.20 can also be written as

$$(2.4.24)\qquad \begin{cases} \dfrac{d\Theta_s}{d\tau} = f(\bar{\theta}_{i,s} - \Theta_s) - g(\tau, \bar{\theta}_{i,s} - \Theta_s) \\ \Theta_s(\tau = 0) = \bar{\theta}_{i,s} \end{cases}$$

The static restoring function $f(\bar{\Theta}_{i,s} - \Theta_s)$ depends only on the nature of the deflagrating substance; the nonautonomous term changes in time according to the first derivatives of the external controlling parameters (see Eq. 2.4.22).

Sec. 2.5 - NATURE OF THE STATIC RESTORING FUNCTION

The static restoring function is an algebraic nonlinear function strictly dependent on the nature of the burning propellant (including the specific way its flame is described, i.e. the flame model implemented and the order of the approximating polynomial used in Sec. 2.4) and the operating conditions. Before examining quantitative plots, consider the qualitative plots of Fig. 12a and Fig. 12b. This allows to extract the basic properties of the static restoring function independenly on the flame description. It is anticipated that the heat release at the surface of the propellant is the most infuential parameter on the shape of the static restoring function.

Consider the qualitative plot of Fig.12a. According to Eq. 2.4.24, when no forcing function is acting on the system, all the points (algebraic roots) for which $f(\bar{\theta}_{i,s} - \theta_s) = 0$ define possible equilibrium configurations for the burning propellant, since they correspond to $d\theta_s/d\tau = 0$. It is seen in Fig.12athat, in addition to the trivial $\theta_s = 0$ (unburning propellant, root C), two more equilibrium solutions (roots A and B) are allowed, in general, for a given set of parameters. Let us consider the equilibrium configuration corresponding to root A. Suppose that, for some unspecified reason, the burning rate or the surface temperature increases a finite amount; then the burning propellant is no longer in a stationary configuration, $d\theta_s/d\tau = f(\bar{\theta}_{i,s} - \theta_s)$ is negative, and the system reacts by decreasing its surface temperature. Conversely, if for an unspecified reason, the surface temperature of a propellant burning according to the configuration of root A decreases, the system reacts by increasing its surface temperature. These movements, around point A, are indicated by arrows in Fig.12a. It is concluded that the equilibrium configuration corresponding to root A is stable because, when disturbed, the system always moves back toward A. By the same arguments, it is concluded that the equilibrium configuration corresponding to root B is unstable; any disturbance yields movement away from the point. Therefore, in steady state experiments, only solution A is observed.

If the set of parameters is changed, for example the pressure is increased from P to P_1, the initial condition of the ODE (see Eq. 2.4.2) is changed so that a new pair of roots, A_1 and B_1, is found in addition to the trivial $\theta_s = 0$ of root C. Again, root A_1 defines a stable equilibrium configuration, while root B_1 defines an unstable equilibrium configuration corresponding to the new set of parameters. Likewise, a new pair of roots, A_2 and B_2, in addition to the trivial $\theta_s = 0$ of root C, is found if the pressure is decreased from P to P_2. It follows that the θ_s axis in Fig.12a includes, in addition to the trivial solution of nonburning propellant at the root C, a segment of stable solution A_i and a segment of associated unstable solution B_i (each pair of roots corresponds to a given set of parameters).

It should be explicitely observed that the trivial $\theta_s = 0$ solution may be obtained only if the exponential Arrhenius-type pyrolysis law for mass production at the surface is dropped. Obviously, the trivial $\theta_s = 0$ solution implies that no external energy source (e.g., radiation) is acting on the solid propellant.

The qualitative picture of Fig. 12a illustrates the general behavior of the static restoring function when the pressure is varied parametrically at fixed ambient temperature and surface heat release. The behavior of the static restoring function when the surface heat release is varied parametrically, at fixed ambient temperature and pressure, is illustrated by the qualitative picture of Fig.12b. Of course, all previous considerations hold true. For example, when the surface heat release is low enough (in a sense which will be better understood below), the system behaves again according to the static restoring function represented by curve CBA (Fig. 12b). However, for increasing values of the surface heat release, it is found that the static restoring function is represented by curve $CB_1A_1D_1E_1$. This is rather surprising; in principle, there are now five equilibrium configurations.

Based on the previous analysis, however, it is immediately recognized that C is the stable equilibrium solution for the unreacting state (trivial solution). But further discussion is required to understand the nature of the remaining four roots. This is easily accomplished by considering the steady state energy balance of the overall combustion wave. For example, the graphic plot of Fig. 9 suggests that for each set of parameters only one solution exists for the reacting state. Conventionally, let us call A that particular root of Figs. 12a and 12b corresponding to the energy balance solution of Fig. 9. It follows that root E_1, although stable according to Lyapunov, is eliminated as being a reacting equilibrium solution. In other words, root E_1 is a false equilibrium solution introduced by the approximate ODE formulation of the problem. The remaing roots B_1 and D_1 are, then, both unstable equilibrium solutions for the reacting state.

For further increase of the surface heat release, it is observed that A- and D-type roots respectively increase (moving to right) and decrease (moving to left) in the plot of Fig. 12b, until coalescence and then crossing over occur with exchange of stability character. This important point will be discussed in detail later (see Sec. 2.6). For further increasing of the surface heat release, B- and D-type roots disappear after coalescence, while both A_2 and E_2 roots, for different reasons, are eliminated as being stable reacting solutions (curve CA_2E_2 in Fig. 12b). Under these circumstances, it follows that the only allowed solution is the trivial unreacting configurations represented by root C. Any attempt to produce a stationary combustion wave with a static restoring function of type CA_2E_2 will inevitably result in extinction. This type of extinction, however, cannot be qualified as "dynamic".

Quantitative plots of the static restoring function $f(\bar{\theta}_{i,s} - \theta_s)$ vs the nondimensional surface temperature θ_s are given for the propellant AP/PBAA No. 941. A quantitative plot requires the choice of a specific flame model and a specific order of the approximating polynomial (see Sec. 2.4). By applying different flame models to the same propellant, different stability properties are predicted : this offers a criterium for discriminating potentially good from bad flame models. In this work MTS and KTSS (both linearized and non linearized) flame models are implemented. As to the order of the approximating polynomial, a cubic law was chosen to represent the space distribution of the disturbance thermal profile. This choice was suggested by a large body of literature on heat transfer problems (e.g., Ref. 32) and by similar solid propellant rocket problems (Refs. 33-34). However, there is no a priori guarantee that is the best (and even, simply, a good) choice. The choice has to be verified, somehow. This is shown in Sec. 2.7.

Plots obtained implementing the MTS and KTSS flame models, with a cubic disturbance thermal profile, are respectively shown in Figs. 13-16 and in Figs. 17-19. The MTS flame model was applied by assuming a combined exponential power pyrolysis law at the burning surface (see Eqs. 2.2.3, with θ_K=0.15 and θ_m=0). The KTSS flame model was applied by assuming a power pyrolysis law (see Eq. 2.2.3b, with w=6 and θ_m =0) over the whole range of surface temperature of interest. Comparative results are shown in Fig. 20 for some standard operating conditions, leading to the conclusion that MTS in perhaps the best flame model but KTSS nonlinearized is strongly competitive. The effect of the order of the approximating polynomial for the disturbance thermal profile is shown in Figs. 21-23 for the MTS flame model only.

The effect of the ambient pressure on the static restoring function vs the nondimensional surface temperature is illustrated in Fig. 13 for the indicated set of parameters (MTS flame and n=3). An increase of pressure implies an increase of the stable equilibrium surface temperature, but a less pronounced increase of the unstable equilibrium surface temperature. The strength of the stability (see Sec. 2.6) is enhanced by an increase of pressure. Similar comments hold true as to the effect of an external radiant flux on the restoring function (Fig.14). It is important, however, to note that an increase of the external radiant flux decreases the unstable equilibrium surface temperature and above a certain value of radiant flux intensity (e.g., 40 cal/cm^2-s for the set of parameters in Fig. 14) no more unstable solutions are found. This implies that, in principle (see Sec. 2.7), at each pressure a minimum value of external radiant flux intensity exists above which the dynamic boundary can no longer be defined. The effects of surface heat release (Figs. 15a and 15b) are more involved. Note that for increasing values of the surface heat release, the behavior of the static restoring function shifts from a CBA - type (see Fig.15a)

curve for Q_s =-150 and -158.2 cal/g, to CBADE (see Fig.15b) for Q_s = -170 and -180 cal/g, and to CBDAE for Q_s = -200 cal/g, with A-D roots coalescence occurring at Q_s=-190 cal/g. This implies that at 30 atm the system will show dynamic stability effects not only in the low range of surface temperature (root B in Fig. 15a) but also in the large range (root D in Fig. 15b). The effects of ambient temperature (Fig. 16) are of little interest in the range investigated.

Similar trends are observed for the nonlinearized KTSS flame model, again with n=3. The effect of the ambient pressure in Fig. 17 is very close to that found with MTS (cf. with Fig. 13) ; minor differences are found in the region near the statically unstable root. The same comments hold true as to the effect of surface heat release (Fig. 18).

Drastically different results are observed for the linearized KTSS flame model, always with n=3. The effect of the ambient pressure in Fig. 19 is virtually the same (as compared both to MTS and KTSS nonlinearized) for surface temperature about or larger than the steady state value, but is physically meaningless for surface temperaure less than about 90% of the steady state value (no zero solution and no unstable root).

The static restoring functions for the three flames are plotted simultaneously in Fig. 20, always with n=3, for the standard conditions specified in the figure (P=30 atm, T_a=300 K, Q_s = -158.2 cal/g, adiabatic). The comparison graphically emphasizes the differences just mentioned. The linearized KTSS is discarded from being in principle an acceptable flame model, the nonlinearized KTSS is acceptable for most of the surface temperature range of values (except near extinction, since chemical kinetics is not considered), the MTS is in principle acceptable over the whole range of surface temperature of interest.

The effect of the order of the polynomial approximating the disturbance thermal profile on the static restoring function is illustrated in Fig. 21 (P=20 atm), Fig.22 (P=30 atm) and Fig. 23 (P=40 atm) for the MTS flame. The shape of the static restoring function is kept for n varying from 2 to 4; the steady state (or stable reacting) solution is always recovered (by construction); the trivial zero solution is also always recovered; the surface temperature associated with the unstable reacting solution slightly increases for n decreasing. Numerical values can be better appreciated in Tab. 3: typically, the surface temperature associated with the B root increases of less than 10% when n decreases from 3 to 2.

Sec. 2.6 - NONLINEAR STATIC STABILITY ANALYSIS

Static stability analysis of a burning propellant relates to the capability of the propellant to keep its burning equilibrium configuration in time. It was shown in Sec. 2.4 that this implies to study the properties of the nonlinear ODE

$$\frac{d\Theta_s}{d\tau} = + f\left(\overline{\Theta}_{i,s} - \Theta_s\right) \tag{2.6.1}$$

which in turn depends on the shape of the algebraic nonlinear static restoring function $f\ (\overline{\Theta}_{i,s} - \Theta_s)$ examined in Sec. 2.5. The following problems are of relevance in the area of static stability:

1. prediction of number and nature of the allowed static solutions (see § 2.6.1).
2. prediction of static stability boundary (see § 2.6.2).
3. measurement of static stability strength (see § 2.6.3).
4. prediction of the pressure deflagration limit.

The first three problems only will be treated in this report.

§ 2.6.1 - Number and nature of the allowed static solutions

It was shown in Ref. 3 that three regions of interest can be distinguished, according to the value of Q_s (see Tab. 4):

1. before A - D roots coalescence, the static reacting solutions is the usual stationary combustion wave strictly defined by root A.
2. after A - D roots coalescence but before B - D roots calescence, the static reacting solution is a self-sustained oscillating combustion wave around root A.
3. after B - D roots coalescence, no static reacting solutions whatsoever is allowed.

Obviously, the trivial unreacting solution $\Theta_s = \mathcal{R} = 0$ is always allowed (being statically stable). Therefore, too much surface energy release excludes any steady reacting solution and under these circumstances the only possible configuration, even in a static environment, is the unreacting state. These predictions were verified by numerical integration of the governing PDE. See Figs. 24-25. The presence of self-sustained oscillations in Fig. 24 suggests the existence of a limit cycle. Being a limit cycle an overall property of the governing partial differential equation, once triggered this oscillatory behavior would not depend on the initial conditions of the system. Indeed, it was found in Ref. 2 that, independently on its past history, under the appropriate circumstances the combustion wave undergoes sharp self-sustained oscillations around root A with amplitude nearly defined by roots D (lower peak) and E (upper peak) and with period corresponding to the characteristic time of the condensed

phase thermal wave.

Under the standard set of parameters indicated, numerical values for the allowed static solutions are given as an example in Tab. 4. In particular, the range of Q_s values for which self-sustained oscillating combustion waves are expected is given, in function of pressure, in Tab. 5. Both calculations were performed for a MTS flame with n=3.

These questions will further be investigated.

§ 2.6.2 - The static stability boundary

An important piece of information in the static stability analysis of a burning propellant is the minimum value of surface temperature (or burning rate) above which stable steady burning is allowed. In order to evaluate this value, a most important feature common to all static restoring functions is emphasized. The specific surface temperature value, Θ_s^S, at which the pair of solutions A_i^S stable and B_i^S unstable coalesces, at a given pressure (Fig. 12a) and for a given set of parameters,

$$A_i^S = B_i^S \equiv \Theta_s^S$$

defines the branching of metastable point at that pressure (and for that set of parameters). Corresponding to this special value of the surface temperature a change of the character of stability occurs at the given pressure, in that for $\Theta_s < \Theta_s^S$ all the equilibrium solutions at that pressure are statically unstable (roots B_i) while for $\Theta_s > \Theta_s^S$ all the equilibrium solutions at that pressure are statically stable (roots A_i). Therefore, the branching point at a given pressure isolates the critical static stability value, Θ_s^S, of the surface temperature at that pressure. Construction of the static stability boundary on the $\mathcal{R}$ vs $\dot{q}_{s,s}$ plane, in a range of pressure, consists of connecting the critical static stability points defined for each pressure of interest in the wanted range (and for a given set of parameters). This implies the search of the branching point at any fixed pressure.

A general method (based on nonadiabaticity of the propellant) for solving this problem is discussed below. However, for the specific case of a solid composite propellant, the search for the branching point may be performed immediately, although not rigorously, based on observation of the physical processes. Consider the qualitative picture superimposed in Fig. 26 on a standard MTS flame model plot. Recall that burning rate and surface temperature are univocally related by an appropriate pyrolysis law. Therefore, it is irrelevant to define the branching point in terms of burning rate or surface temperature. Now, as schematically indicated in Fig. 26, the branching point is determined at each pressure by the geometrical condition of vertical tangent, i.e., infinite slope or maximum heat feedback. Indeed, for $\Theta_s > \Theta_s^S$ a change of burning rate or surface temperature produces opposing effects on the thermal gradients at the surface from the condensed and the gas phase sides; for example, the former increases but the latter decreases when the burning rate is disturbed upward. This competition is the stabilizing mechanism. For $\Theta_s < \Theta_s^S$ a change of burning rate affects, in the same direction, both thermal gradients; this

is destabilizing.Just at the point with vertical tangent, the two unstable and stable static roots $A_s = B_s$ coalesce and an exchange of the stability character of the solutions occurs; therefore, we may identify this point as the wanted branching or metastable point Θ_s^S .For $\Theta_s = \Theta_s^S$the behavior of the system depends on the direction of the perturbation. Now, in order to construct a static stability boundary in the plane $\mathcal{R}$ vs $\dot{q}_{g,s}$ it is enough to connect the branching points Θ_s^S, $\dot{q}_{g,s}^S$ associated with each pressure. This boundary separates the region where static solutions are allowed from the region where no static solution can be found.

This method, first suggested in Ref. 3, is not rigorous since the contribution from the surface reactions is neglected. Its advantage is simplicity. For accurate results, the procedure illustrated in Figs. 27 (Q_s = -120 cal/g), Fig. 28 (Q_s=- 158.2 cal/g) and Fig. 29 (Q_s=-200 cal/g) for a MTS flame has to be used. This consists in assigning a larger and larger heat loss to the burning propellant until just one solution is found (coalescing from the stable and unstable static roots). Obviously, this search can be made directly for any flame model without knowledge of the static restoring function. However, the same results should be obtained by searching the coalescence of the corresponding A and B roots of the static restoring function. This is illustrated in Fig. 30 (P=20 atm), Fig. 31 (P=30 atm) and Fig. 32 (P=40 atm) for the MTS flame with n=3. The closeness of the two set of results confirms the validity of the ODE formulation of the problem. Obviously, this second approach is affected by the choice of the approximating polynomial order. The quantitative differences between the two set of results may be appreciated by comparison of Tab. 6 (heat feedback) with Tab. 7 (static restoring function with n=3).

§ 2.6.3 - Measurement of static stability strength

The static stability analysis can be put on a quantitative basis by means of the "first" Lyapunov criterion. According to this, the solution of the nonlinear autonomous ODE of Eq. 2.6.1 is stable in the neighborhood of a point Θ_s^* if

$$\left[\frac{df(\Theta_{i,s} - \Theta_s)}{d\Theta_s}\right]_{\Theta_s = \Theta_s^*} < 0$$

at the point of interest Θ_s^*. The physical meaning of this criterion was explained in Sec. 2.5. In keeping with the spirit of this physical interpretation, the strength of the stability of the solution at a point Θ_s^* may be measured by the magnitude of the derivative $df/d\Theta_s$ evaluated at $\Theta_s = \Theta_s^*$. How this value is affected by typical parameters is shown in Tab. 8. In the exceptional case of a branching, or metastable, point in which the unstable and the stable solutions coalesce, the above first criterion is not valid. In the present situation, however, it is enough to say that the point Θ_s^S is stable from one side ($\Theta_s \geq \Theta_s^S + \varepsilon$) while it is unstable on the other side ($\Theta_s \leq \Theta_s^S - \varepsilon$), so that, overall, the point Θ_s^S is said to be unstable. It should be clear that the first Lyapunov criterion (used for measuring the strength of the stability) is essentially a lineariza-

tion criterion of the originally nonlinear ODE. However, it is plausible that both roots C and A are stable to finite disturbances of an unknown size, also. The extent of the stability region around the stable roots could be estimated by the Lyapunov "direct" method; but this is not one of the purposes of this analysis. Physically, it is expected that the range of stability of C root (always stable) is limited upward by B, while the range of stability of A root (if stable) is limited downward by B. But dynamic effetcs may increase the range of stability of C root against the range of stability of A root.

Values of the static stability strength in various conditions are summarized in Tab. 8.

Sec. 2.7 - NONLINEAR DYNAMIC STABILITY ANALYSIS

It is wished to predict, under an appropriate set of assumptions, the behavior of an heterogeneous deflagration wave initially propagating steadily under a given set of external parameters and then subjected to arbitrary but known changes in time of pressure and/or radiant flux. This is easily done if an ODE formulation of the problem is available.

Dynamic stability of a burning propellant relates to transition of the propellant from a given initial configuration to a wanted final configuration. A burning propellant is dynamically stable if the transition is successful; if the transition leads to a final configuration different from the wanted one, the burning propellant is dynamically unstable.

It was shown in Ref. 3 that for the wide range of controlling parameters varying in time according to monotonically decreasing functions (see Fig. 33), the statically unstable root of the static restoring function evaluated at the final operating conditions is also the asymptotic (in time) dynamic limit (see Fig. 34). It was verified in Ref.4 that this limit holds true for any monotonic decrease in time of pressure or radiant flux intensity. It was shown in Ref. 3 that this limit is a unique property of the propellant at the final operating conditions; in particularitdoes notdepend on optical trasparency of the condensed phase.

Dynamic effects are associated both with a B-type root (see Figs. 12a - 12b) and with a D-type root (see Fig. 12b). The former is called lower dynamic stability and relates to extinction; the latteris called upper dynamic stability and relates to vigorous accelerations of the combustion wave possibly followed by extinction due to overstability (Fig. 24). Discussions and results concerning this point are given in Refs. 2 - 3.

Note that in the general ODE formulation of Eq. 2.4.19 the influence of time varying external parameters is felt only through their time derivatives. This implies that, if no change of pressure and/or radiant flux occurs, the system is only subjected to random intrinsic fluctuations and the results from the static stability analysis apply. It is also implied that, in the case that $g(\tau, \bar{\Theta}_{i,s} - \Theta_s) \ll f(\Theta_{i,s} - \Theta_s)$ in Eq. 2.4.24, the dynamic stability boundary is a no-return boundary for any τ (even finite) and for any external law (even non monotonic or increasing).

A graphical summary of this nonlinear stability analysis is offered in Fig. 35 (MTS flame plot) and Fig. 36 (standard $\mathcal{R}$ vs P plot). According to the value of the surface heat release, upper static and dynamic stability boundaries may also be found.

Checks of the lower dynamic stability boundary were performed for several deradiation and depressurization transients. See Tabs. 9 - 10 and Figs. 37 - 47. The computer checks were performed by solving numerically the PDE formulation of the general quasi-steady gas phase transient problem, whereas the stability boundaries were determined by analytical means from

considerations of the approximately equivalent ODE formulation. Since the lower dynamic stability boundary corresponds to statically unstable roots, it cannot be observed directly either experimentally or theoretically. A go/no-go technique is required (see Fig. 37). The results shown in Figs. 38 - 47 and summarized in Tab. 10 suggest that $n = 3$ gives an excellent agreement for final pressures not larger than, say 30 atm. For large values of pressure, $2 < n < 3$ seemes more successful (see Fig. 45).

Sec. 2.8 - STATE OF THE ART OF THE NONLINEAR APPROACH

The problem of the quasi-steady gas phase burning of a solid propellant in a rather general form is being dealt with. In order to retain the nonlinearity of the problem, an approximate formulation in terms of an ODE was written. This was done by means of an integral approach limited to situations in which no inflection point in the history of the condensed phase thermal profiles would occur. It is shown that the important facts (see below) of heterogeneous combustion may be ascertained. The two fundamental regimes of the static (intrinsic random perturbations) and of the dynamic (externally assigned changes of the controlling parameters) stability of heterogeneous flames, allowing for finite size disturbances, are examined.

The following facts emerge from the nonlinear static stability analysis. For a given set of parameters:

1. a stable stationary nonreacting equilibrium configuration (trivial solution) is always found.
2. a stable, stationary (low Q_s) or self-sustained oscillating (large Q_s), reacting equilibrium configuration may be found.
3. a stable stationary reacting equilibrium configuration is found before A-D roots coalescence occurs.
4. self-sustained oscillations are found between A-D roots coalescence and B-D roots coalescence.
5. after B-D roots coalescence, no stable reacting equilibrium solution is found.
6. the static stability boundary, for small but finite size random intrinsic disturbances, is the locus of the branching points (A-B roots coalescence).
7. the stability of the steady state equilibrium configurations can be measured by the slope of the static restoring function vs the surface temperature at the point $\bar{\theta}_{i,s}$ of interest.
8. The effect of the relevant parameters can be easily evaluated by considering the corresponding static restoring function.

The following facts emerge from the nonlinear dynamic stability analysis. For a given monotonic law of timewise decrease of the controlling parameters:

1. extinction may occur even though the final point of the transition is statically stable.
2. the lower dynamic stability boundary, for finite size disturbances consequent to timewise monotonical changes of the controlling parameters, is the locus of the statically unstable roots (B-type) associated with the final operating conditions.

3. the lower dynamic stability boundary holds true both for deradiation and depressurization runs, and is not affected by the specific forcing law.

4. upper dynamic instability is related to D root and may cause vigorous acceleration of the combustion wave or dynamic extinction.

The following facts emerge by comparing several flame models:

1. the KTSS linearized flame model is physically meaningless for burning rate less than about 90% of the steady value.

2. the KTSS nonlinearized flame model is physically questionable for burning rate near zero.

3. the MTS flame model is in principle acceptable over the whole range of burning rate.

The following facts emerge by changing the order n of the polynomial approximating the disturbance thermal profile:

1. C and A roots are not affected.

2. B, D, and E roots are affected.

3. the static stability boundary can be evaluated independently of n.

4. the dynamic stability boundaries (both lower and upper) are determined in function of n.

5. the polynomial of order n=3 gives accurate results up to 30 atm of final pressure, while $3 > n > 2$ is more suitable for larger values of pressure.

The physical meaning of the stability boundaries is the following. The static stability boundary defines a line of separation between a region where stable steady state solutions are allowed and a region where only unstable or no steady solutions are found. The dynamic stability boundary defines that ultimate burning condition (in terms of burning rate or surface temperature) beyond which extinction necessarily follows. The fundamental importance of this distinction is stressed by the fact that, under dynamic conditions, the propellant may momentarily burn also in a region of statically unstable configurations. It is shown that the dynamic stability boundary collapses to the static stability boundary when the rate of change of the externally controlled parameters is negligible.

Notice that numerical values have been given only for a particular composite propellant (AP/PBAA No. 941). This was done simply because the properties of that particular propellant and good flame models were readily available. It is felt, however, that all analyses were conducted from a broad point of view, and in no way were they dependent on the particular type of propellant chosen as the datum case. Therefore, the conceptual results are expected to hold, although in different ranges of the relevant parameters, for any kind of solid propellant.

Sec. 2.9 - SHOCK TUBE EXPERIMENTS

The pressure deflagration limits of the three propellant formulations under consideration (an AP-based composite, a catalyzed DB and a noncatalyzed DB) were determined in the actual operating conditions of the shock tube (Fig. 48a). These experiments were conducted statically, i.e. a propellant sample was placed in the test section of the shock tube (end wall) and ignition was attempted by means of an electrically heated wire (Fig.48b). The ignition was considered successful only if a self-sustained flame would develop. The test was repeated for several pressurizing gases (nitrogen,air,oxygen) and for ambient pressure parametrically changed. Results for the composite propellant are shown in Fig. 49 (not self-sustained flame means that a visible flame would develop but disappear immediately after an electrical heating of several seconds duration). The samples were cylindrical pellets of 8 mm diameter and about 10 mm thickness. Tests with noncatalyzed DB samples of 16 mm diameter did not show any appreciable difference.

Samples were then placed at the same location, ignited by an electrically heated wire and, once steadily burning, subjected to shock waves of different strength. The light emitted by the burning propellant was detected by means of a photodiode directionally selective and sensitive in the visible and near infrared (spectral response peak at 0.8 μm) . Several tests with different propellants, ignition pressures, pressurizing gases, and shock speeds failed to show conclusive trends as to the dynamic burning rate behavior (as revealed by the light emission). The basic difficulty is the fast succession of shock waves and expansion fans impinging on the surface of the burning propellant during the same test. For example, see Figs. 50-51 (in which the period of the pressure pulse is about 10 ms). In this series of tests, complete extinguishment of the propellant was never achieved.

In order to overcome the problem just mentioned, the shock tube was slightly modified to work as a piston tube. At present, a teflon piston weighting 150 g is being used. In this operating configuration, a longer period (about 50 ms) of the pressure pulses can be obtained and, in general, a better control of the whole experimental apparatus is possible. Work in this direction is now in progress. Preliminary results obtained with a noncatalyzed DB are shown in Figs. 52-55. Again the propellant was located at the end wall of the shock tube and electrically ignited before the run. The test of Figs. 52-53 was run with an initial pressure of 0.5 atm of air; the emitted light reached the maximum value at the peak pressure and then decreased during the expansion. In this test the propellant was extinguished and then reignited by the subsequent shocks. A test conducted at an initial pressure of 0.75 atm of air is shown in Figs. 54-55. In this case the emitted light reached the maximum value before the peak pressure and then decreased while the pressure was still rising. In this test the propellant was completely extinguished.

REFERENCES

1) De Luca, L., "Nonlinear Stability Analysis of Solid Propellant Combustion", II Symposium (International) on Dynamics of Chemical Reactions, University of Padova (Italy), 15-17 Dec. 1975, pp. 245-256.

2) De Luca, L., "Instability of Heterogeneous Deflagration Waves", VI Symposium (International) on Detonation, San Diego (California) USA, 24-27 Aug. 1976, pp. 281-289.

3) De Luca, L., "Solid Propellant Ignition and Other Unsteady Combustion Phenomena Induced by Radiation", Ph. D. Thesis, Department of Aerospace and Mechanical Sciences, AMS Report No. 1192-T, Princeton University, 15 Nov. 1976.

4) De Luca, L., Galfetti, L.and Zanotti, C., "Dynamic Extinction of Composite Solid Propellants", XIX Israel Annual Conference on Aviation and Astronautics, Technion, Haifa (Israel), 2-3 March 1977.

5) De Luca, L. and Zanotti, C., "Measurement of Steady Solid Propellant Burning Rate and Data Processing", Technical Note, XXXII Congresso ATI, Roma, 20-23 Sept. 1977, pp. 256-275.

6) De Luca, L., Galfetti, L. and Zanotti, C.,"Evaluating the Kinetic and Diffusion Time Constants in the MTS Flame Model", Technical Note, XXXII Congresso ATI, Roma, 20-23 Sept. 1977, pp. 278-301.

7) Coghe, A., De Luca, L., Spizzamiglio, A., "Flame Structure of Double Base Propellants by Laser-Doppler Anemometry", V International Symposium on Combustion Processes, Krakow, (Poland), 12-17 Sept.1977, pp. 149-150.

8) De Luca, L., "Theoretical Studies on Heterogeneous Deflagration Waves : I. A Partial Differential Equation Formulation of the Problem", offered for pubblication, Meccanica.

9) De Luca, L., "Theoretical Studies on Heterogeneous Deflagration Waves : II. An Approximate Ordinary Differential Equation Formulation of the Problem", offered for pubblication, Meccanica.

10) De Luca, L., Galfetti, L. and Zanotti, C.,"Comparison of Two Flame Models used in Solid Rocket Propellant Unsteady Combustion", XXVI Convegno Internazionale delle Comunicazioni, Genova (Italy), 5-7 October 1978.

11) Friedley, J. C. and Petersen E. E., "Influence of Combustion Parameters on Instability in Solid Propellant Motors: Part II. Nonlinear Analysis", AIAA Journal, Vol. 11, No. 4, April 1966, pp. 1932-1937.

12) Horton, M. D., Bruno, P. S. and Graesser, E. C., "Depressurization Induced Extinction of Burning Solid Propellant", AIAA Journal, Vol. 6, No. 2, February 1968, pp. 292-297.

13) Von Elbe, G. and McHale, E. T., "Extinguishment of Solid Propellants by Rapid Depressurization", AIAA Journal, Vol. 6, No. 7, July 1968, pp. 1417-1419.

14) Marxman, G. A. and Wooldridge, C. E., "Nonlinear Solid Propellant Burning Rate Behavior During Abrupt Pressure Excursion", AIAA Paper, No. 68-172, 1969.

15) Brown, R. S. and Muzzy, R. J., "Linear and Nonlinear Pressure Coupled Combustion Instability of Solid Propellants AIAA Journal, Vol. 8, No. 8, August 1970, pp. 1492-1500.

16) Coates, R. L. and Horton, M. D., "Predicted Effects of Motor Parameters on Solid Propellant Extinguishment", JSR, Vol. 7, No. 12, December 1970, pp. 1468-1470.

17) Park, C. P., Ryan, N. W. and Baer, A. A., "Extinguishment of Composite Propellants at Low Pressures", AIAA Preprint No. 73-175.

18) Istratov, A. G. and Librovich, V. B., "Burning Stability of Powder", PMTF. Translation AFSC #FTD-MT-65-161.

19) Barrère, M., "Réponse à un Regime Transitoire de la Surface de Combustion d'un Propergol Solide Hétérogène", ONERA T. P. No. 748, 1969.

20) Summerfield, M., and Krier, H., "Errors in Non Steady Combustion Theory in the Past Decade (A Review)", AIAA Paper No. 69-178, 1969.

21a) Merkle, C. L., Turk, S. L., and Summerfield, M., "Extinguishment of Solid Propellants by Depressurization: Effects of Propellant Parameters", AIAA Paper No. 69-176, 1969.

21b) Merkle, C. L., Turk,S. L. and Summerfield M., "Extinguishment of Solid Propellants by Rapid Depressurization", AMS Report No. 880, July 1969, Princeton University, Princeton, N.J.

21c) Merkle, C. L. and Summerfield, M., "Extinguishment of Solid Propellant Flames : a Theory Based on a New Feedback Law", AMS Report No.838, Presentation Version, June 1968, Princeton University.

22) Ohlemiller, T. J., Caveny, L. H., DeLuca, L. and Summerfield, M., "Dynamic Effects on Ignitability Limits of Solid Propellants Subjected to Radiative Heating", XIV Symposium (International) on Combustion, 1973, pp. 1297-1307.

23a) DeLuca, L., Ohlemiller, T. J., Caveny, L. H. and Summerfield, M., "Radiative Ignition of Double Base Propellants: I. Some Formulation Effects", AIAA Journal, Vol. 14, No. 7, July 1976, pp. 940-946.

23b) DeLuca, L., Ohlemiller, T. J., Caveny. L. H. and Summerfield M., "Radiative Ignition of Double Base Propellants: II. Pre-Ignition Events and Source Effects", AIAA Journal, Vol. 14, No. 8., August 1976, pp. 1111 -1117.

24) T'ien, J. S., "A Theoretical Criterion for Dynamic Extinction of Solid Propellants by Fast Depressurization", Combustion Science and Technology, Vol. 9, No. 1-2, March-April 1974, pp. 37-39.

25) T'ien, J. S., "The Effects of Perturbations on the Flammability Limits", Combustion Science and Technology, Vol. 7, No. 4, June 1973,pp. 185-188.

26) Istratov, A. G., Librovich, V. B. and Novozhilov, B. V., "An Approximate Method in the Theory of Unsteady Burning Velocity of Powder", PMTF, No. 3, 1964. Translation AFSC #FTD-MT-64-319, pp. 233-242.

27) Novozhilov, B. V., "Nonstationary Burning of Powders Having a Variable Surface Temperature", PMTF, No. 1, pp. 54-63, January-February 1967. Translation AFSC #FTD-MT-24-376-68.

28) Summerfield, M., Caveny, L. H., Battista, R. A., Kubota, N., Gostintsev, Yu. A., and Isoda, H., "Theory of Dynamic Extinguishment of Solid Propellant with Special Reference to Non-steady Heat Feedback Law", JSR, Vol. 8, No. 3, March 1971, pp. 251-258.

29) Battista, R. A., Caveny, L. H. and Summerfield, M., "Nonsteady Combustion of Solid Propellants", AMS Report #1049, October 1972, Princeton University, Princeton, N.J.

30) Novozhilov, B. V., Nonstationary Combustion of Solid Rocket Fuels, 1973. Translation FTD-MT24-317-74.

31) Boggs, T. L. and Beckstead, N. W., "Failure of Existing Theories to Correlate Experimental Nonacoustic Combustion Instability Data", AIAA Journal, Vol. 8, No. 4, April 1970, pp. 626-631.

32) Goodman, T.R., "Application of Integral Methods to Transient Nonlinear Heat Transfer", Advances in Heat Transfer, Vol. 1, 1964, Academic Press, New York, pp. 51-122.

33) Peters, N., "Theory of Heterogeneous Combustion Instabilities of Spherical Particles", XV Symposium (International) on Combustion, 1975, pp. 363-375.

34) Kuo, K.K., "Theory of Flame Front Propagation in Porous Propellant Charges under Confinement", Ph. D. Thesis, Aerospace and Mechanical Sciences Dept., Princeton University, August 1971.

35) Peretz, A., Caveny, L.H., Kuo, K.K. and Summerfield, M. "The Starting Transient of Solid Propellant Rocket Motors with High Internal Gas Velocities", Aerospace and Mechanical Sciences Dept., Report No. 1100, Princeton University, April 1973.

36) Gostintsev, Ya. A., "Method of Reduction to Ordinary Differential Equations in Problems of the Nonstationary Burning of Solid Propellants", Combustion, Explosion, and Shock Waves, Vol. 3, No. 3, 1967, pp. 355-361.

37) Librovich, V. B., "Ignition of Powders and Explosives", PMTF, No. 6, November-December 1963, pp. 74-80.

38) Rozenbad, V. I., Averson, A. E., Barzykin, V. V., and Merzhanov, A. G., "Some Characteristics of Dynamic Ignition Regimes", Combustion, Explosion and Shock Waves, Vol. 4, No. 4, 1968, pp. 494-500.

39) Gostintsev, Ya. A. and Margolin, A. D., "On Nonstationary Burning of Powder", PMTF, No. 5, 1964.

40) Gostinsev, Ya. A. and Margolin, A. D. , "Nonstationary Combustion of a Powder Under the Action of a Pressure Pulse", Combustion, Explosion, and Shock Waves, Vol. 1, No. 2, March-April 1965, pp. 69-75.

41) Anisimov, S. I. and Perel'man, "On One Nonlinear Problem of Thermal Conduction", PMTF, No. 5, 1963. Translation AFSC No. FTD-MT-64-61, pp. 223-228.

42a) Krier, H., T'ien, J.S., Sirignano, W.A. and Summerfield, M., "Nonsteady Burning Phenomena of Solid Propellants : Theory and Experiments", AIAA Journal, Vol. 6, No. 2, February 1968, pp. 278-285.

42b) Summerfield, M., Krier, H., T'ien, J.S. and Sirignano, W.A., "Non-steady Burning Phenomena of Solid Propellants : Theory and Experiment (U)" , AMS Report No. 793, July 1967, Princeton University.

42c) Krier, H., "Solid Propellant Burning in Nonsteady Pressure Fields", Ph. D. Thesis, Sept. 1968, Princeton University.

43a) Steinz, J.A., Stang, P.L. and Summerfield, M., "The Burning Mechanism of Ammonium Perchlorate Based Composite Propellants", AMS Report No. 830, February 1969, (AD 688 944), Princeton University.

43b) Steinz, J.A.,Stang, P.L. and Summerfield, M., "Effects of Oxidizer Particle Size on Composite Solid Propellant Burning : Normal Burning, Plateau Burning and Intermediate Pressure Extinction", AMS Report No. 810, Presentation Version, October 1967, Princeton University.

43c) Steinz, J.A. and Summerfield, M., "Low Pressure Burning of Composite Solid Propellants", Reprinted from Advances in Chemistry Series No. 88, 1969, Princeton University.

43d) Steinz,J.A., "State of Knowledge of Mechanism of Steady State Burning of Composite Ammonium Perchlorate Solid Propellant", manuscript, March 1965, Princeton University.

43e) Steinz,J.A. and Stang, P.L., "The Burning Mechanism of Ammonium Perchlorate Based Composite Solid Propellant", AIAA Paper No. 68-658, 10-14 June 1968.

44a) Summerfield, M., Sutherland, G. S., Webb, M. J., Taback, H. J. and Hall, U.P., "Burning Mechanism of Ammonium Perchlorate Propellants", ARS Progress in Astronautics and Rocketry: Solid Propellant Rocket Research, Vol.1, edited by M. Summerfield, Academic Press, New York, 1960, pp. 141-182.

44b) Blair, D.W., Bastress, E.K., Hermance,C.E., Hall, K.P. and Summerfield, M., "Some Research Problem in the Steady State Burning of Composite Solid Propellant", ARS Journal, 28-29 January 1960.

45) Andronov, A.A., Vitt, A.A. and Khaikin, S.E., "Theory of Oscillators",English Edition by Pergamon Press Ltd., London ; U.S.A. Edition distributed by Addison-Wesley, Mass., 1966.

NOMENCLATURE

a	= volume absorption coefficient, cm^{-1}
A_M	= constant used in MTS flame model (see Eq. 2.3.2)
B_M	= constant used in MTS flame model (see Eq. 2.3.3)
B_p	= nondimensional depressurization rate coefficient (see Tab. 8)
B_r	= nondimensional deradiation rate coefficient (see Tab. 8)
C	= specific heat, cal/g-K
d	= layer thickness, cm
E	= activation energy, cal/gmole
$f\ (\bar{\theta}_{i,s}-\theta_s)$	= static restoring function (see Eq. 2.4.21)
F	= nondimensional radiant flux intensity
$g\ (\tau, \bar{\theta}_{i,s}-\theta_s)$	= nonautonomous function (see Eq. 2.4.22)
H	= nondimensional surface heat release
I	= radiant flux intensity, cal/cm^2-s
I_o	= radiant flux intensity impinging at the propellant surface, cal/cm^2-s
$\bar{m}$	= average molecular weight, g/gmole
n	= exponent in ballistic burning rate law; also: order of the approximating polynomial (see Eq. 2.4.9)
N_t	= transparency factor (see Eq. 2.2.2)
p	= ammonium perchlorate percent, %
P	= pressure, atm
$\mathcal{P}$	= nondimensional pressure
$\dot{q}$	= energy flux intensity, cal/cm^2-s
$q_{g,s}$	= nondimensional heat feedback from the gas phase
Q	= nondimensional flame heat release
Q_f	= flame heat release, cal/g
Q_s	= surface heat release, cal/g
r	= surface reflectivity
$\mathcal{R}$	= universal gas constant, cal/gmole-k
R	= burning rate, cm/s
$\mathcal{R}$	= nondimensional burning rate
s	= volume scattering coefficient, cm^{-1}
t	= time, s
T	= temperature, K

Υ = nondimensional temperature (see Eq. 2.2.1b)

u = nondimensional finite size disturbance of temperature (see Eq. 2.4.1)

u_X = nondimensional finite size disturbance of thermal gradient (see Eq. 2.4.8)

U = gas velocity, cm/s

$\mathfrak{U}$ = nondimensional gas velocity

x = space variable, cm

X = nondimensional space variable

w = exponent in KTSS surface pyrolysis law (see Eq.2.2.3b)

Greek Symbols:

α = thermal diffusivity, cm^2/s

δ = nondimensional layer thickness

Δ = finite difference of a quantity evaluated between $X = 0$ and $X = -\xi$ (see Eq. 2.4.14)

ε = small quantity

θ = nondimensional temperature (see Eq. 2.2.1a)

λ = thermal conductivity, cal/cm-s-K; also: wavelength, μm

ξ = nondimensional thickness of disturbance thermal layer (see Eq. 2.4.11)

ρ = density, g/cm^3

τ = nondimensional time

τ' = nondimensional time parameter defined in Eqs. 2.32 - 2.3.4

Subscripts and Superscripts:

a = ambient value; also: absorption layer

B = binder

c = condensed phase value

cr = crystal

ξ = penetration depth

f = final value; also: flame

g = gas

i = initial value

k = matching value

ℓ	= energy loss
m	= minimum value for chemical reactions to occur
p	= pressure
r	= radiant
s	= surface value
S	= static
di	= diffusion
ki	= kinetic
re	= reaction
th	= thermal
ext	= external
ref	= reference value
-	= steady state or average value of a parameter
v	= vaporization
$-\infty$	= condition far upstream
$+\infty$	= condition far downstream

Abbreviations:

A	= ammonia (NH_3)
AFSC	= Air Force System Command
AIAA	= American Institute of Aeronautics and Astronautics
AIMETA	= Associazione Italiana di Meccanica Teorica ed Applicata
AMS	= Aerospace and Mechanical Sciences Department
AP	= ammonium perchlorate (NH_4ClO_4)
ATI	= Associazione Termotecnica Italiana
BC	= boundary condition
BC1	= boundary condition at x = 0
BC2	= boundary condition at $x = -\infty$
BRL	= Ballistic Research Laboratory
CPIA	= Chemical Propulsion Information Agency
DB	= double base
GDF	= granular diffusion flame (model of steady state burning)
IC	= initial condition
JSR	= Journal of Spacecraft and Rockets
KTSS	= Krier-T'ien-Sirignano-Summerfield
HTPB	= hydroxyl-terminated polybutadiene

MTS = Merkle-Turk-Summerfield

NC = nitrocellulose

NOTS = Naval Ordnance Test Station

NWC = Naval Weapons Center

ODE = ordinary differential equation

ONERA = Office National d'Etudes et de Recherches Aérospatiales

PBAA = polybutadiene-acrylic acid

PA = perchloric acid ($HClO_4$)

PDE = partial differential equation

PMTF = Journal of Applied Mechanics and Technical Physics

PU = polyurethane

SRI = Stanford Research Institute

UTC = United Technology Center

LIST OF TABLES

Tab. 8b Compared stabilizing effect of large pressure on stability strength of steady reacting solution measured according to Lyapunov. Nonlinear static restoring function evaluated for MTS, KTSS nonlinearized and KTSS linearized flames with $n = 3$ at standard conditions (Q_s=-158.2 cal/g, T_a = 300 K, adiabatic burning).

Tab. 9 Forcing laws used for computer simulated deradiation and depressurization transients.

Tab.10 Computer simulated go/no-go transient tests showing agreement with the predicted lower dynamic boundary and strong dependence of dynamic extinction on the initial conditions. All runs performed according to MTS flame for adiabatic opaque strands with T_a = 300 K and Q_s = -158.2 cal/g.

TABLE 1

Properties of solid composite propellant AP/PBAA No. 941 used as datum case in this study.

ASSUMED OR MEASURED PROPERTIES	
Endoth. crystal. transition heat, Q_{cr}	20 cal/g of AP
Endoth. AP vaporiz. heat, $Q_{v,AP}$	526 cal/g of AP
Exoth. AP decomposition heat, $Q_{A/PA}$	800 cal/g of AP
Endoth. binder vapor. heat, $Q_{v,B}$	225 cal/g of binder
AP content, p	80%
Ballistic exponent, n	0.46
KTSS pyrolysis law power, w	6.38
Surface activation energy, E_s	16000 cal/gmole
Flame activation energy, E_f	20000 cal/gmole
Condensed phase density, ρ_c	1.54 g/cm^3
Condensed phase specific heat, C_c	0.33 cal/g-K
Condensed phase thermal diffusivity α_c	1.4×10^{-3} cm^2/s
Gas phase specific heat, C_g	0.33 cal/g-K
Gas phase thermal conducivity, λ_g	1×10^{-4} cal/cm-K-s
Average products molecular weight, $\overline{m}$	26 g/gmole
Reflectivity of propellant surface, r	0 %
Optical absorption coefficient, a	∞ cm^{-1}
Minimum surface temp. for reactions, T_m	300 K
Matching surface temp. for pyrolysis, T_k	405 K
EVALUATED PROPERTIES	
Cond. phase thermal conductivity, λ_c	7.12×10^{-4} cal/cm-K-s
Refer. frequency factor, $A_{s,ref}$	2705 cm/s
Surface gasification heat, Q_s	-158.2 cal/g (+endoth.)
Chemical time constant, A_M	0.338
Diffusion time costant, B_M	2.350
REFERENCE PROPERTIES	
Pressure, P_{ref}	68 atm
Temperature, T_{ref}	300 K
Burning Rate, $R_{ref} = R\ (P_{ref})$	0.837 cm/s
Surface temperature, $T_{s,ref} = T_s(P_{ref})$	1000 K
Flame temperature, $T_{f,ref}$	2430 K
Distance, $x_{ref} = \alpha_c / R_{ref}$	1.673×10^{-3} cm
Time, $t_{ref} = \alpha_c / R_{ref}$	1.998×10^{-3} s
Heat, $Q_{ref} = C_c (T_{s,ref} - T_{ref})$	231 cal/g
Energy flux, $I_{ref} = \rho_c c_c R_{ref} (T_{s,ref} - T_{ref})$	297.8 cal/cm^2 - s

TABLE 2

Q_s, cal/g	P=10 atm	P=20 atm	P=30 atm	P=40 atm	P=50 atm	P=60 atm
-120	0.823	0.875	0.906	0.927	0.943	0.956
-140	0.839	0.890	0.921	0.941	0.957	0.969
-158.2	0.860	0.909	0.937	0.957	0.972	0.984
-170	0.876	0.922	0.949	0.969	0.984	0.996
-180	0.891	0.935	0.962	0.980	0.995	1.013
-200	0.932	0.969	0.992	1.009	1.022	1.033
-220	0.986	1.014	1.032	1.047	1.061	1.066

TABLE 3

P, atm	$A(\theta_s)$	$A(\mathfrak{R})$	n=2		n=2.5		n=3	
			$B(\theta_s)$	$B(\mathfrak{R})$	$B(\theta_s)$	$B(\mathfrak{R})$	$B(\theta_s)$	$B(\mathfrak{R})$
10	0.860	0.415	0.667	0.084	0.643	0.066	0.618	0.052
20	0.909	0.575	0.691	0.107	0.670	0.088	0.646	0.070
30	0.937	0.687	0.709	0.126	0.684	0.101	0.663	0.083
40	0.957	0.775	0.719	0.138	0.698	0.115	0.674	0.093
50	0.972	0.849	0.729	0.151	0.704	0.121	0.684	0.101
60	0.984	0.913	0.737	0.161	0.712	0.130	0.692	0.108

TABLE 4

	surface heat release, Q_s, cal/g	Nondimensional surface temperature, θ_s root B (lower dynamic stability)	root A	root D (upper dynamic stability)	root E
steady burning	-150	0.66	0.929	=	=
	-155	0.66	0.934	=	=
	-158.2	0.67	0.937	=	=
	-165	0.67	0.944	=	=
	-170	0.68	0.949	1.14	1.29
	-175	0.68	0.955	1.08	1.38
	-180	0.69	0.962	1.04	1.43
	-185	0.69	0.968	1.00	1.48
self-sustained oscillations	-190	0.70	0.976	0.976	1.53
	-195	0.71	0.984	0.96	1.57
	-200	0.72	0.992	0.94	1.61
	-205	0.73	1.001	0.92	1.64
	-210	0.75	1.011	0.90	1.68
	-215	0.76	1.021	0.88	1.71
	-220	0.78	1.032	0.86	1.75
extinction	-225	=	1.044	=	1.78
	-230	=	1.057	=	1.81

TABLE 5

P, atm	Surface Heat Release Q_s, cal/g	
	A-D coalescence	B-D coalescence
10	-168	-197
20	-182	-212
30	-190	-225
40	-195	-230
50	-200	-235
60	-205	-240

TABLE 6

P,atm	$\dot{q}_{\ell}$, cal/cm^2-s	$\dot{q}_{g,s}$	θ_s	$\mathcal{R}$
10	-40.5	1.40×10^{-1}	7.12×10^{-1}	1.30×10^{-1}
20	-65.0	2.36×10^{-1}	7.69×10^{-1}	2.10×10^{-1}
30	-85.0	3.14×10^{-1}	7.91×10^{-1}	2.60×10^{-1}
40	-101.5	3.80×10^{-1}	8.15×10^{-1}	3.00×10^{-1}
50	-116.0	4.36×10^{-1}	8.23×10^{-1}	3.20×10^{-1}
60	-129.5	4.91×10^{-1}	8.40×10^{-1}	3.60×10^{-1}

TABLE 7

P, atm	$\dot{q}_\ell$, cal/cm^2-s	θ_s	$\mathcal{R}$
10	-38	0.747	0.175
20	-62	0.793	0.255
30	-82	0.817	0.305
40	-98	0.837	0.354
50	-112	0.853	0.396
60	-126	0.863	0.423

TABLE 8a

I_o, cal/cm^2-s (x)	Q_s, cal/g	$(df/d\Theta_s)_{\bar{\Theta}_{i,s}}$
0	-158.2	-3.53
10	-158.2	-3.89
20	-158.2	-4.03
30	-158.2	-4.27
40	-158.2	-4.50
60	-158.2	-5.18
80	-158.2	-6.01
-10	-158.2	-3.33
-20	-158.2	-3.14
-30	-158.2	-2.78
-40	-158.2	-2.33
-50	-158.2	-1.85
-60	-158.2	-1.50
-70	-158.2	-1.35
-80	-158.2	-0.52
0	-110	-0.71
0	-120	-2.10
0	-130	-3.02
0	-140	-3.59
0	-150	-3.74
0	-160	-3.51
0	-170	-2.86
0	-180	-1.74
0	-190	0
0	-200	2.41
0	-210	5.85
0	-220	10.60

(x) negative values represent heat loss from the burning surface.

TABLE 8b

P,atm	$(df/d\theta_s)_{\bar{\theta}_{i,s}}$		
	MTS	KTSS NONLIN.	KTSS LIN.
10	-0.54	-0.74	-0.73
20	-2.10	-2.29	-2.27
30	-3.53	-3.86	-3.79
40	-4.92	-5.40	-5.24
50	-6.02	-6.90	-6.63
60	-7.26	-8.37	-7.96

TABLE 9

Linear deradiation	$F(\tau) = (1-r)\ (F_i - B_r \cdot \tau)$
Bilinear deradiation	$F(\tau) = (1-r)\ (F_i - B_{r,1}\ \tau) \quad F_i \geq F(\tau) \geq F_m$ $F(\tau) = (1-r)\ (F_m - B_{r,2}\ \tau) \quad F_m \geq F(\tau) \geq F_f$
Parabolic deradiation	$F(\tau) = (1-r)\ (F_i - B_r\ \tau^2)$
Exponential deradiation	$F(\tau) = (F_i - (F_i - F_f)\ (1-\exp(B_r \tau)))\ (1-r)$
Exponential depressurization	$\mathcal{P}(\tau) = \mathcal{P}_i - (\mathcal{P}_i - \mathcal{P}_f)\ (1-\exp(B_p\ \tau))$

TABLE 10

(*) P,atm	Forcing Law	B_p	B_r	Observed dynamic limit		(n=3) Predicted dynamic limit	
				$\mathcal{R}$	θ_s	$\mathcal{R}$	θ_s
10	linear deradiation	0	100	0.058	0.627	0.052	0.618
10	bilinear derad.	0	100 and 20	0.057	0.626	0.052	0.618
10	parabolic derad.	0	640	0.056	0.625	0.052	0.618
10	exponential derad.	0	5	0.058	0.627	0.052	0.618
10	exponential derad.	0	10	0.054	0.621	0.052	0.618
20	exponential derad.	0	10	0.072	0.649	0.071	0.647
30	exponential derad.	0	10	0.102	0.685	0.083	0.663
40	exponential derad.	0	10	0.123	0.706	0.093	0.674
10	exponential depress.	10	0	0.051	0.615	0.052	0.618
10	exponential depress.	3.336	0	0.054	0.621	0.052	0.618

(*) final pressure in the case of depressurization transients.

LIST OF FIGURES

Fig. 15b - Coalescence of A-D roots at Q_s = -190 cal/g; the steady reacting mode is stationary for $|Q_s| < 190$ cal/g and self-sustained oscillating for $|Q_s| > 190$ cal/g. (MTS flame, n = 3). See Fig. 24.

Fig. 16 - Negligible influence of ambient temperature on nonlinear static restoring function (for the indicated range of values). (MTS flame, n = 3).

Fig. 17 - Stabilizing effect of pressure on both reacting modes. (KTSS nonlinearized flame, n = 3).

Fig. 18 - Effect of surface heat release on static restoring function according to KTSS nonlinearized flame (n = 3).

Fig. 19 - KTSS linearized flame (n = 3) applying for surface temperatures near or above the steady reacting value.

Fig. 20 - Compared static restoring functions (n = 3) for MTS, KTSS nonlinearized and KTSS linearized flames.

Fig. 21 - Effect of the approximating polynomial order on the static restoring function at 20 atm of pressure (MTS flame).

Fig. 22 - Effect of the approximating polynomial order on the static restoring function at 30 atm of pressure (MTS flame).

Fig. 23 - Effect of the approximating polynomial order on the static restoring function at 40 atm of pressure (MTS flame).

Fig. 24 - Computer simulated pressurization tests confirming the existence of three possible static regimes (stationary for Q_s = -180 cal/g, self-sustained oscillating for $Q_s = \pm$ 200 cal/g, extinguished for Q_s = - 220 cal/g). Cf. Tab. 4.

Fig. 25 - Static instability of burning propellants for large surface heat release.

Fig. 26 - Approximate construction of the static stability boundary and its meaning (MTS flame).

Fig. 27 - Rigorous construction of the static stability boundary for Q_s = - 120 cal/g (MTS flame).

Fig. 28 - Rigorous construction of the static stability boundary for Q_s = - 158. 2 cal/g (MTS flame).

Fig. 29 - Rigorous construction of the static stability boundary for Q_s = - 200 cal/g (MTS flame).

Fig. 30 - Evaluating the static stability limit through the static restoring function at 20 atm of pressure (MTS flame, n = 3).

Fig. 31 - Evaluating the static stability limit through the static restoring function at 30 atm of pressure (MTS flame, n = 3).

Fig. 32 - Evaluating the static stability limit through the static restoring function at 40 atm of pressure (MTS flame, n = 3).

Fig. 33a - Representative time histories of burning rate during deradiation showing possible occurence of dynamic extinction.

Fig. 33b - Corresponding trajectories in burning rate vs heat feedback plane.

Fig. 33c - Nomenclature used for deradiation transients.

Fig. 33d - Nature of nonautonomous function considered in this study.

Fig. 34 - The range of possible unstable equilibrium points in dynamic burning regime is limited by the no-return point M (the unstable root associated to the static restoring function for $\tau \to \infty$).

Fig. 35 - Static and dynamic stability boundaries on a burning rate vs heat feedback plot (MTS flame).

Fig. 36 - Static and dynamic (MTS flame, n = 3) stability boundaries on a burning rate is pressure plot.

Fig. 37 - Go/no-go computed deradiation tests showing occurrence of dynamic extinction ($B_r = 5$).

Fig. 38 - Go/no-go computed deradiation tests showing occurrence of dynamic extinction ($B_r = 10$).

Fig. 39 - Dynamic extinction following linear deradiation.

Fig. 40 - Dynamic extinction following bilinear deradiation.

Fig. 41 - Dynamic extinction following parabolic deradiation.

Fig. 42 - Dynamic extinction following exponential deradiation at 10 atm of pressure.

Fig. 43 - Dynamic extinction following exponential deradiation at 20 atm of pressure.

Fig. 44 - Dynamic extinction following exponential deradiation at 30 atm of pressure.

Fig. 45 - Dynamic extinction following exponential deradiation at 40 atm of pressure.

Fig. 46 - Dynamic extinction following exponential depressurization from a parametically changed initial pressure.

Fig. 47 - Dynamic extinction following exponential depressurization with a parametrically changed depressurization rate.

Fig. 48a - Sketch of the shock tube apparatus.

Fig. 48b - Sketch of the shock tube test section.

Fig. 49 - Static pressure deflagration limits of the composite propellant as measured in the shock tube test section.

Fig. 50 - Composite propellant tested in the shock tube. Ignition at 1 atm of nitrogen. Upper trace : pressure (10 atm/div), lower trace : emitted radiation (relative intensity). Time scale : 5 ms/div.

Fig. 51 - See above. Time scale: 1 ms/div.

Fig. 52 - Noncatalyzed DB tested in the piston tube. Ignition at 0.50 atm of air. Upper trace : pressure (20 atm/div), lower trace : emitted radiation (relative intensity). Time scale : 5 ms/div.

Fig. 53 - See above. Time scale : 50 ms/div.

Fig. 54 - Noncatalyzed DB tested in the piston tube. Ignition at 0.75 atm of air. Upper trace : pressure (20 atm/div), lower trace: emitted radiation (relative intensity). Time scale : 5 ms/div.

Fig. 55 - See above. Time scale : 50 ms/div.

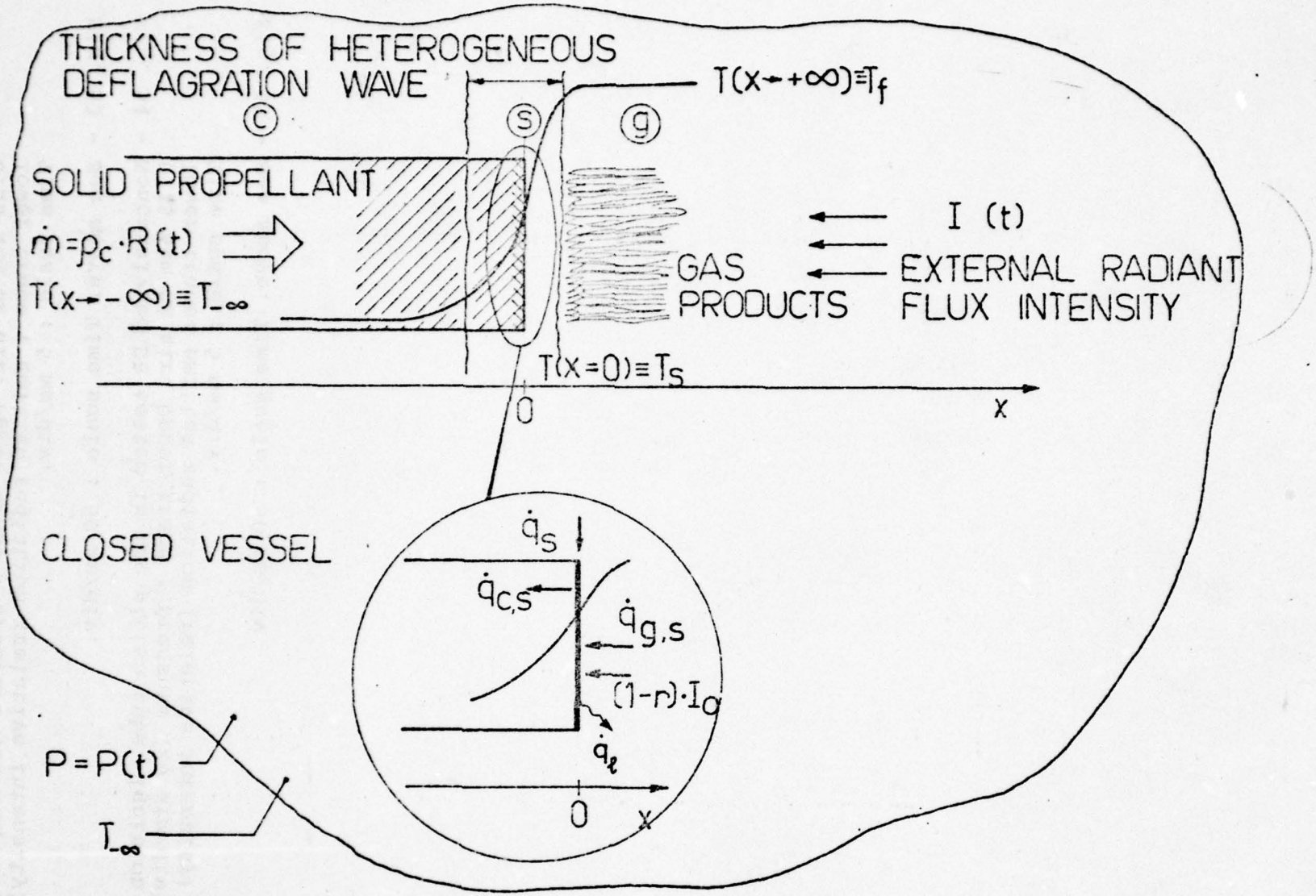
THICKNESS OF HETEROGENEOUS
DEFLAGRATION WAVE
T(x→+∞)≡Tf
c
s
g
SOLID PROPELLANT
ṁ=ρc·R(t)
T(x→-∞)≡T∞
I (t)
GAS
PRODUCTS
EXTERNAL RADIANT
FLUX INTENSITY
T(x=0)≡Ts
0
x
CLOSED VESSEL
q̇s
q̇c,s
q̇g,s
(1-r)·I0
q̇ℓ
0
x
P=P(t)
T∞

FIG. 1

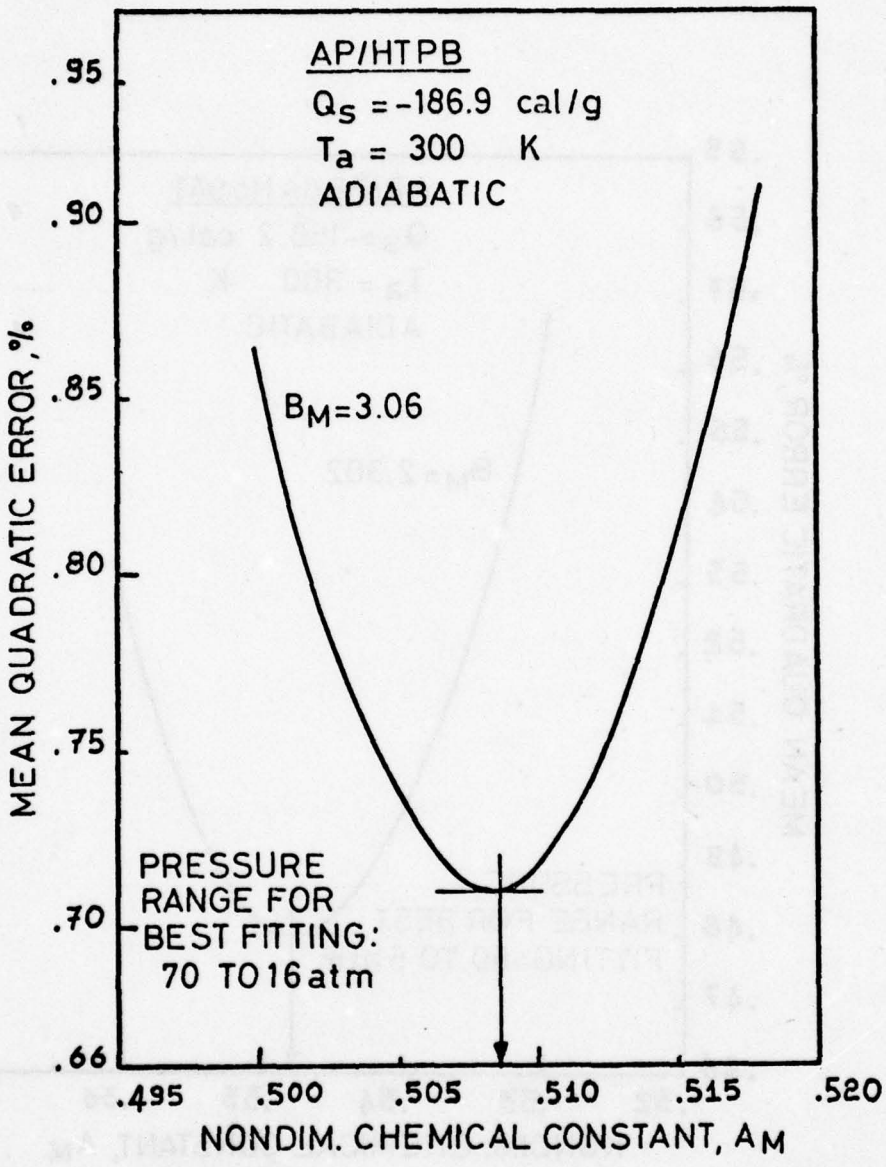
AP/HTPB
Q_S = -186.9 cal/g
T_a = 300 K
ADIABATIC
B_M=3.06
PRESSURE
RANGE FOR
BEST FITTING:
70 TO 16 atm
MEAN QUADRATIC ERROR, %
.95
.90
.85
.80
.75
.70
.66
.495
.500
.505
.510
.515
.520
NONDIM. CHEMICAL CONSTANT, A_M

FIG. 2a

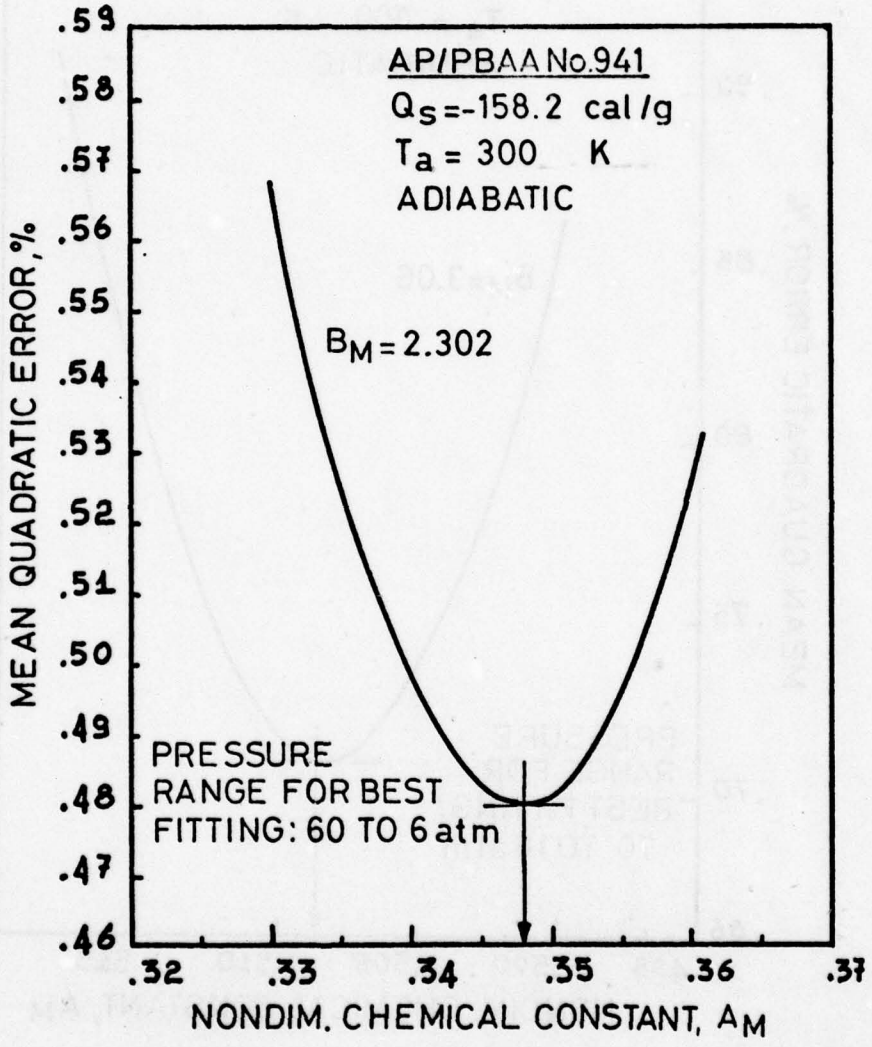
AP/PBAA No.941
Q_S = -158.2 cal/g
T_a = 300 K
ADIABATIC
B_M = 2.302
PRESSURE
RANGE FOR BEST
FITTING: 60 TO 6 atm
MEAN QUADRATIC ERROR, %
.59
.58
.57
.56
.55
.54
.53
.52
.51
.50
.49
.48
.47
.46
.32
.33
.34
.35
.36
.37
NONDIM. CHEMICAL CONSTANT, A_M

FIG. 2b

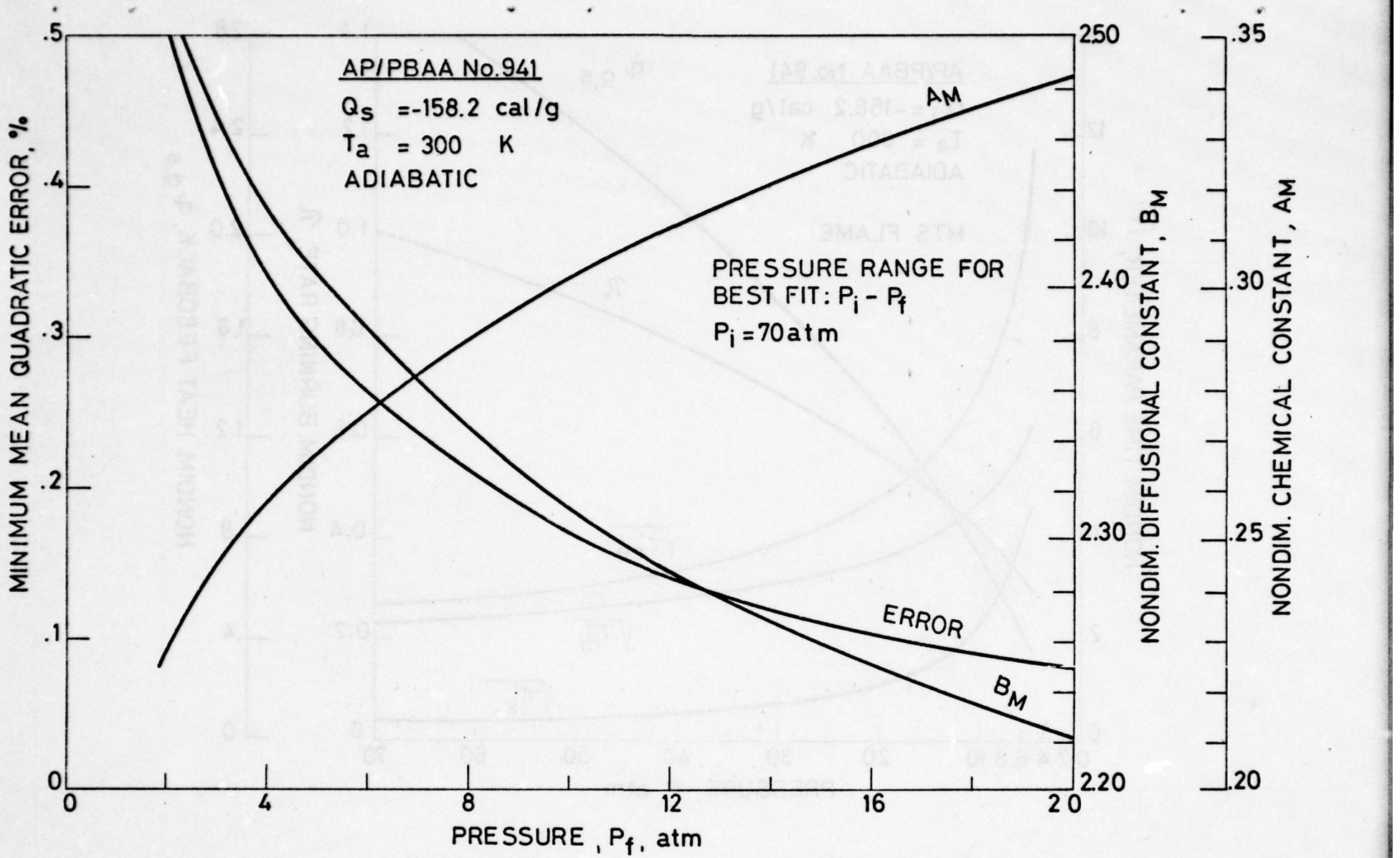
AP/PBAA No.941
Q_s =-158.2 cal/g
T_a = 300 K
ADIABATIC
PRESSURE RANGE FOR BEST FIT: P_i - P_f
P_i = 70 atm
AM
ERROR
B_M
MINIMUM MEAN QUADRATIC ERROR, %
NONDIM. DIFFUSIONAL CONSTANT, B_M
NONDIM. CHEMICAL CONSTANT, A_M
PRESSURE, P_f, atm
0
.1
.2
.3
.4
.5
4
8
12
16
20
2.20
2.30
2.40
2.50
.20
.25
.30
.35

FIG. 3

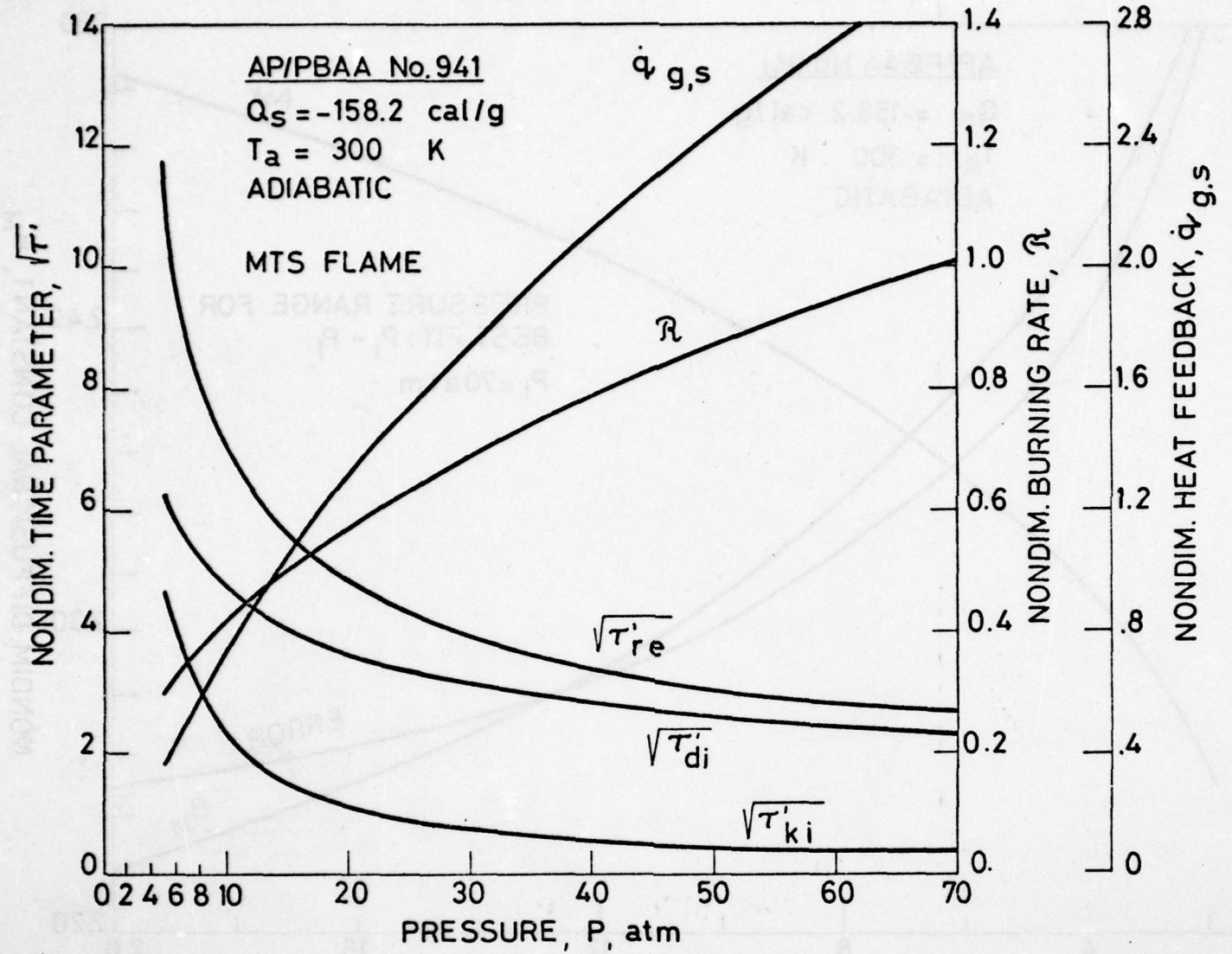
AP/PBAA No. 941
Q_s = -158.2 cal/g
T_a = 300 K
ADIABATIC
MTS FLAME
$\dot{q}_{g,s}$
$\mathcal{R}$
$\sqrt{\tau'_{re}}$
$\sqrt{\tau'_{di}}$
$\sqrt{\tau'_{ki}}$
NONDIM. TIME PARAMETER, $\sqrt{\tau'}$
NONDIM. BURNING RATE, $\mathcal{R}$
NONDIM. HEAT FEEDBACK, $\dot{q}_{g,s}$
PRESSURE, P, atm
0 2 4 6 8 10 20 30 40 50 60 70
0 2 4 6 8 10 12 14
0 0.2 0.4 0.6 0.8 1.0 1.2 1.4
0 .4 .8 1.2 1.6 2.0 2.4 2.8

FIG. 4

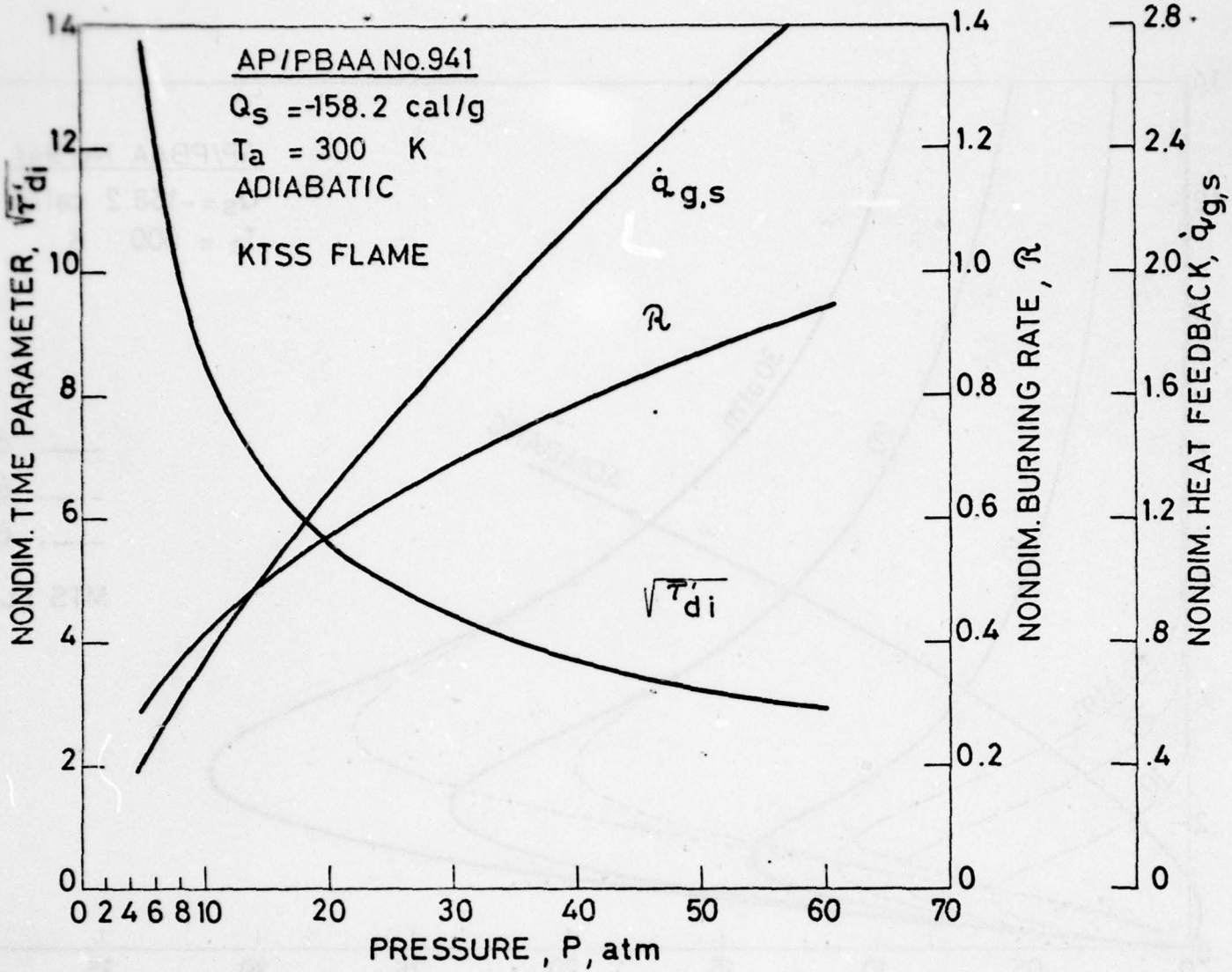
AP/PBAA No.941
Q_s = -158.2 cal/g
T_a = 300 K
ADIABATIC
KTSS FLAME
$\dot{q}_{g,s}$
$\mathcal{R}$
$\sqrt{\tau'_{di}}$
NONDIM. TIME PARAMETER, $\sqrt{\tau'_{di}}$
NONDIM. BURNING RATE, $\mathcal{R}$
NONDIM. HEAT FEEDBACK, $\dot{q}_{g,s}$
PRESSURE, P, atm
0 2 4 6 8 10 20 30 40 50 60 70
0 2 4 6 8 10 12 14
0 0.2 0.4 0.6 0.8 1.0 1.2 1.4
0 .4 .8 1.2 1.6 2.0 2.4 2.8

FIG. 5

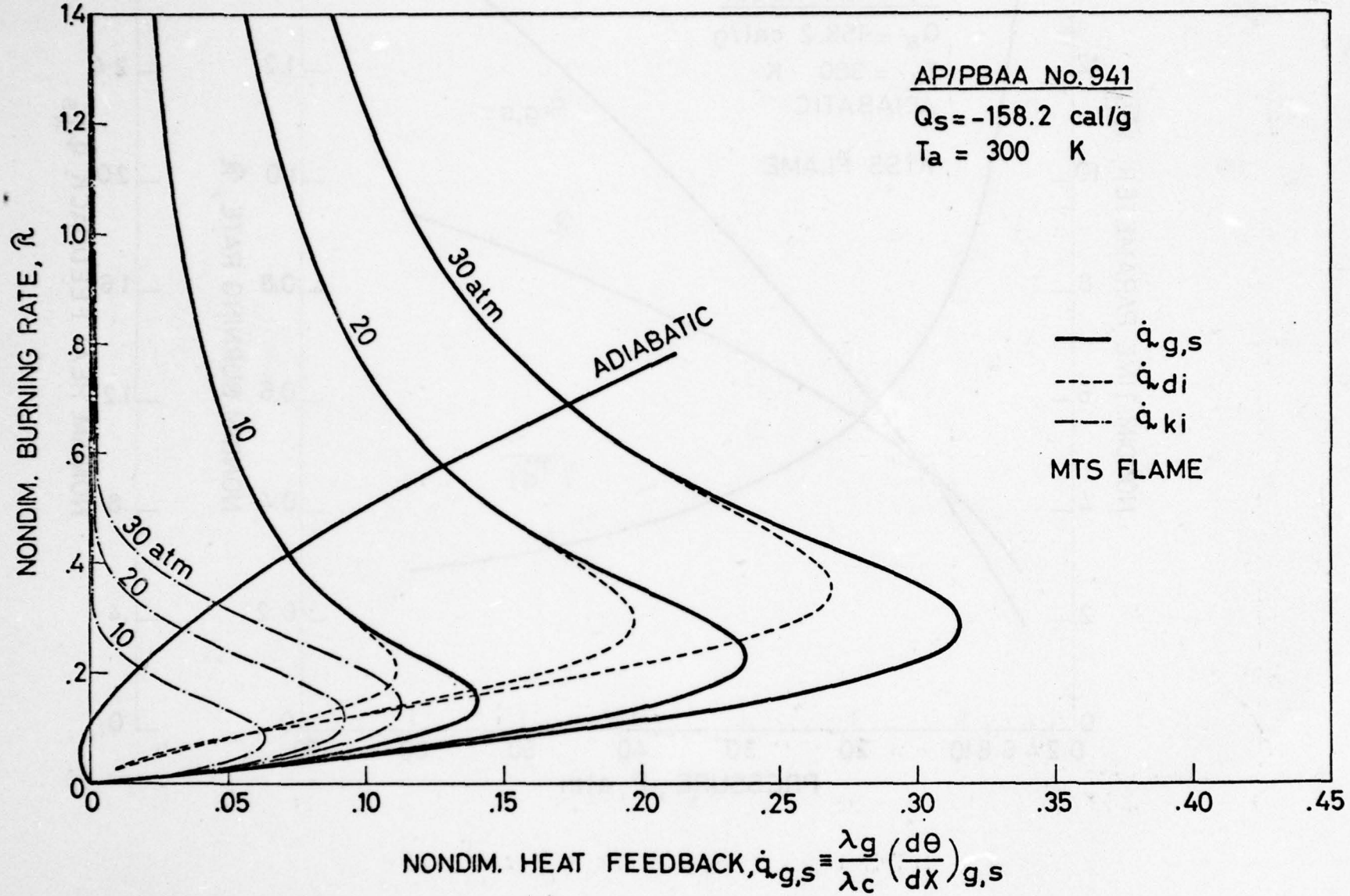
AP/PBAA No. 941
Q_s = -158.2 cal/g
T_a = 300 K
$\dot{q}_{g,s}$
$\dot{q}_{di}$
$\dot{q}_{ki}$
MTS FLAME
ADIABATIC
30 atm
20
10
30 atm
20
10
NONDIM. BURNING RATE, $\mathcal{R}$
NONDIM. HEAT FEEDBACK, $\dot{q}_{g,s} \equiv \frac{\lambda_g}{\lambda_c}\left(\frac{d\theta}{dX}\right)_{g,s}$
0
.2
.4
.6
.8
1.0
1.2
1.4
0
.05
.10
.15
.20
.25
.30
.35
.40
.45

FIG. 6

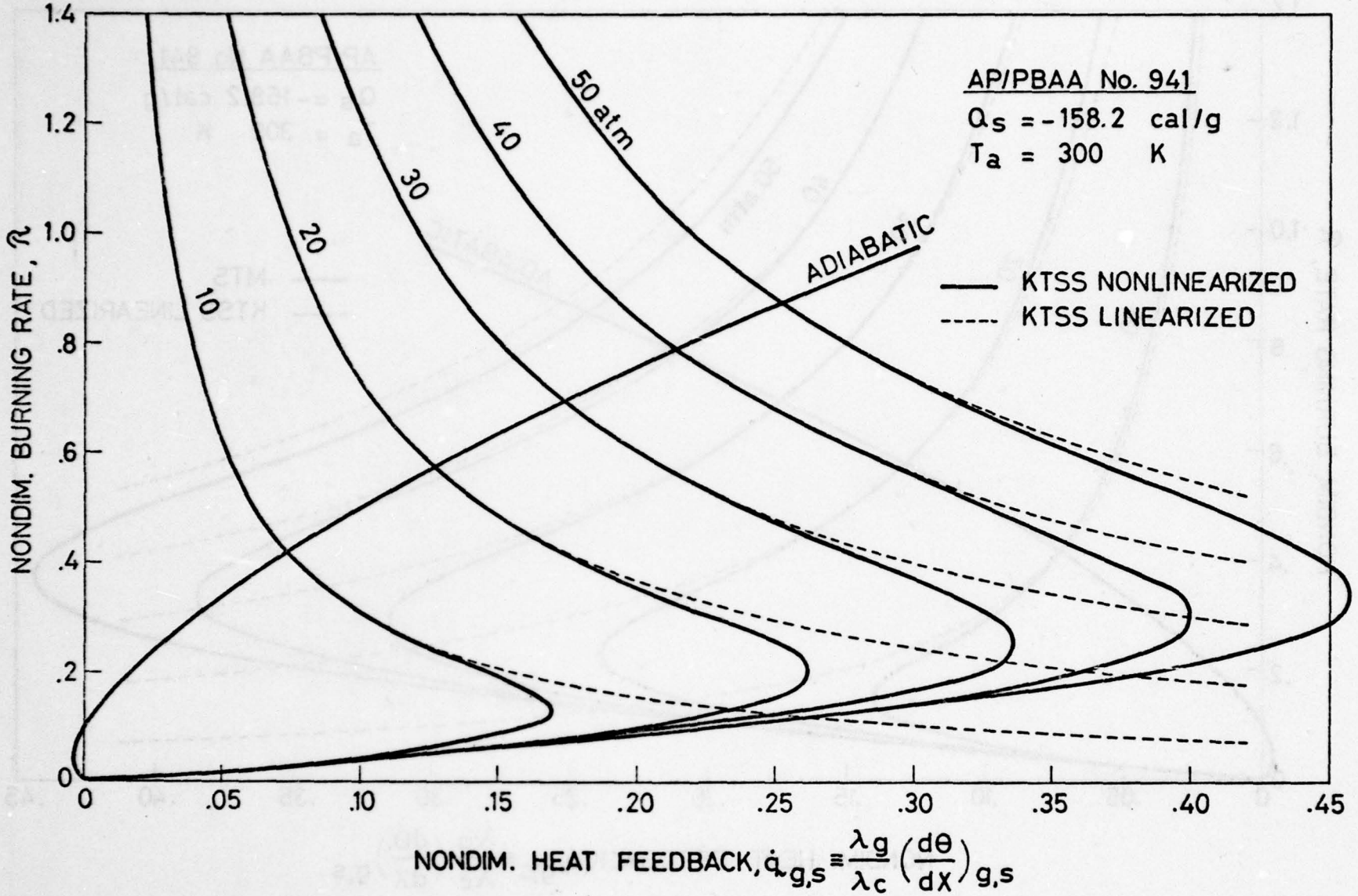
AP/PBAA No. 941
Q_s = -158.2 cal/g
T_a = 300 K
KTSS NONLINEARIZED
KTSS LINEARIZED
ADIABATIC
10
20
30
40
50 atm
NONDIM. BURNING RATE, $\dot{R}$
NONDIM. HEAT FEEDBACK, $\dot{q}_{g,s} \equiv \frac{\lambda_g}{\lambda_c}\left(\frac{d\theta}{dX}\right)_{g,s}$
0
.2
.4
.6
.8
1.0
1.2
1.4
0
.05
.10
.15
.20
.25
.30
.35
.40
.45

FIG. 7

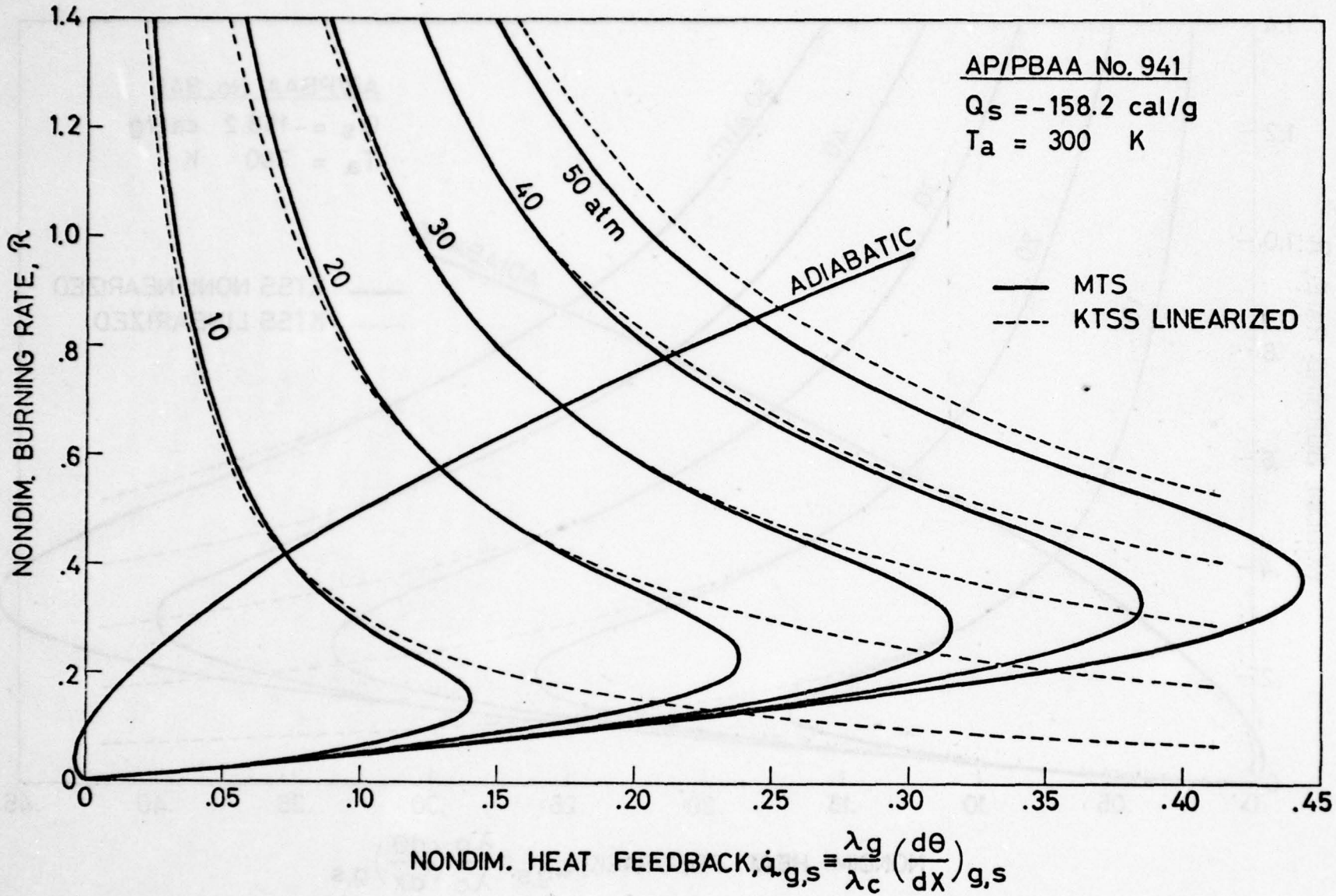
AP/PBAA No. 941
Q_s = -158.2 cal/g
T_a = 300 K
MTS
KTSS LINEARIZED
ADIABATIC
10
20
30
40
50 atm
NONDIM. BURNING RATE, R
NONDIM. HEAT FEEDBACK, $\dot{q}_{g,s} \equiv \frac{\lambda_g}{\lambda_c}\left(\frac{d\theta}{dX}\right)_{g,s}$
0
.2
.4
.6
.8
1.0
1.2
1.4
.05
.10
.15
.20
.25
.30
.35
.40
.45

FIG. 8

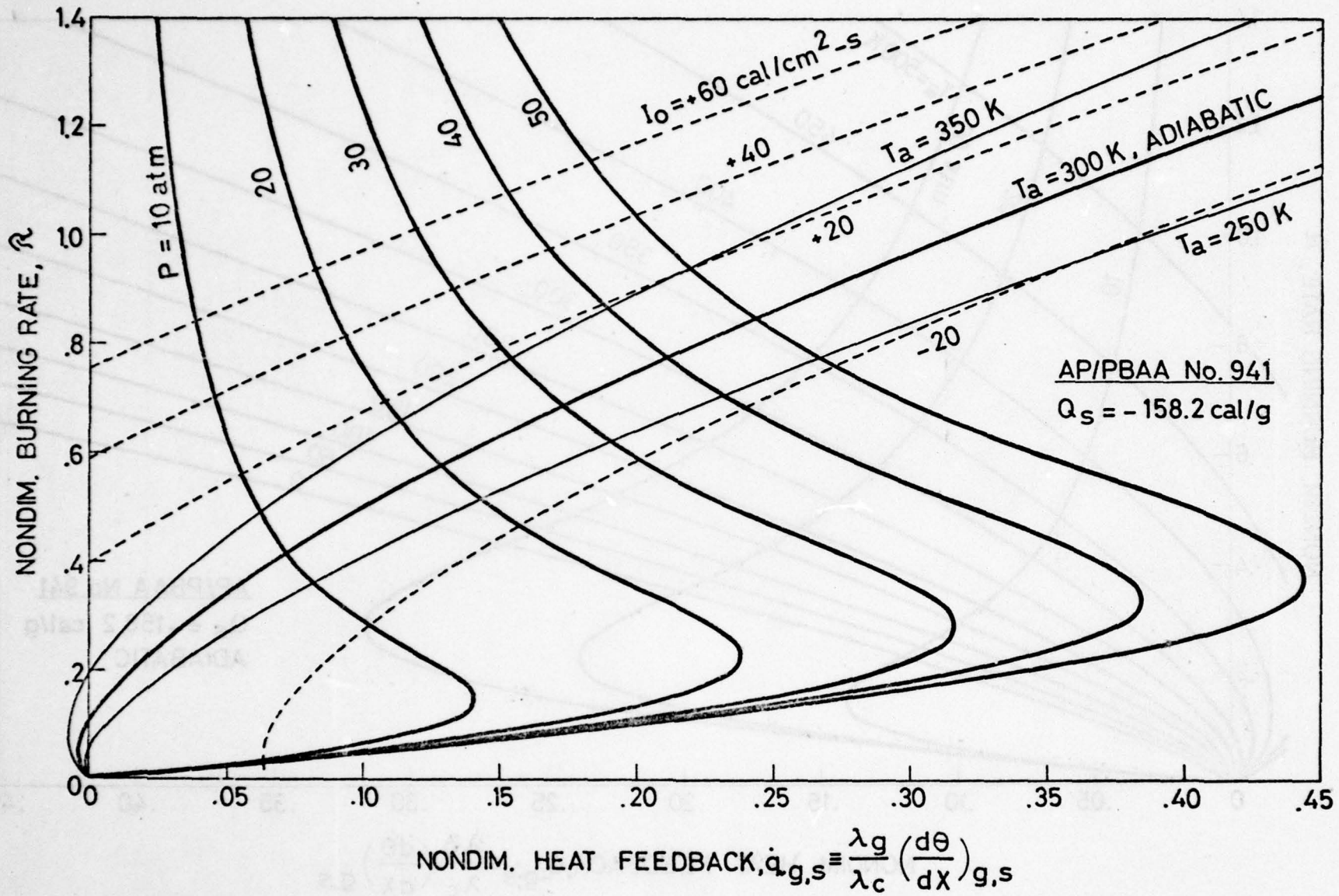
NONDIM. BURNING RATE, R
NONDIM. HEAT FEEDBACK, $\dot{q}_{g,s} \equiv \frac{\lambda_g}{\lambda_c}\left(\frac{d\theta}{dX}\right)_{g,s}$
P = 10 atm
20
30
40
50
I_o = +60 cal/cm^2-s
+40
+20
-20
Ta = 350 K
Ta = 300 K, ADIABATIC
Ta = 250 K
AP/PBAA No. 941
Q_s = - 158.2 cal/g
0
.2
.4
.6
.8
1.0
1.2
1.4
.05
.10
.15
.20
.25
.30
.35
.40
.45

FIG. 9

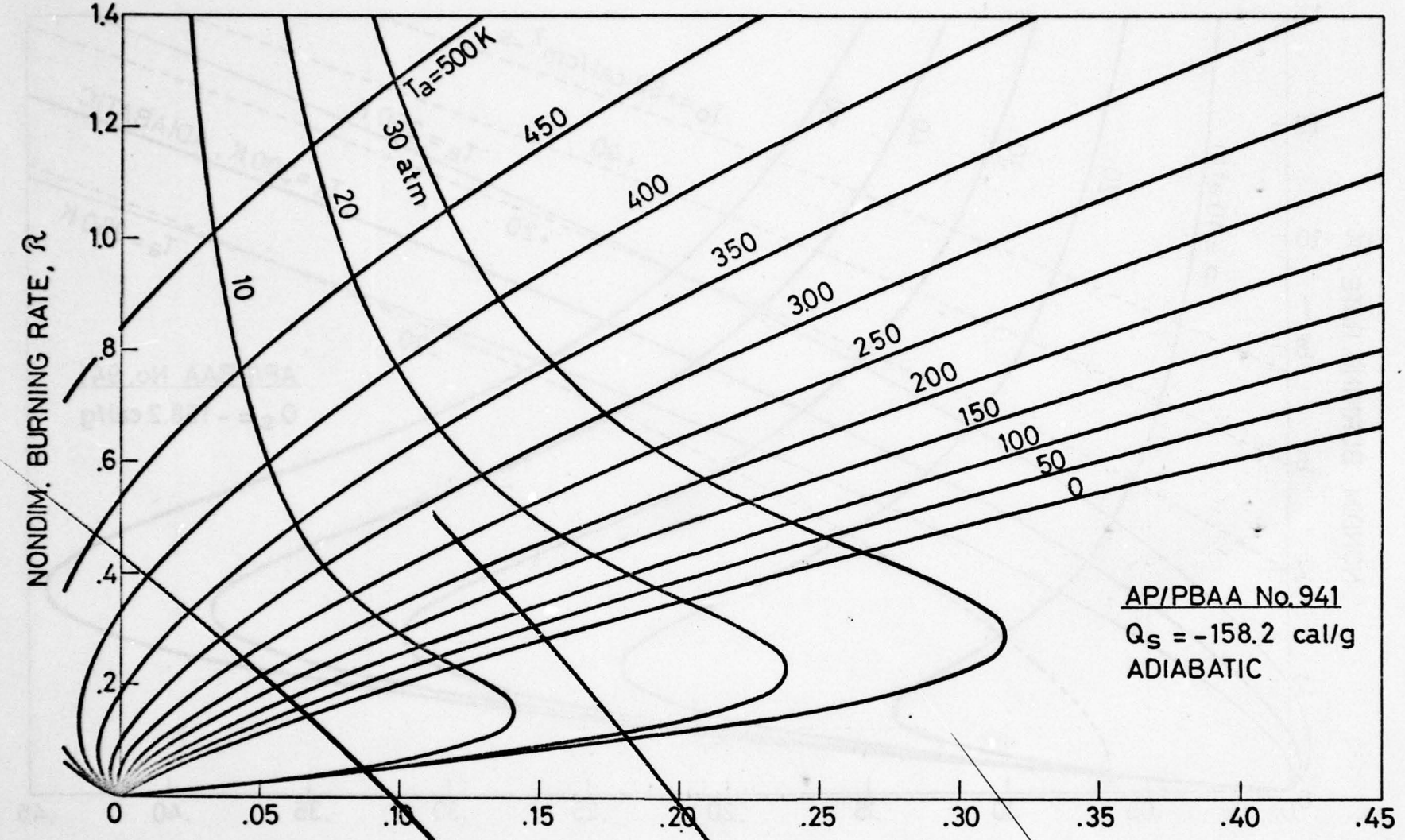
NONDIM. BURNING RATE, R
1.4
1.2
1.0
.8
.6
.4
.2
0
.05
.10
.15
.20
.25
.30
.35
.40
.45
Ta=500K
450
400
350
300
250
200
150
100
50
0
30 atm
20
10
AP/PBAA No. 941
Qs = -158.2 cal/g
ADIABATIC
NONDIM. HEAT FEEDBACK, $\dot{q}_{g,s} \equiv \frac{\lambda_g}{\lambda_c}\left(\frac{d\theta}{dX}\right)_{g,s}$

FIG. 10

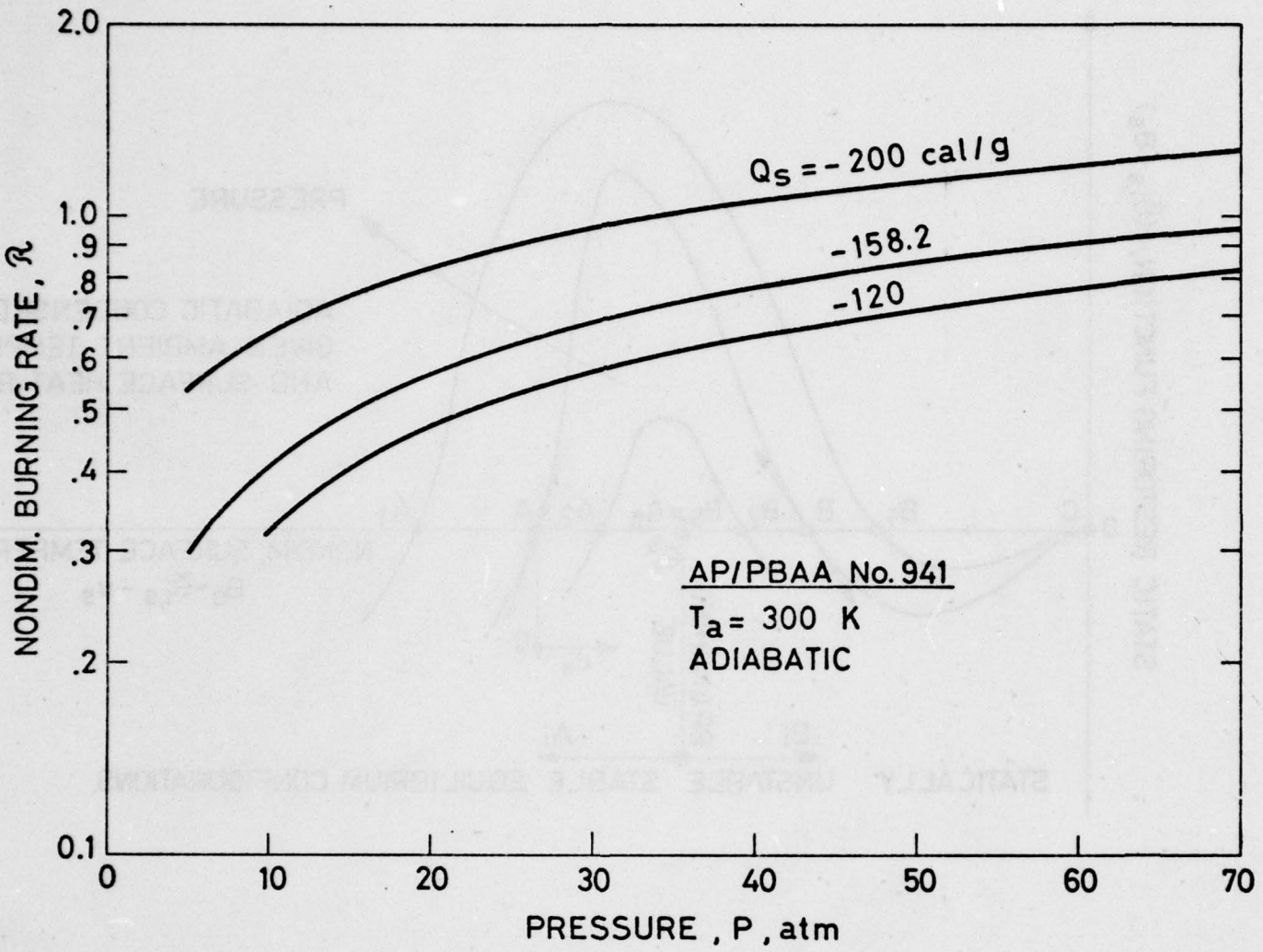
2.0
1.0
.9
.8
.7
.6
.5
.4
.3
.2
0.1
NONDIM. BURNING RATE, $\mathcal{R}$
Q_s = - 200 cal/g
-158.2
-120
AP/PBAA No. 941
T_a = 300 K
ADIABATIC
0
10
20
30
40
50
60
70
PRESSURE , P , atm

FIG. 11

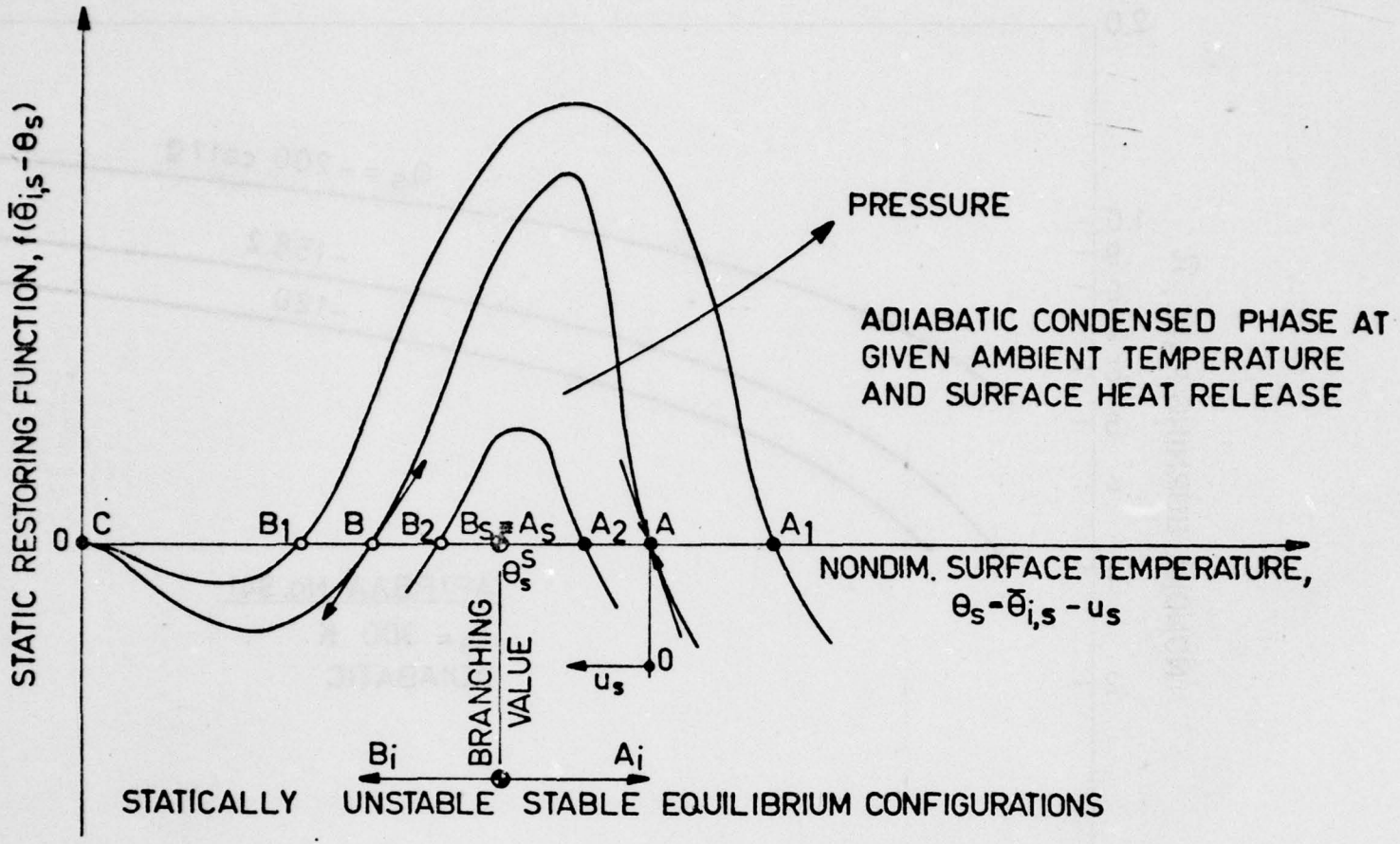
STATIC RESTORING FUNCTION, $f(\bar{\theta}_{i,s}-\theta_s)$
PRESSURE
ADIABATIC CONDENSED PHASE AT
GIVEN AMBIENT TEMPERATURE
AND SURFACE HEAT RELEASE
0
C
B_1
B
B_2
$B_S \equiv A_S$
A_2
A
A_1
θ_s^S
u_s
0
NONDIM. SURFACE TEMPERATURE,
$\theta_s-\bar{\theta}_{i,s}-u_s$
BRANCHING VALUE
B_i
A_i
STATICALLY UNSTABLE STABLE EQUILIBRIUM CONFIGURATIONS

FIG. 12a

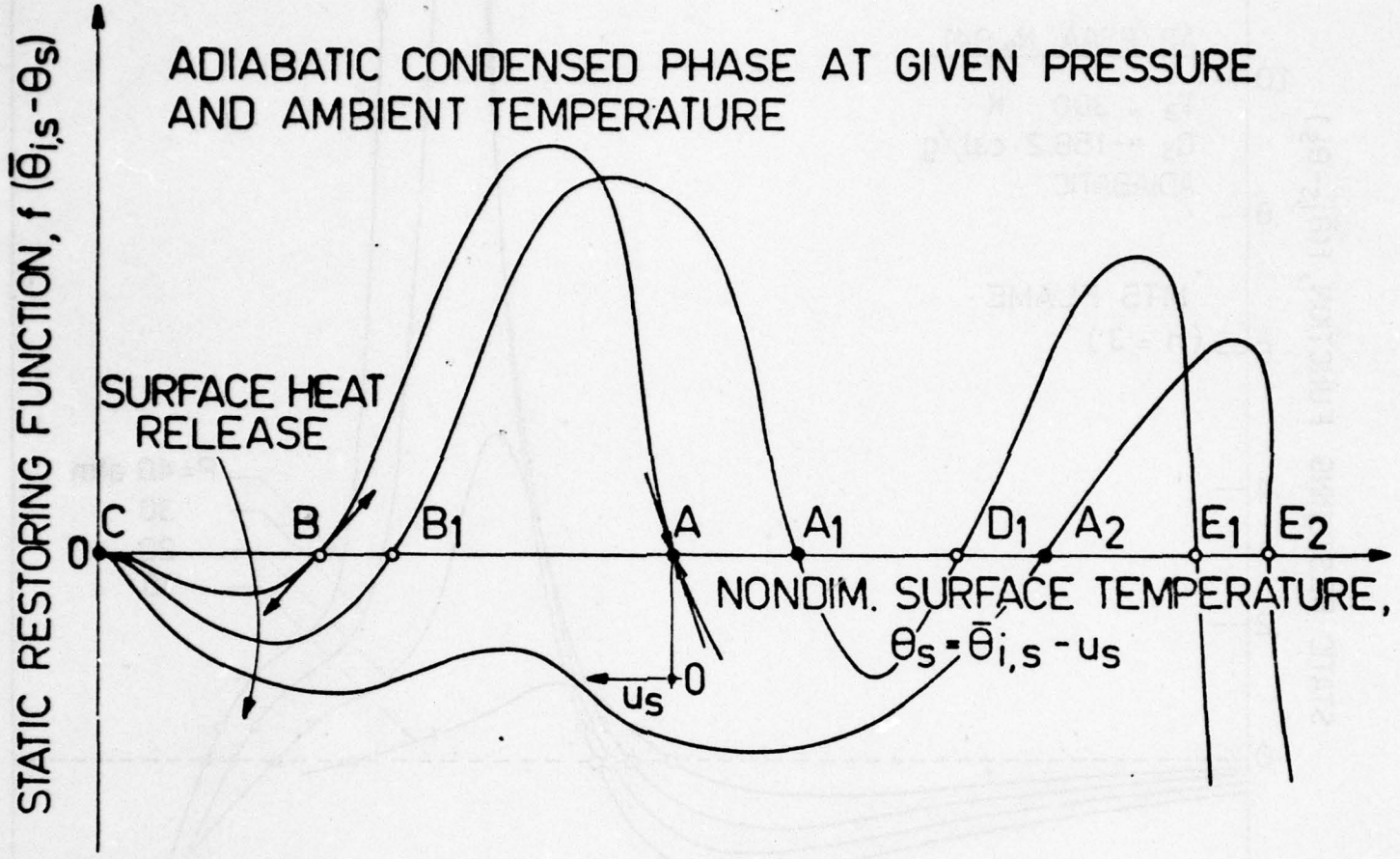
ADIABATIC CONDENSED PHASE AT GIVEN PRESSURE
AND AMBIENT TEMPERATURE
STATIC RESTORING FUNCTION, f $(\bar{\theta}_{i,s}-\theta_s)$
SURFACE HEAT
RELEASE
C
B
B_1
A
A_1
D_1
A_2
E_1
E_2
0
u_s
0
NONDIM. SURFACE TEMPERATURE,
$\theta_s = \bar{\theta}_{i,s} - u_s$

FIG. 12b

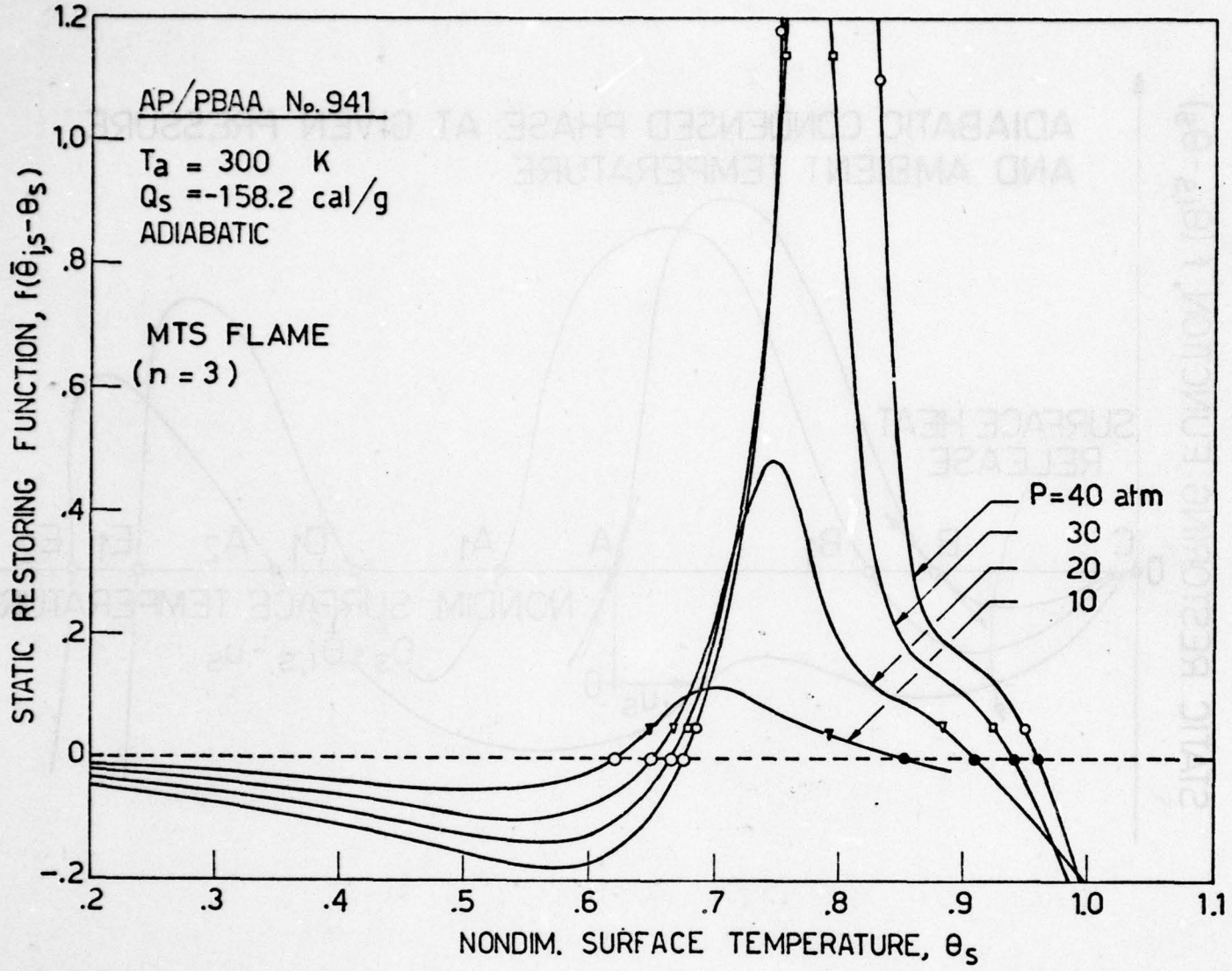
AP/PBAA No. 941
T_a = 300 K
Q_s =-158.2 cal/g
ADIABATIC
MTS FLAME
(n = 3)
P=40 atm
30
20
10
STATIC RESTORING FUNCTION, $f(\bar{\theta}_{i,s}-\theta_s)$
NONDIM. SURFACE TEMPERATURE, θ_s
1.2
1.0
.8
.6
.4
.2
0
-.2
.2
.3
.4
.5
.6
.7
.8
.9
1.0
1.1

FIG. 13

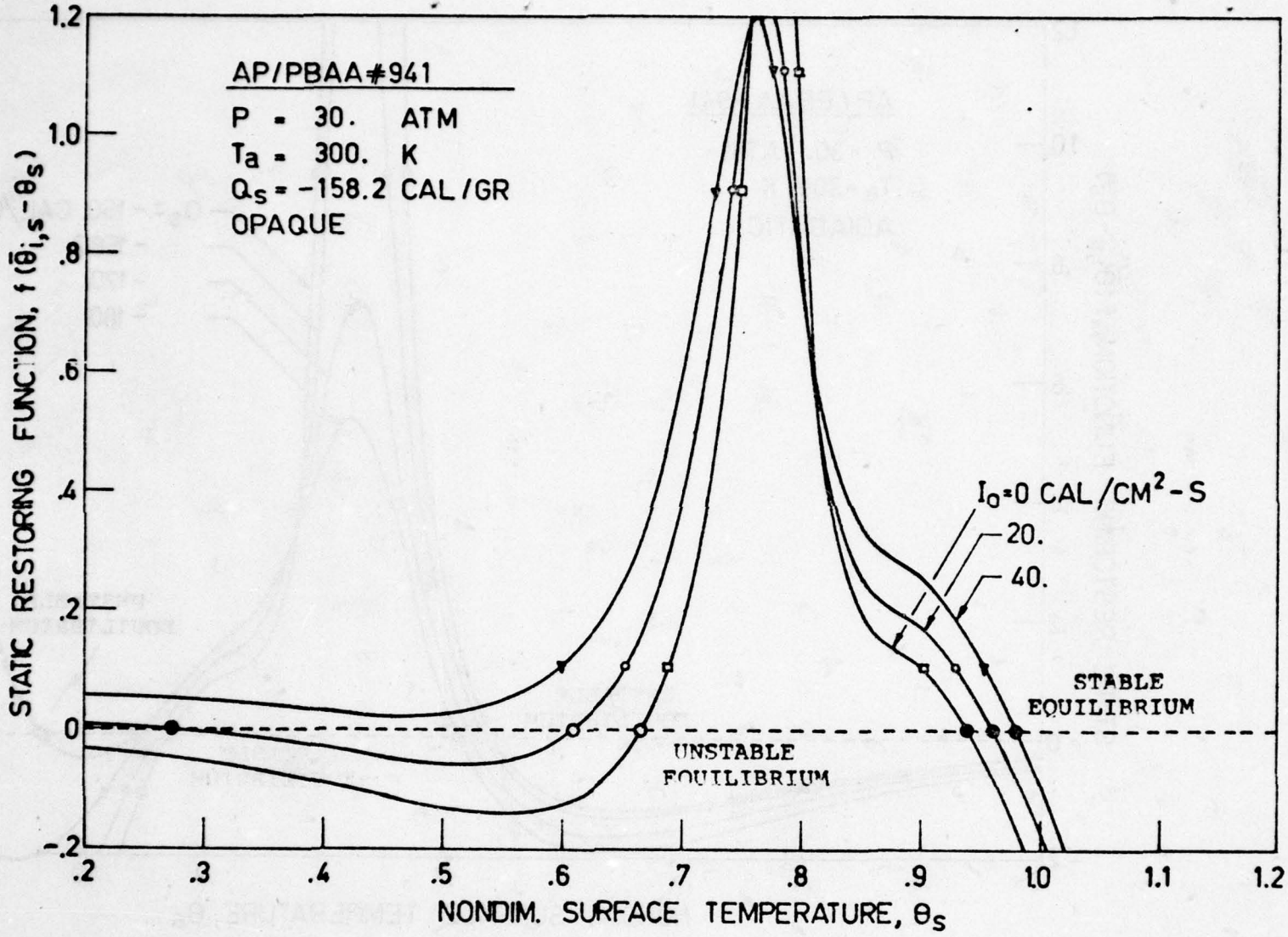
AP/PBAA#941
P = 30. ATM
Ta = 300. K
Qs = -158.2 CAL/GR
OPAQUE
STATIC RESTORING FUNCTION, f(θ̄i,s - θs)
NONDIM. SURFACE TEMPERATURE, θs
Io=0 CAL/CM2-S
20.
40.
STABLE EQUILIBRIUM
UNSTABLE EQUILIBRIUM
1.2
1.0
.8
.6
.4
.2
0
-.2
.2
.3
.4
.5
.6
.7
.8
.9
1.0
1.1
1.2

FIG. 14

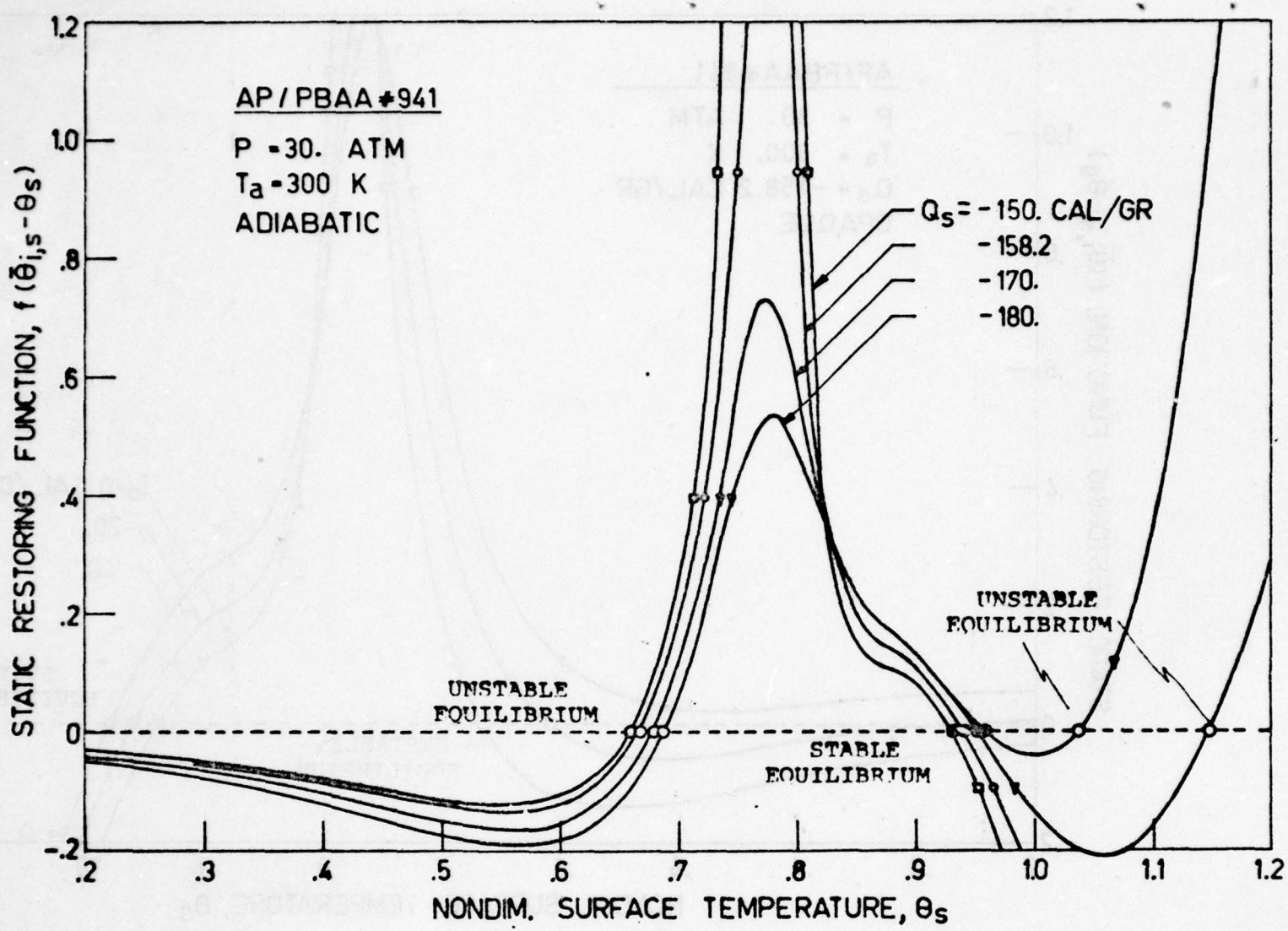
AP / PBAA #941
P = 30. ATM
T_a = 300 K
ADIABATIC
Q_s = - 150. CAL/GR
- 158.2
- 170.
- 180.
UNSTABLE EQUILIBRIUM
STABLE EQUILIBRIUM
UNSTABLE EQUILIBRIUM
STATIC RESTORING FUNCTION, $f(\theta_{i,s}-\theta_s)$
NONDIM. SURFACE TEMPERATURE, θ_s
1.2
1.0
.8
.6
.4
.2
0
-.2
.2
.3
.4
.5
.6
.7
.8
.9
1.0
1.1
1.2

FIG. 15a

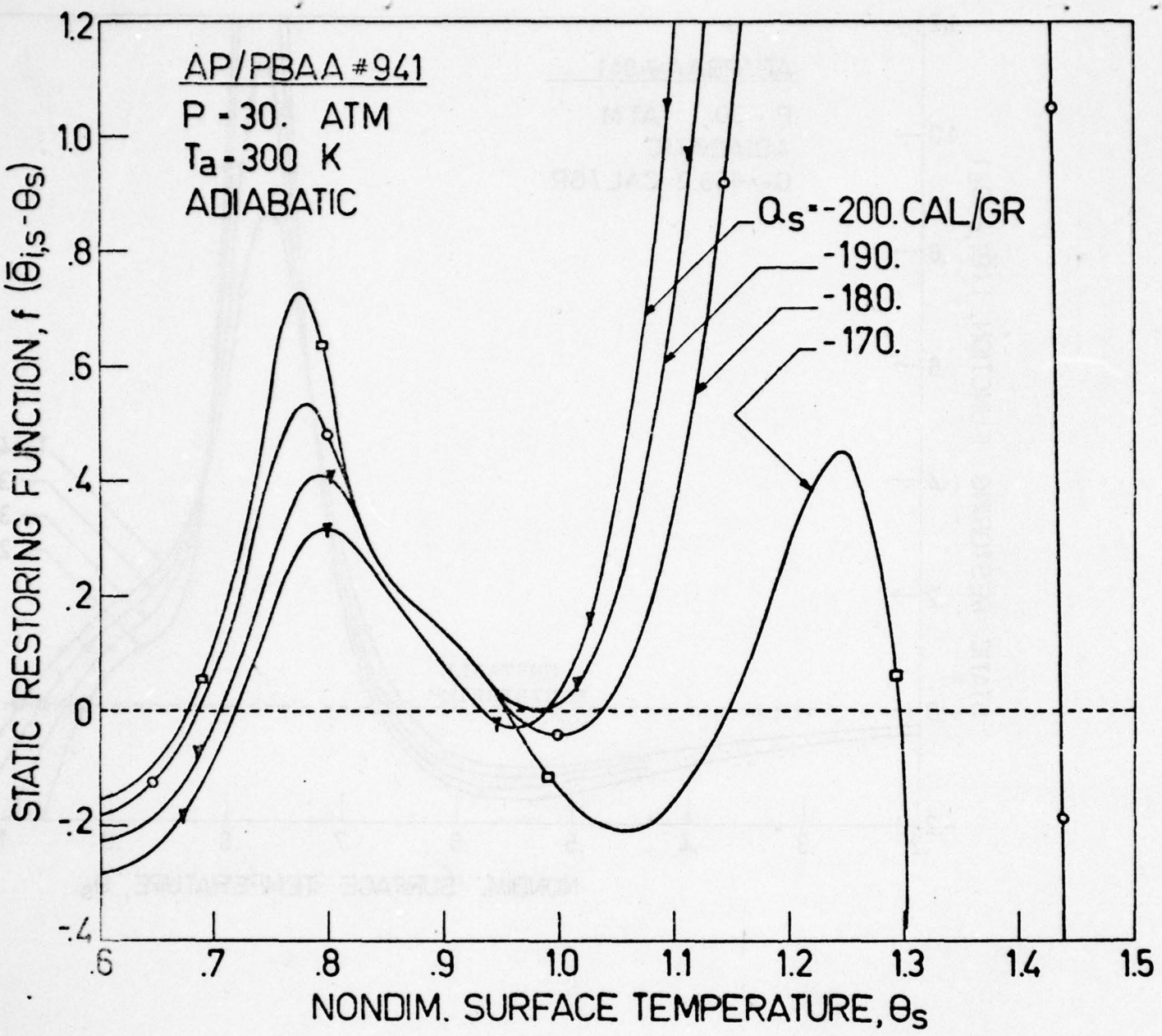
AP/PBAA #941
P - 30. ATM
Ta - 300 K
ADIABATIC
Qs = -200. CAL/GR
-190.
-180.
-170.
STATIC RESTORING FUNCTION, f (θi,s - θs)
NONDIM. SURFACE TEMPERATURE, θs
1.2
1.0
.8
.6
.4
.2
0
-.2
-.4
.6
.7
.8
.9
1.0
1.1
1.2
1.3
1.4
1.5

FIG. 15b

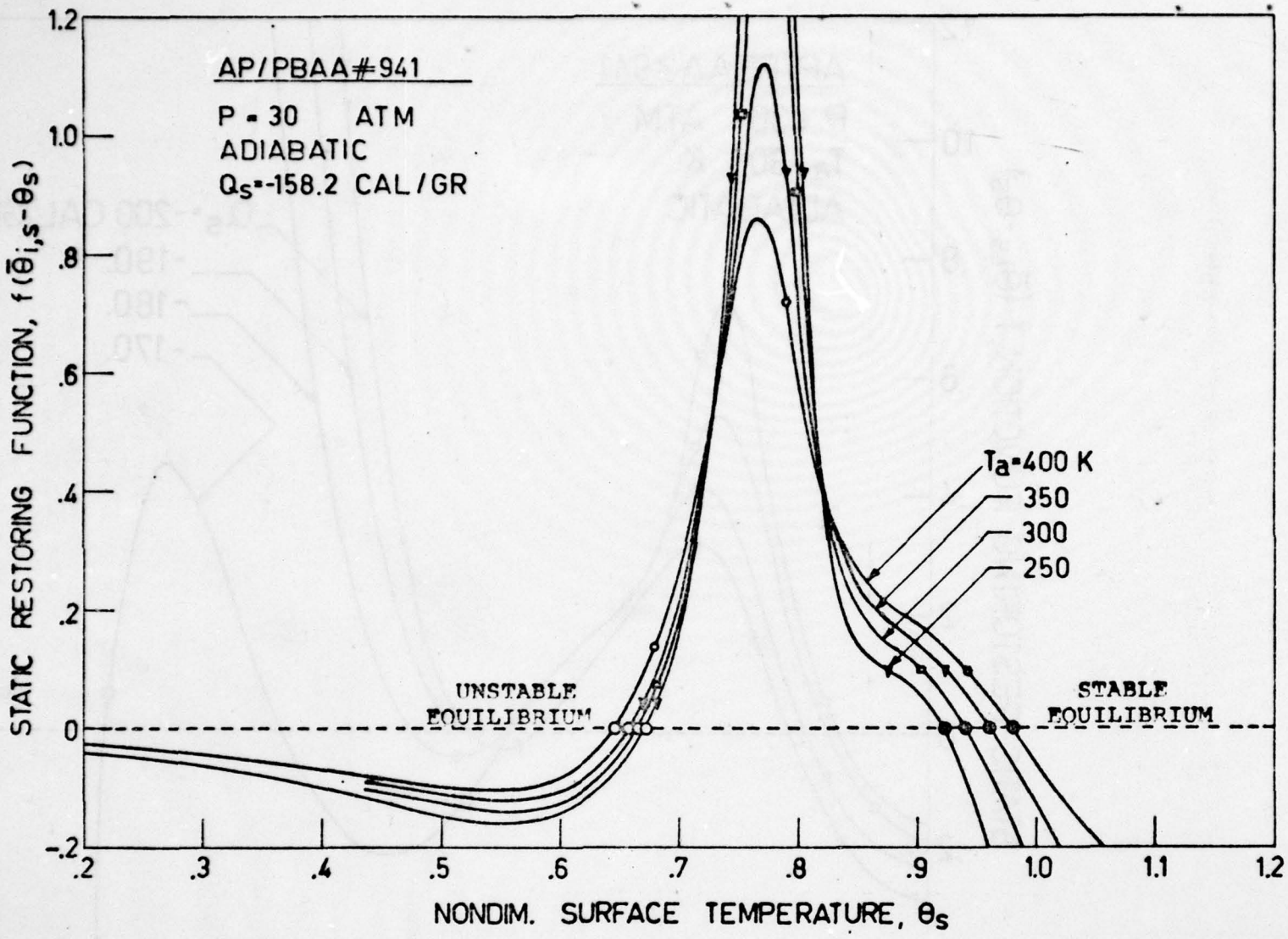
AP/PBAA#941
P = 30 ATM
ADIABATIC
Qs=-158.2 CAL/GR
Ta=400 K
350
300
250
UNSTABLE EQUILIBRIUM
STABLE EQUILIBRIUM
STATIC RESTORING FUNCTION, f(θi,s-θs)
NONDIM. SURFACE TEMPERATURE, θs
1.2
1.0
.8
.6
.4
.2
0
-.2
.2
.3
.4
.5
.6
.7
.8
.9
1.0
1.1
1.2

FIG. 16

AD-A065 064 POLITECNICO DI MILANO (ITALY) IST DI MACCHINE F/G 19/1
THE DYNAMICS OF SOLID PROPELLANT COMBUSTION.(U)
SEP 78 L DE LUCA, A COGHE, A REGGIORI DAERO-78-G-029

UNCLASSIFIED NL

2 OF 2
ADA
065064

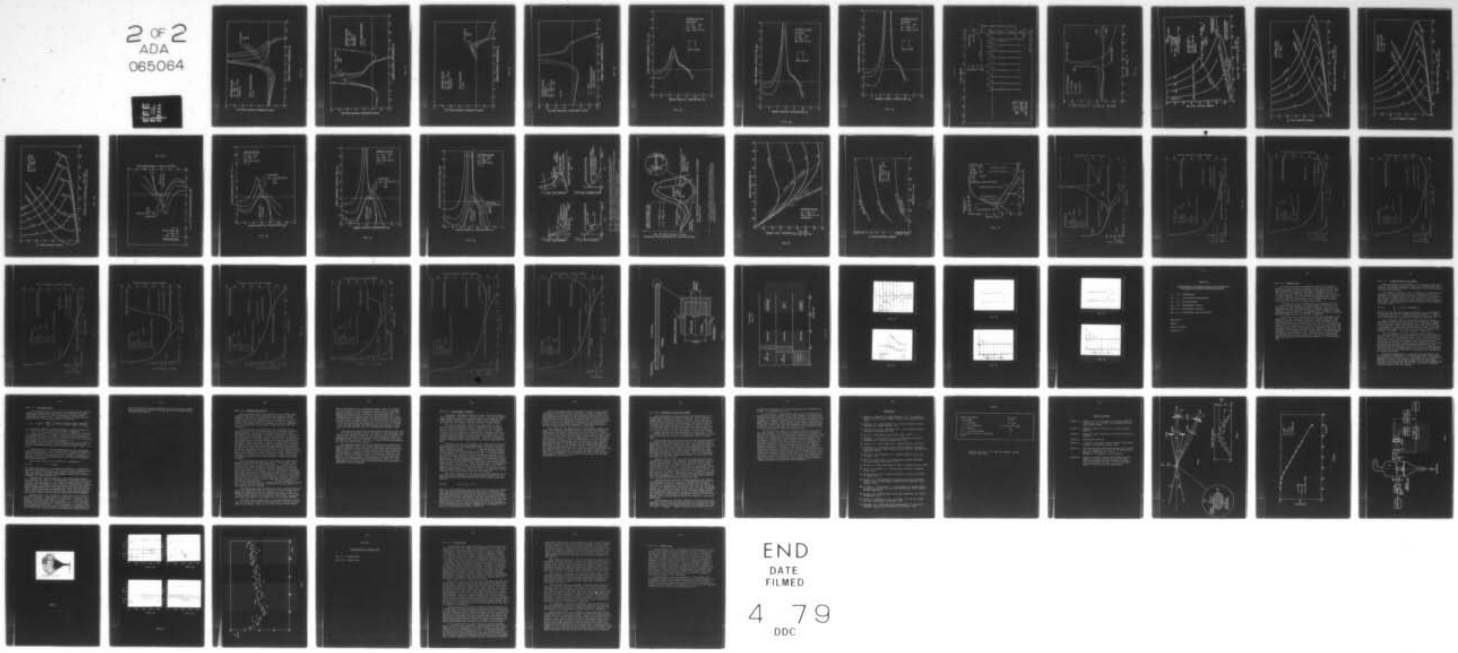

END
DATE
FILMED
4 79
DDC

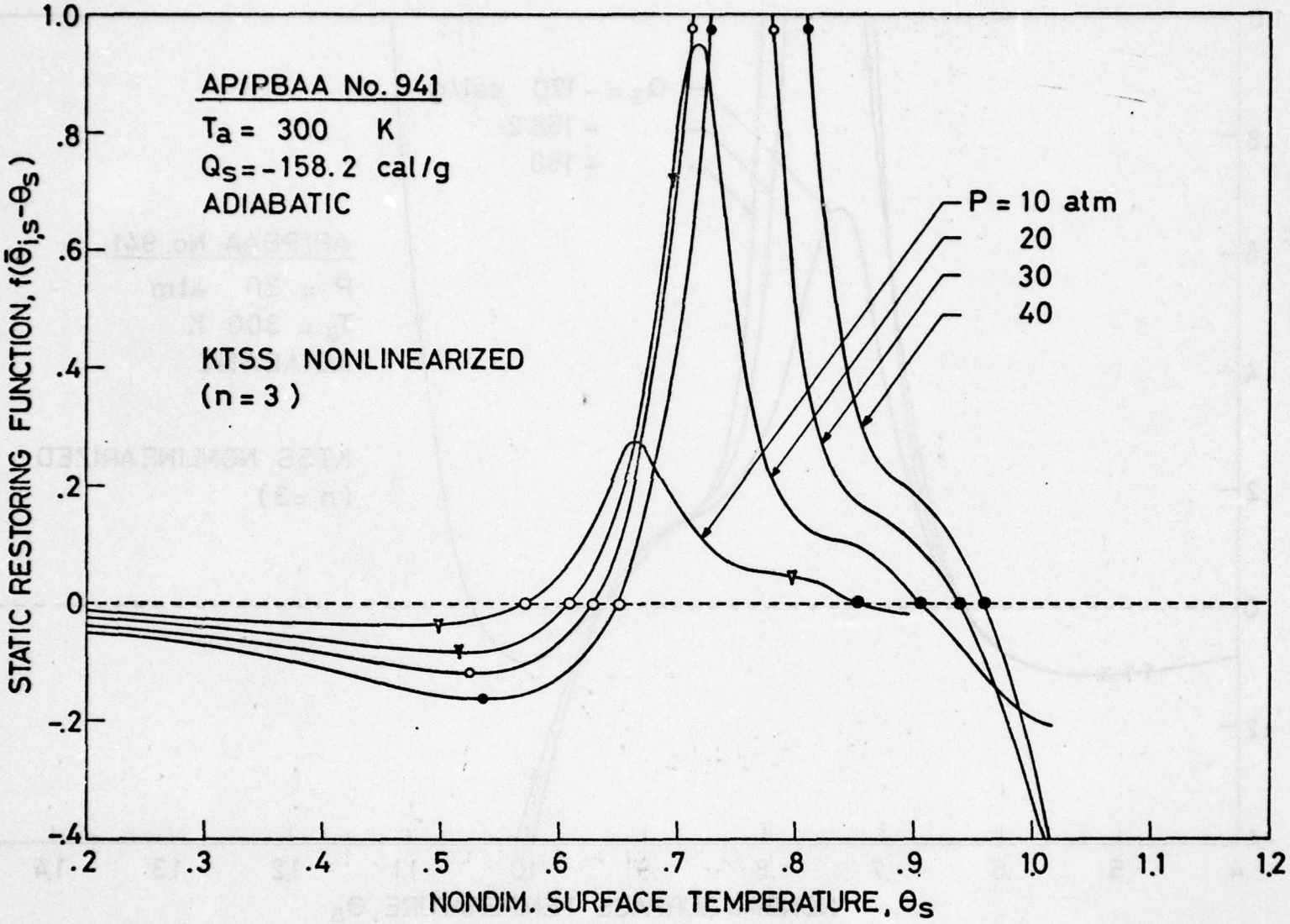
AP/PBAA No. 941
T_a = 300 K
Q_s = -158.2 cal/g
ADIABATIC
KTSS NONLINEARIZED
(n = 3)
P = 10 atm
20
30
40
STATIC RESTORING FUNCTION, $f(\bar{\theta}_{i,s}-\theta_s)$
NONDIM. SURFACE TEMPERATURE, θ_s
1.0
.8
.6
.4
.2
0
-.2
-.4
.2
.3
.4
.5
.6
.7
.8
.9
1.0
1.1
1.2

FIG. 17

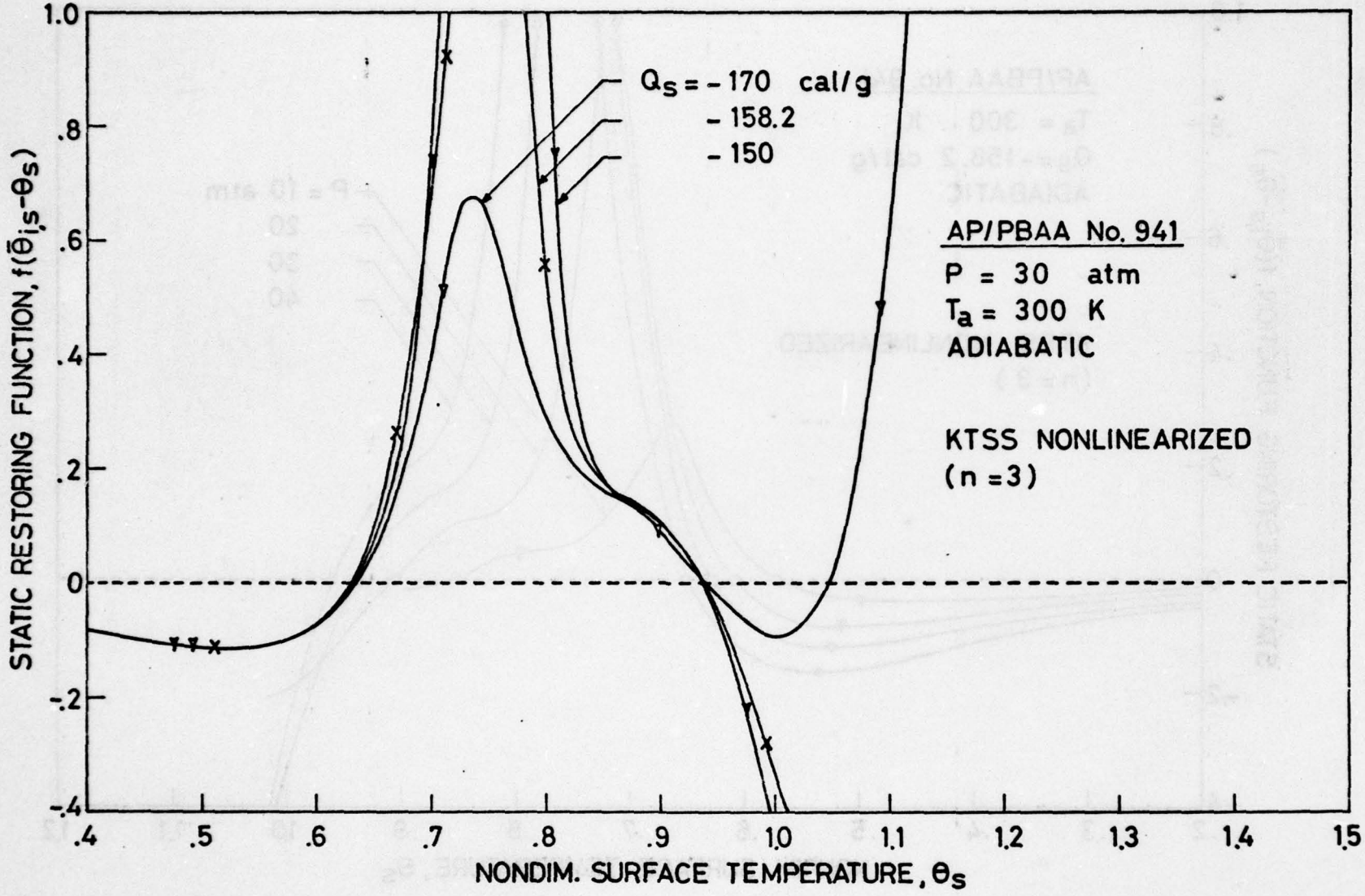
1.0
.8
.6
.4
.2
0
-.2
-.4
.4
.5
.6
.7
.8
.9
1.0
1.1
1.2
1.3
1.4
1.5
STATIC RESTORING FUNCTION, $f(\bar{\theta}_{is}-\theta_s)$
NONDIM. SURFACE TEMPERATURE, θ_s
Q_s = - 170 cal/g
- 158.2
- 150
AP/PBAA No. 941
P = 30 atm
T_a = 300 K
ADIABATIC
KTSS NONLINEARIZED
(n = 3)

FIG. 18

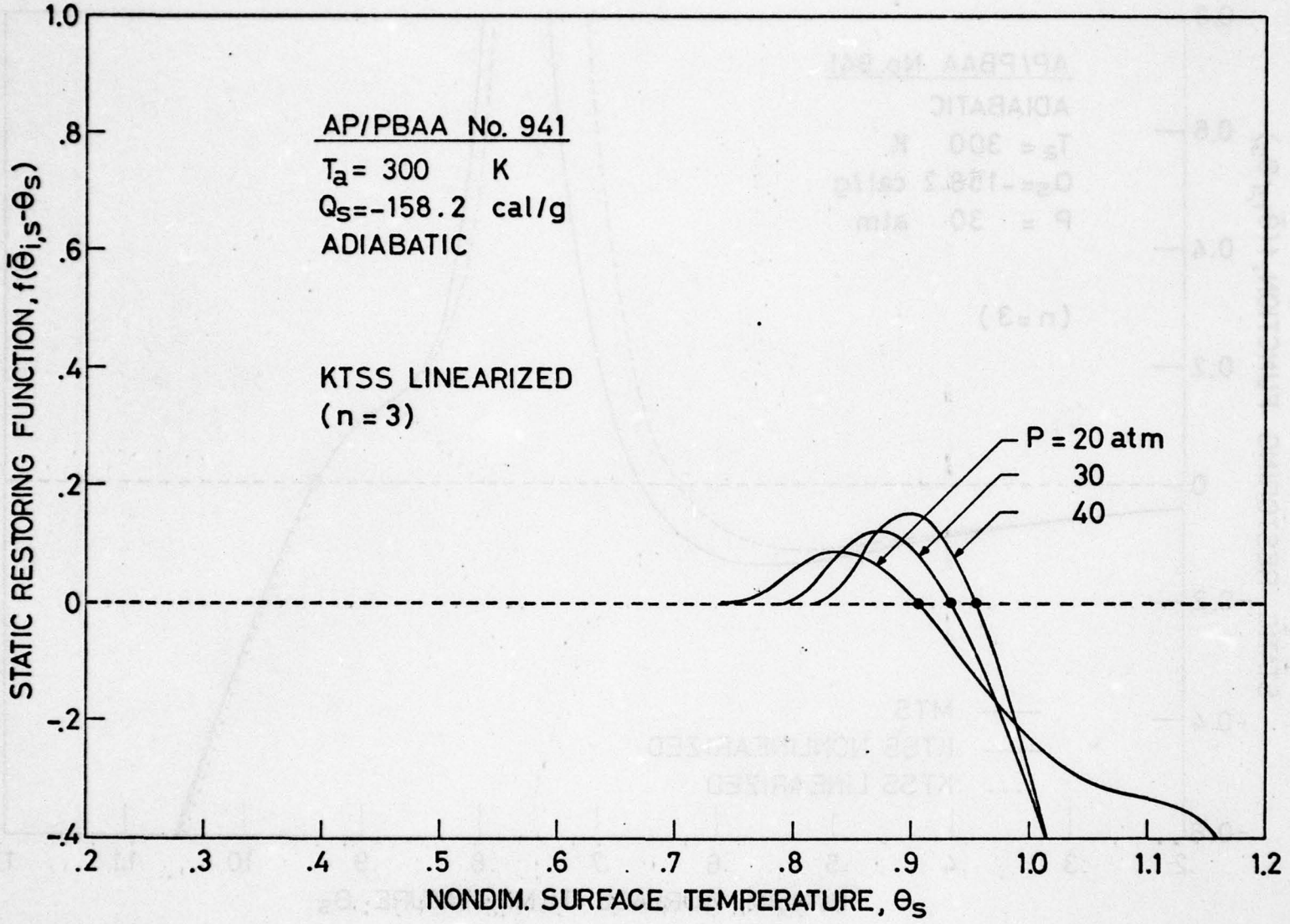
AP/PBAA No. 941
T_a= 300 K
Q_s=-158.2 cal/g
ADIABATIC
KTSS LINEARIZED
(n = 3)
P = 20 atm
30
40
STATIC RESTORING FUNCTION, $f(\bar{\theta}_{i,s}-\theta_s)$
NONDIM. SURFACE TEMPERATURE, θ_s
1.0
.8
.6
.4
.2
0
-.2
-.4
.2
.3
.4
.5
.6
.7
.8
.9
1.0
1.1
1.2

FIG. 19

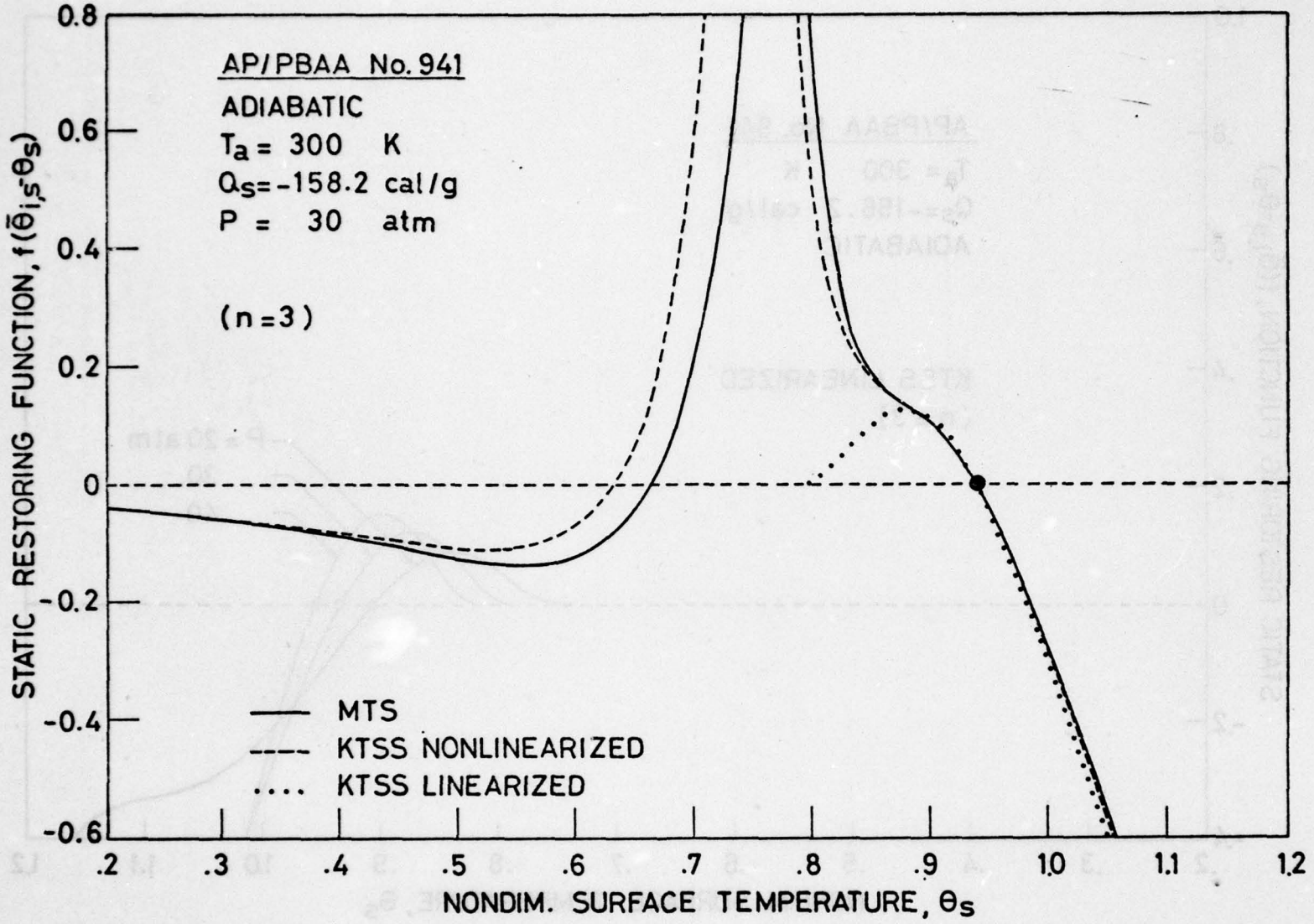
AP/PBAA No. 941
ADIABATIC
T_a = 300 K
Q_s = -158.2 cal/g
P = 30 atm
(n = 3)
MTS
KTSS NONLINEARIZED
KTSS LINEARIZED
STATIC RESTORING FUNCTION, $f(\tilde{\theta}_{i,s}-\theta_s)$
NONDIM. SURFACE TEMPERATURE, θ_s
0.8
0.6
0.4
0.2
0
-0.2
-0.4
-0.6
.2
.3
.4
.5
.6
.7
.8
.9
1.0
1.1
1.2

FIG. 20

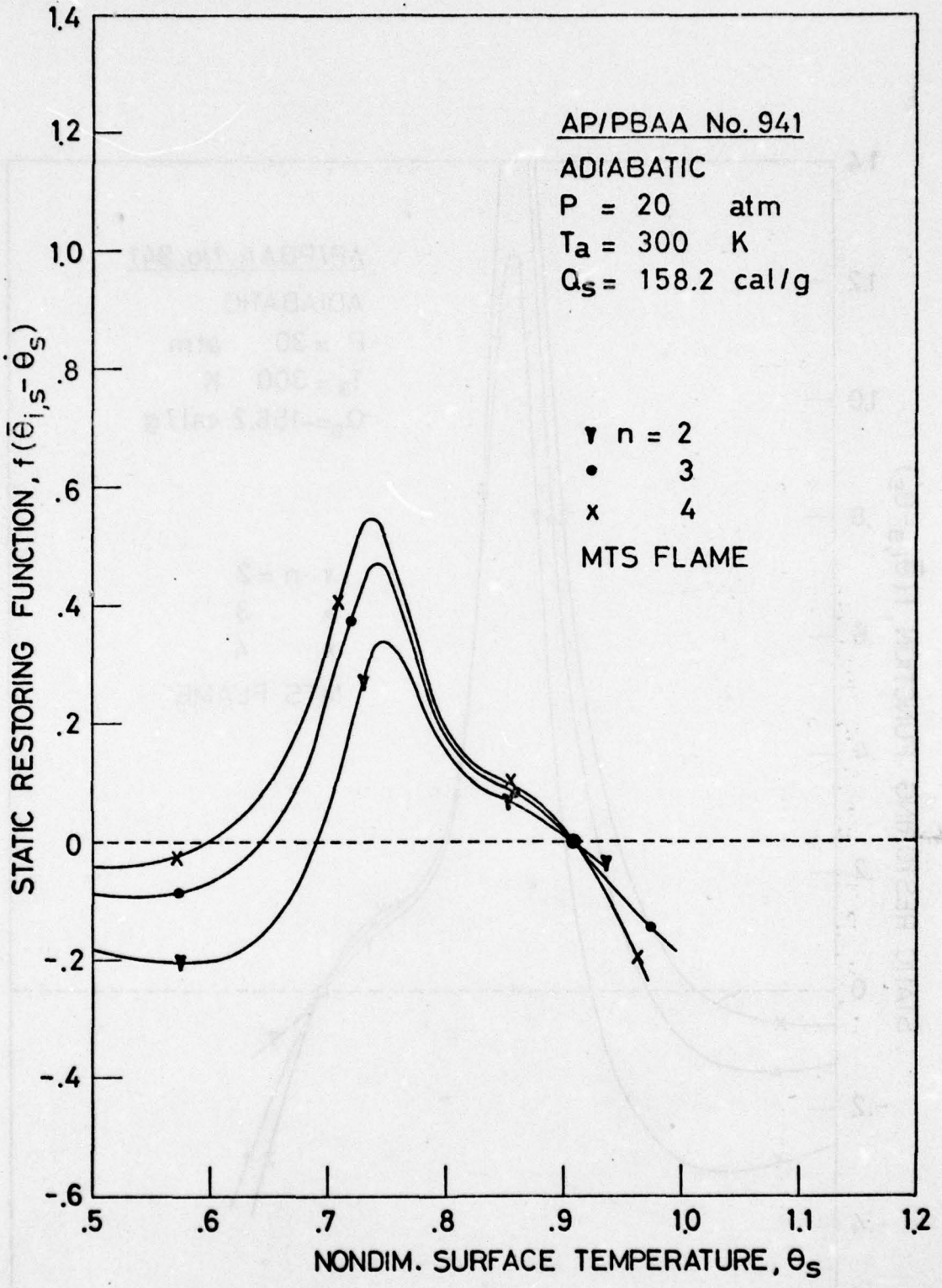
AP/PBAA No. 941
ADIABATIC
P = 20 atm
Ta = 300 K
Qs = 158.2 cal/g
n = 2
3
4
MTS FLAME
STATIC RESTORING FUNCTION, f(θ̄i,s - θ̇s)
NONDIM. SURFACE TEMPERATURE, θs
1.4
1.2
1.0
.8
.6
.4
.2
0
-.2
-.4
-.6
.5
.6
.7
.8
.9
1.0
1.1
1.2

FIG. 21

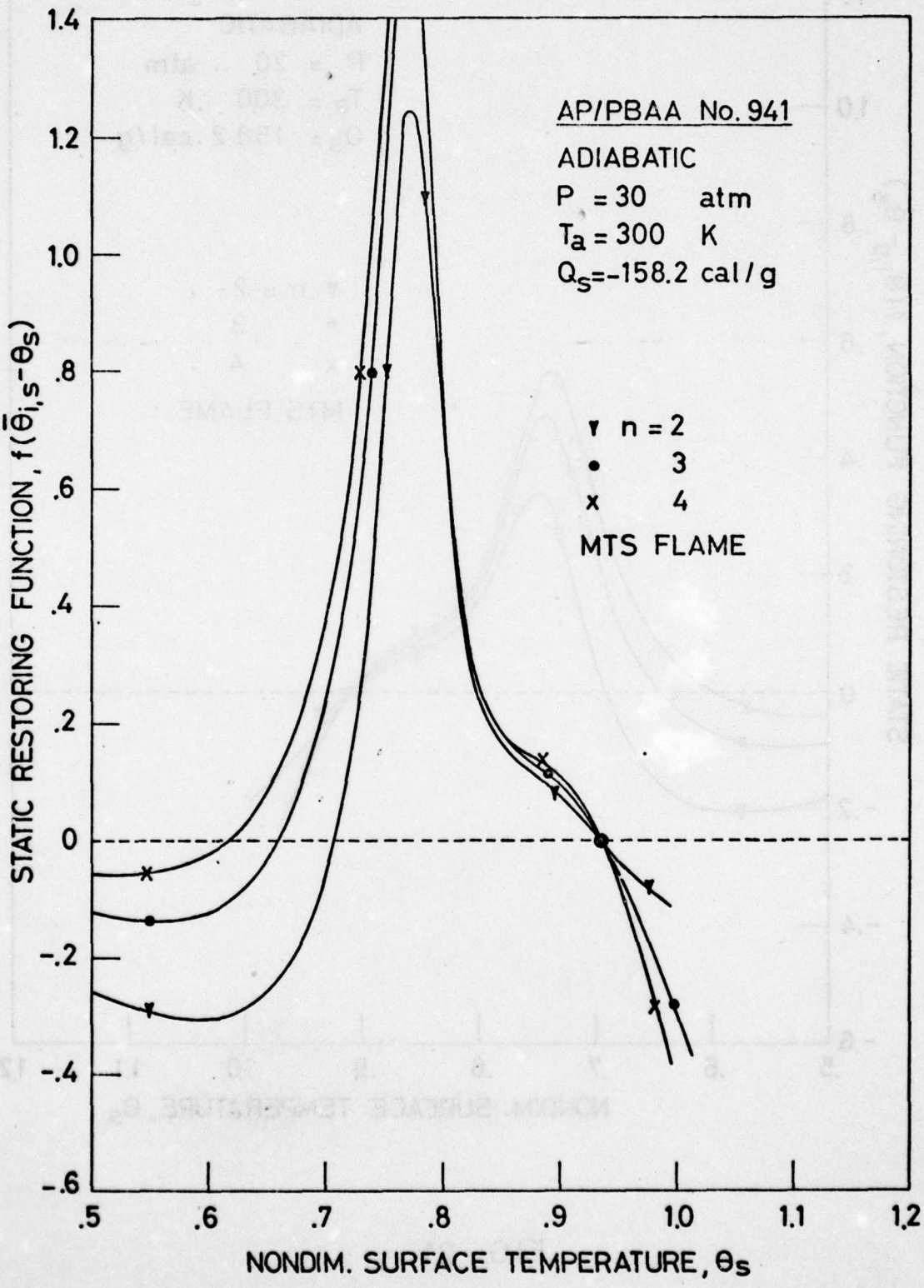
AP/PBAA No. 941
ADIABATIC
P = 30 atm
T_a = 300 K
Q_s=-158.2 cal/g
n = 2
3
4
MTS FLAME
STATIC RESTORING FUNCTION, $f(\bar{\theta}_{i,s}-\theta_s)$
NONDIM. SURFACE TEMPERATURE, θ_s
1.4
1.2
1.0
.8
.6
.4
.2
0
-.2
-.4
-.6
.5
.6
.7
.8
.9
1.0
1.1
1.2

FIG. 22

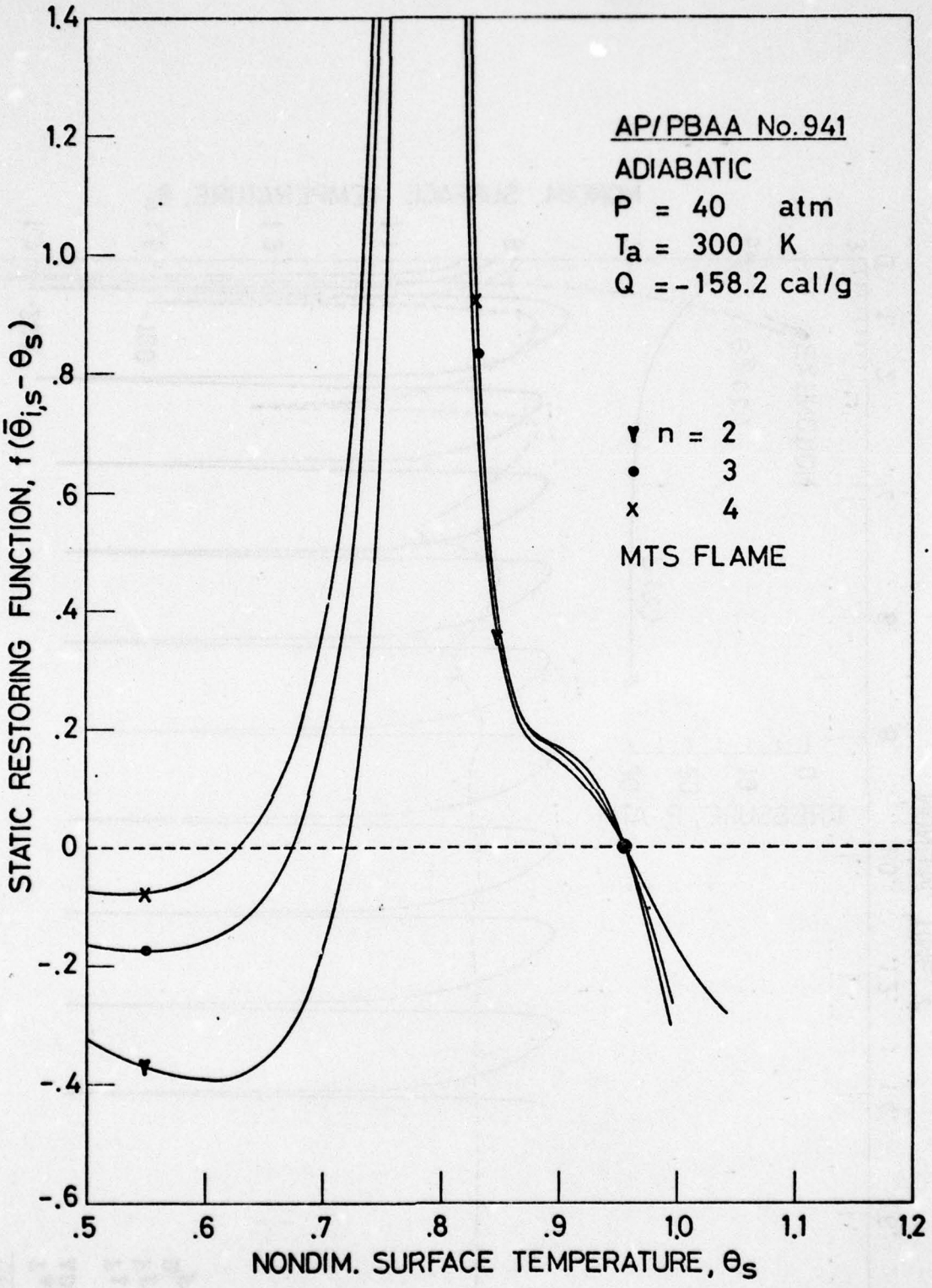
AP/PBAA No. 941
ADIABATIC
P = 40 atm
T_a = 300 K
Q = -158.2 cal/g
n = 2
3
4
MTS FLAME
STATIC RESTORING FUNCTION, $f(\bar{\theta}_{i,s}-\theta_s)$
NONDIM. SURFACE TEMPERATURE, θ_s
1.4
1.2
1.0
.8
.6
.4
.2
0
-.2
-.4
-.6
.5
.6
.7
.8
.9
1.0
1.1
1.2

FIG. 23

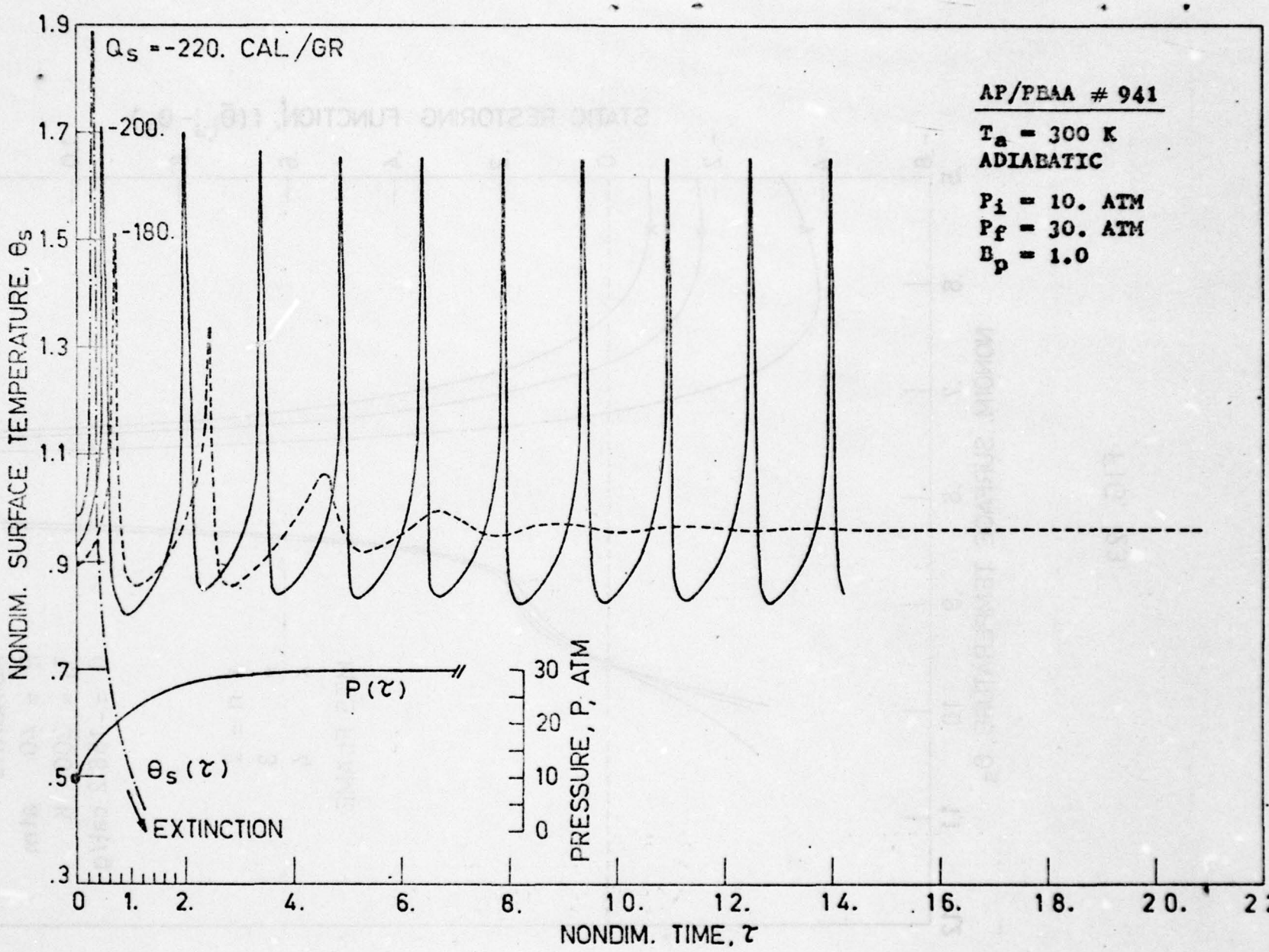
Q_s = -220. CAL/GR
-200.
-180.
AP/PBAA # 941
T_a = 300 K
ADIABATIC
P_i = 10. ATM
P_f = 30. ATM
B_p = 1.0
NONDIM. SURFACE TEMPERATURE, θ_s
1.9
1.7
1.5
1.3
1.1
.9
.7
.5
.3
P(τ)
$\theta_s(\tau)$
EXTINCTION
30
20
10
0
PRESSURE, P, ATM
0
1.
2.
4.
6.
8.
10.
12.
14.
16.
18.
20.
22.
NONDIM. TIME, τ

FIG. 24

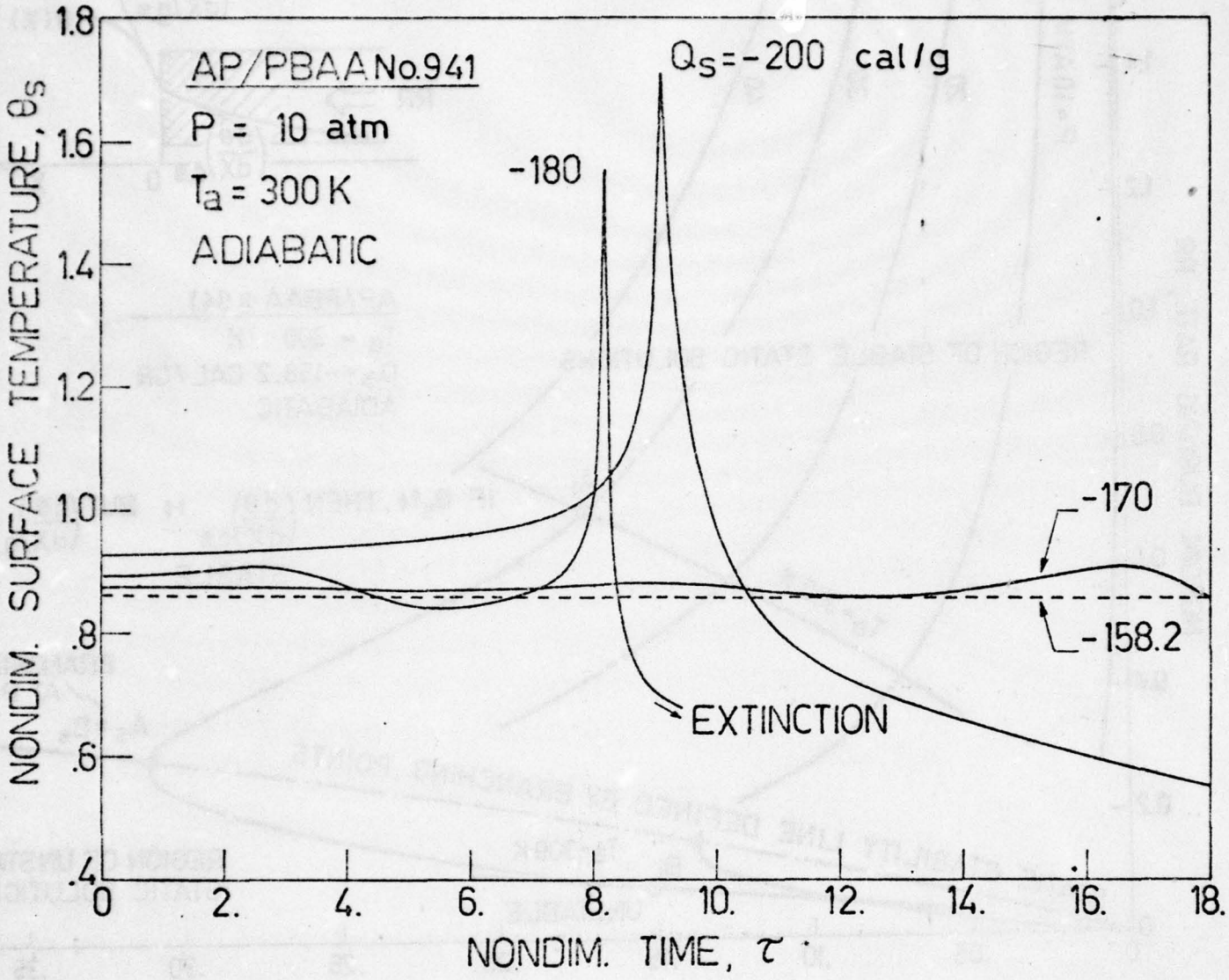
AP/PBAA No.941
P = 10 atm
T_a = 300 K
ADIABATIC
Q_S = -200 cal/g
-180
-170
-158.2
EXTINCTION
NONDIM. SURFACE TEMPERATURE, θ_S
NONDIM. TIME, τ
1.8
1.6
1.4
1.2
1.0
.8
.6
.4
0
2.
4.
6.
8.
10.
12.
14.
16.
18.

FIG. 25

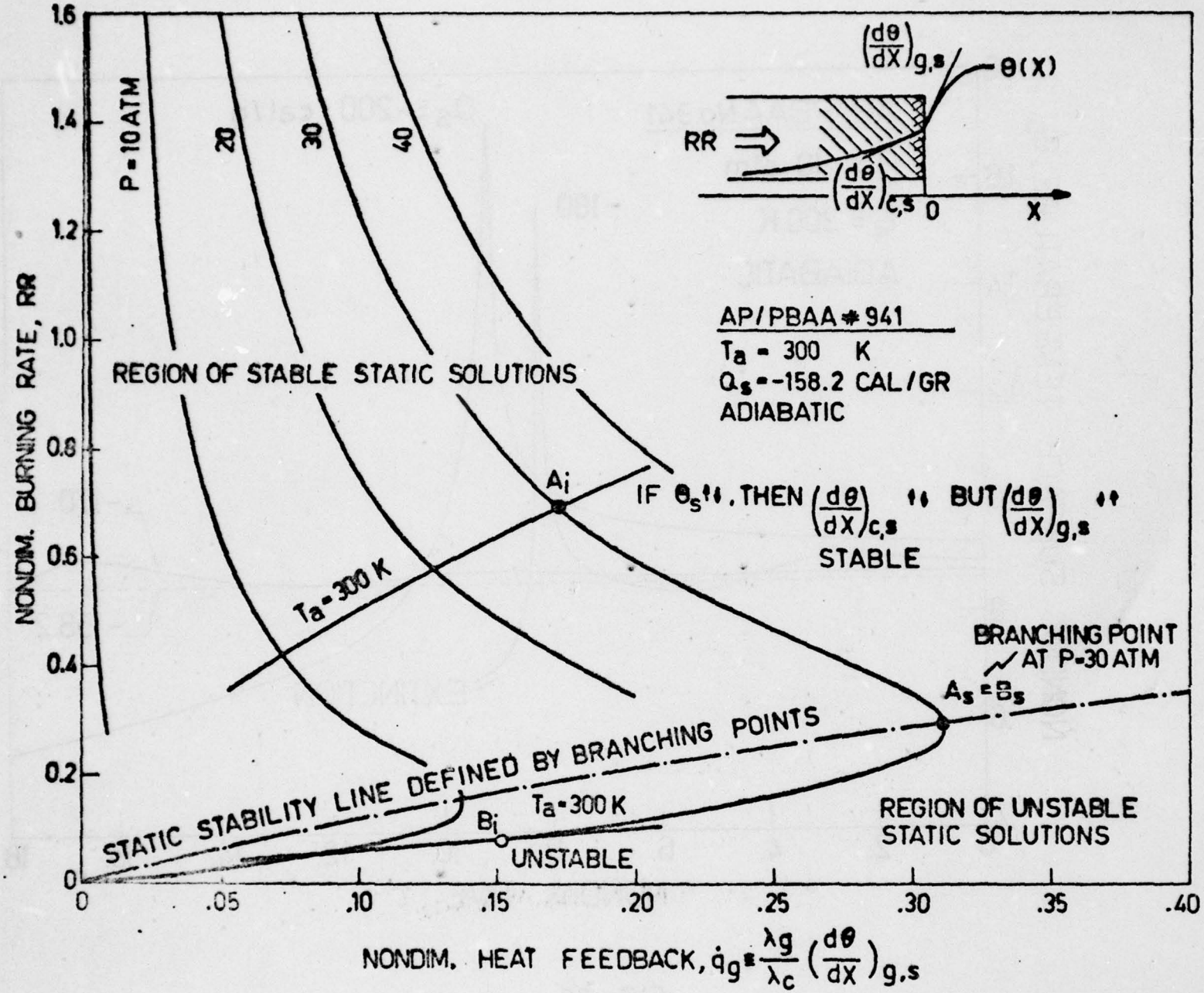
NONDIM. BURNING RATE, RR
NONDIM. HEAT FEEDBACK, $\dot{q}_g = \frac{\lambda_g}{\lambda_c}\left(\frac{d\theta}{dX}\right)_{g,s}$
P=10 ATM
20
30
40
REGION OF STABLE STATIC SOLUTIONS
AP/PBAA #941
T_a = 300 K
Q_s = -158.2 CAL/GR
ADIABATIC
$\left(\frac{d\theta}{dX}\right)_{g,s}$
$\theta(X)$
RR
$\left(\frac{d\theta}{dX}\right)_{c,s}$
0
X
A_i
IF $\theta_s \uparrow$, THEN $\left(\frac{d\theta}{dX}\right)_{c,s} \uparrow$ BUT $\left(\frac{d\theta}{dX}\right)_{g,s} \downarrow$
STABLE
T_a=300 K
BRANCHING POINT
AT P=30 ATM
$A_s = B_s$
STATIC STABILITY LINE DEFINED BY BRANCHING POINTS
B_i
T_a=300 K
UNSTABLE
REGION OF UNSTABLE
STATIC SOLUTIONS
0
.05
.10
.15
.20
.25
.30
.35
.40
0.2
0.4
0.6
0.8
1.0
1.2
1.4
1.6

FIG. 26

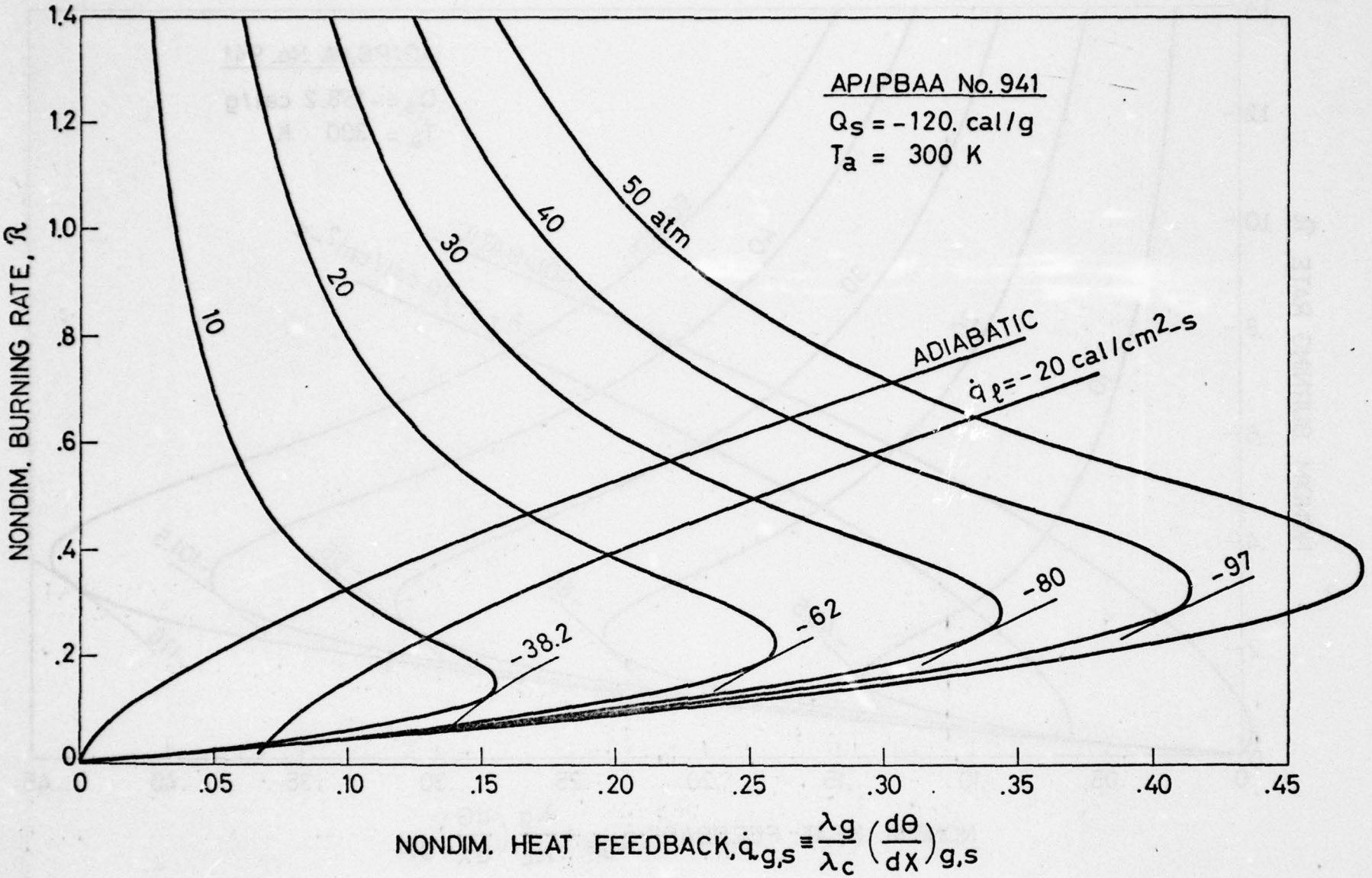
AP/PBAA No. 941
$Q_s = -120.$ cal/g
$T_a = 300$ K
50 atm
40
30
20
10
ADIABATIC
$\dot{q}_\ell = -20$ cal/cm^2-s
-97
-80
-62
-38.2
NONDIM. BURNING RATE, $\mathcal{R}$
NONDIM. HEAT FEEDBACK, $\dot{q}_{g,s} \equiv \frac{\lambda_g}{\lambda_c}\left(\frac{d\theta}{dX}\right)_{g,s}$
0
.2
.4
.6
.8
1.0
1.2
1.4
0
.05
.10
.15
.20
.25
.30
.35
.40
.45

FIG. 27

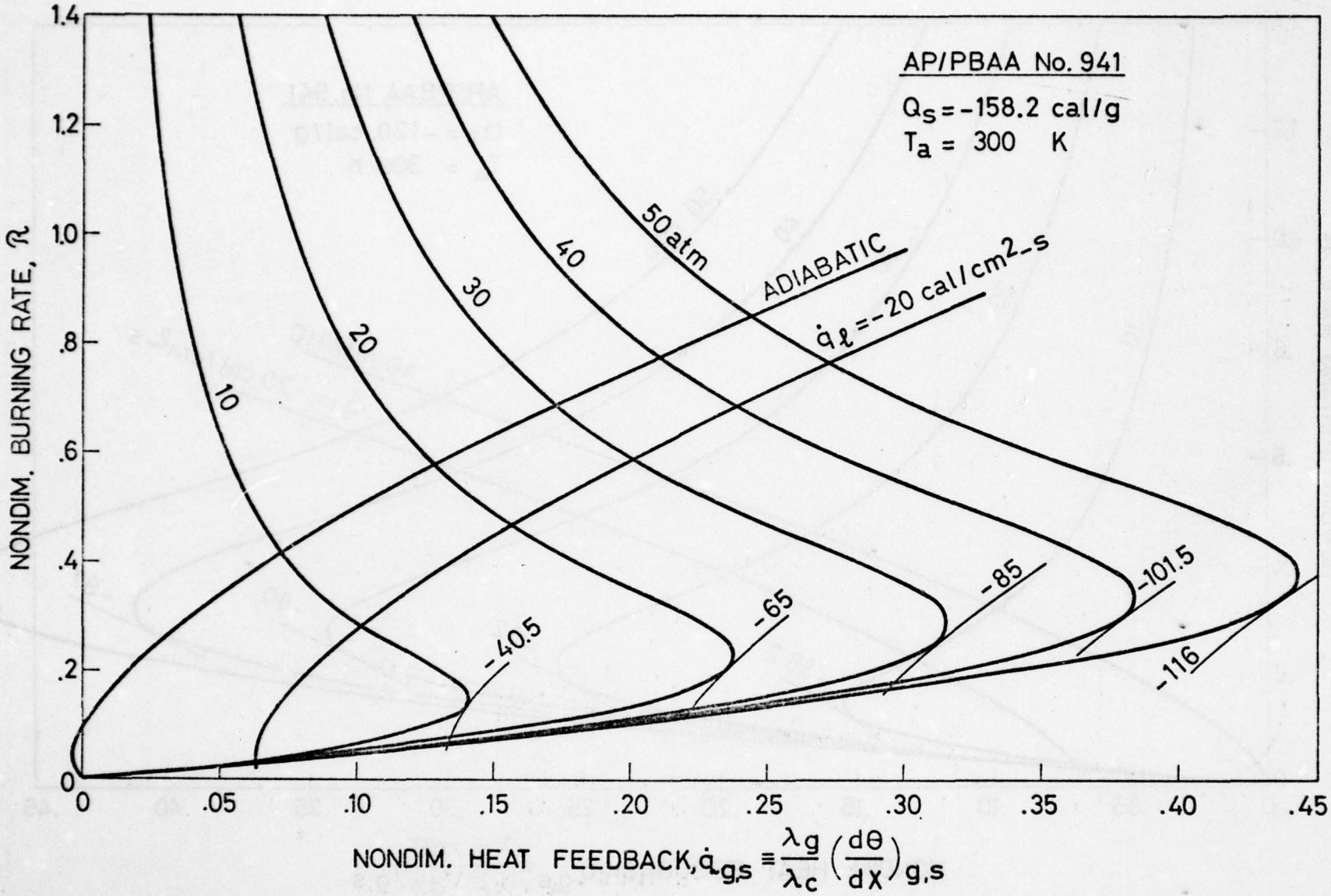
AP/PBAA No. 941
Q_s = -158.2 cal/g
T_a = 300 K
50 atm
40
30
20
10
ADIABATIC
$\dot{q}_\ell$ = -20 cal/cm2-s
-40.5
-65
-85
-101.5
-116
NONDIM. BURNING RATE, $\mathcal{R}$
NONDIM. HEAT FEEDBACK, $\dot{q}_{g,s} \equiv \frac{\lambda_g}{\lambda_c}\left(\frac{d\theta}{dX}\right)_{g,s}$
0
.2
.4
.6
.8
1.0
1.2
1.4
.05
.10
.15
.20
.25
.30
.35
.40
.45

FIG. 28

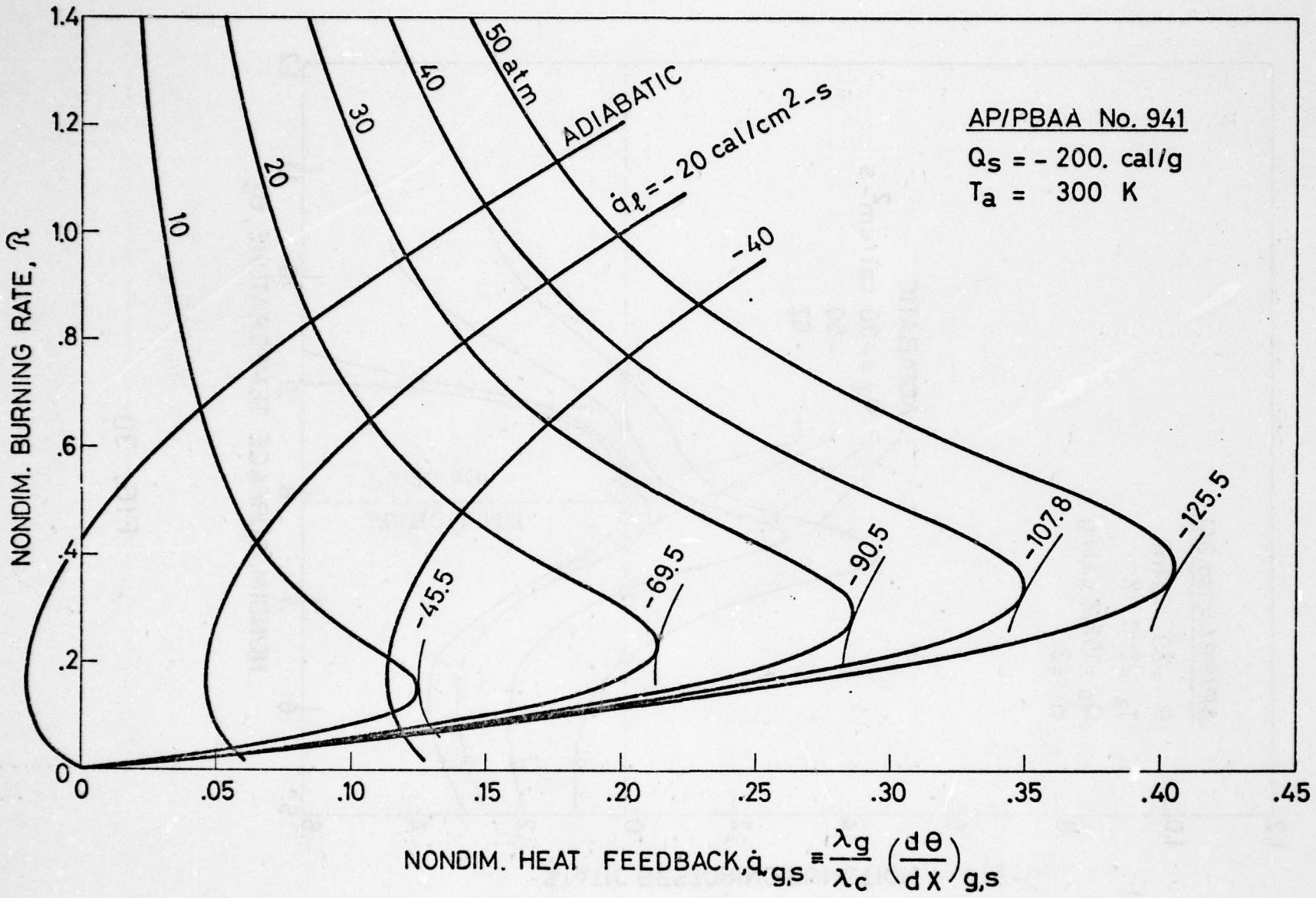
AP/PBAA No. 941
Q_s = - 200. cal/g
T_a = 300 K
ADIABATIC
$\dot{q}_\ell$ = - 20 cal/cm²-s
50 atm
40
30
20
10
-40
-45.5
-69.5
-90.5
-107.8
-125.5
NONDIM. BURNING RATE, R
NONDIM. HEAT FEEDBACK, $\dot{q}_{g,s} \equiv \frac{\lambda_g}{\lambda_c}\left(\frac{d\theta}{dX}\right)_{g,s}$
0
.2
.4
.6
.8
1.0
1.2
1.4
.05
.10
.15
.20
.25
.30
.35
.40
.45

FIG. 29

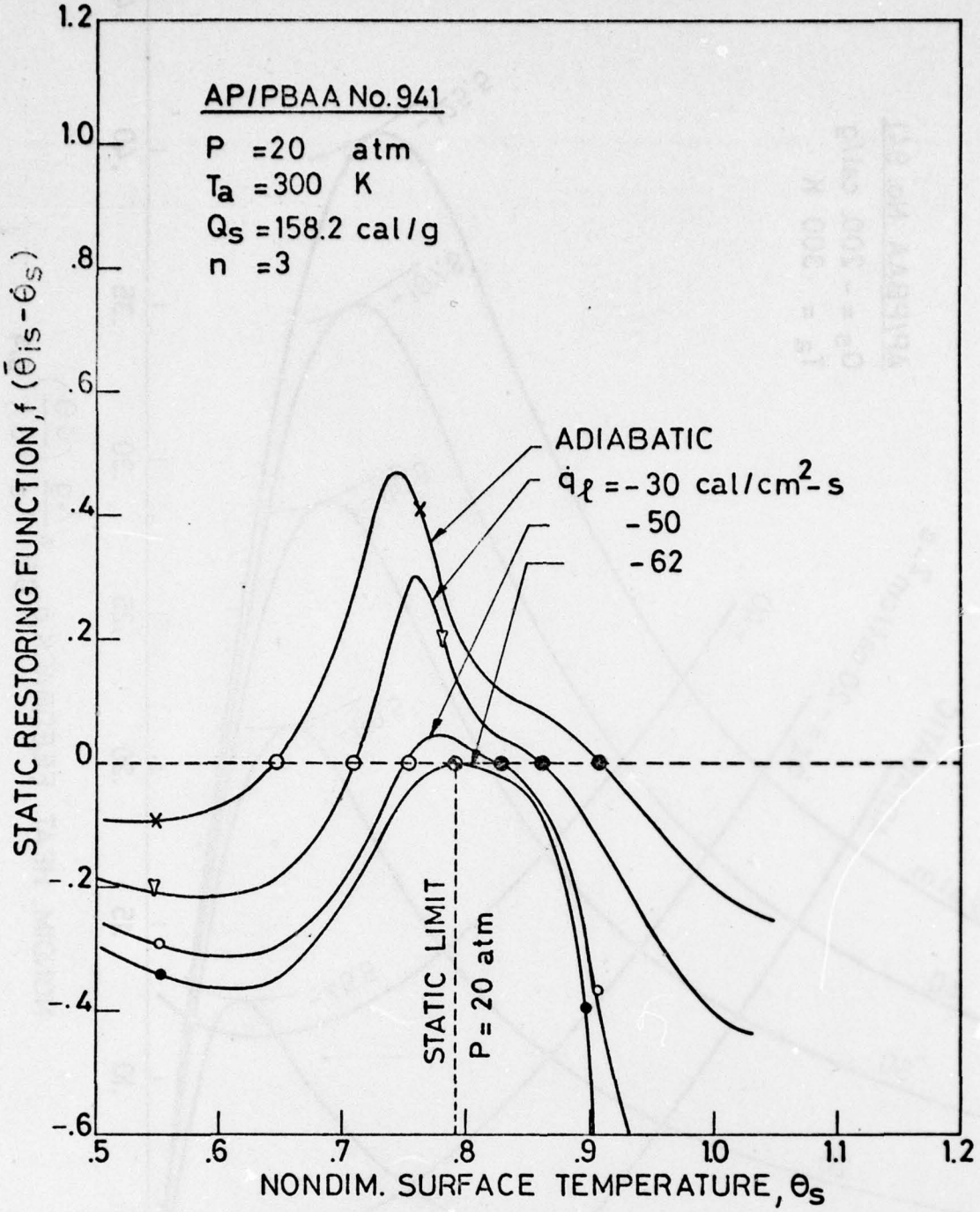
AP/PBAA No. 941
P =20 atm
T_a =300 K
Q_s =158.2 cal/g
n =3
ADIABATIC
$\dot{q}_\ell$ = -30 cal/cm^2-s
-50
-62
STATIC LIMIT
P= 20 atm
STATIC RESTORING FUNCTION, $f(\bar{\theta}_{is} - \dot{\theta}_s)$
NONDIM. SURFACE TEMPERATURE, θ_s
1.2
1.0
.8
.6
.4
.2
0
-.2
-.4
-.6
.5
.6
.7
.8
.9
1.0
1.1
1.2

FIG. 30

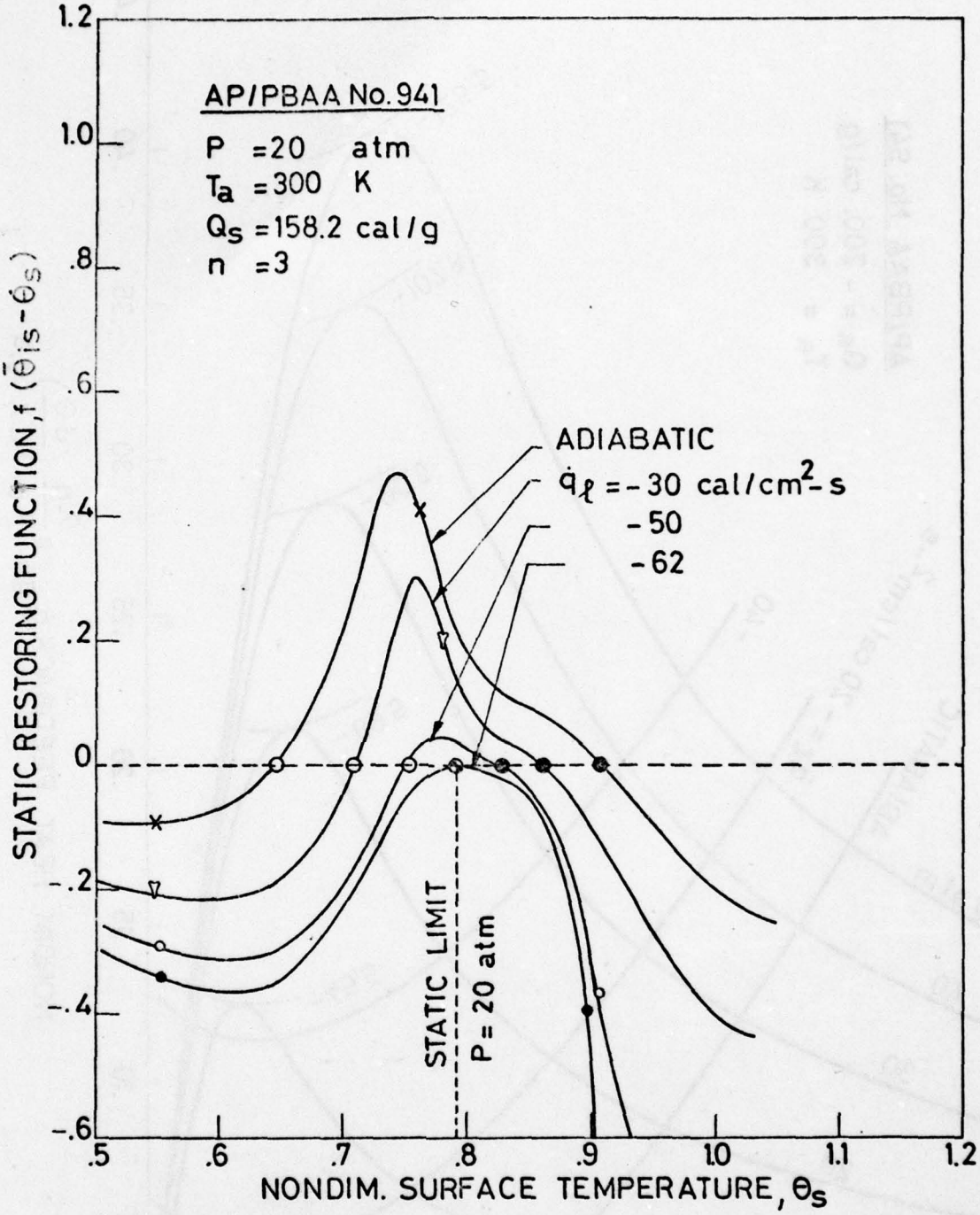
AP/PBAA No. 941
P =20 atm
T_a =300 K
Q_s =158.2 cal/g
n =3
ADIABATIC
$\dot{q}_\ell$ = -30 cal/cm²-s
-50
-62
STATIC LIMIT
P= 20 atm
STATIC RESTORING FUNCTION, $f(\bar{\theta}_{is}-\theta_s)$
NONDIM. SURFACE TEMPERATURE, θ_s
1.2
1.0
.8
.6
.4
.2
0
-.2
-.4
-.6
.5
.6
.7
.8
.9
1.0
1.1
1.2

FIG. 30

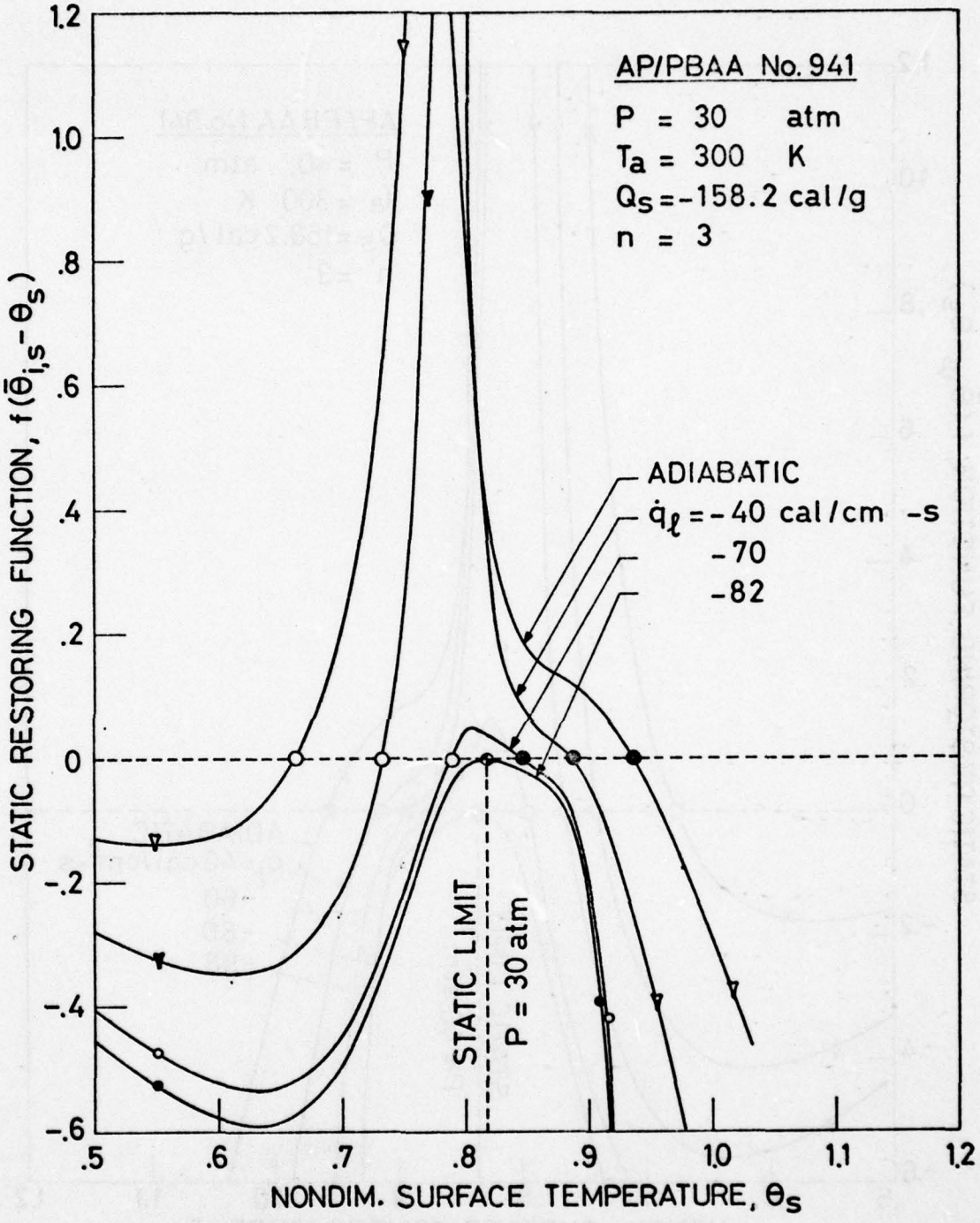
AP/PBAA No. 941
P = 30 atm
T_a = 300 K
Q_s = -158.2 cal/g
n = 3
ADIABATIC
$\dot{q}_\ell$ = -40 cal/cm -s
-70
-82
STATIC LIMIT
P = 30 atm
STATIC RESTORING FUNCTION, $f(\bar{\theta}_{i,s} - \theta_s)$
NONDIM. SURFACE TEMPERATURE, θ_s
1.2
1.0
.8
.6
.4
.2
0
-.2
-.4
-.6
.5
.6
.7
.8
.9
1.0
1.1
1.2

FIG. 31

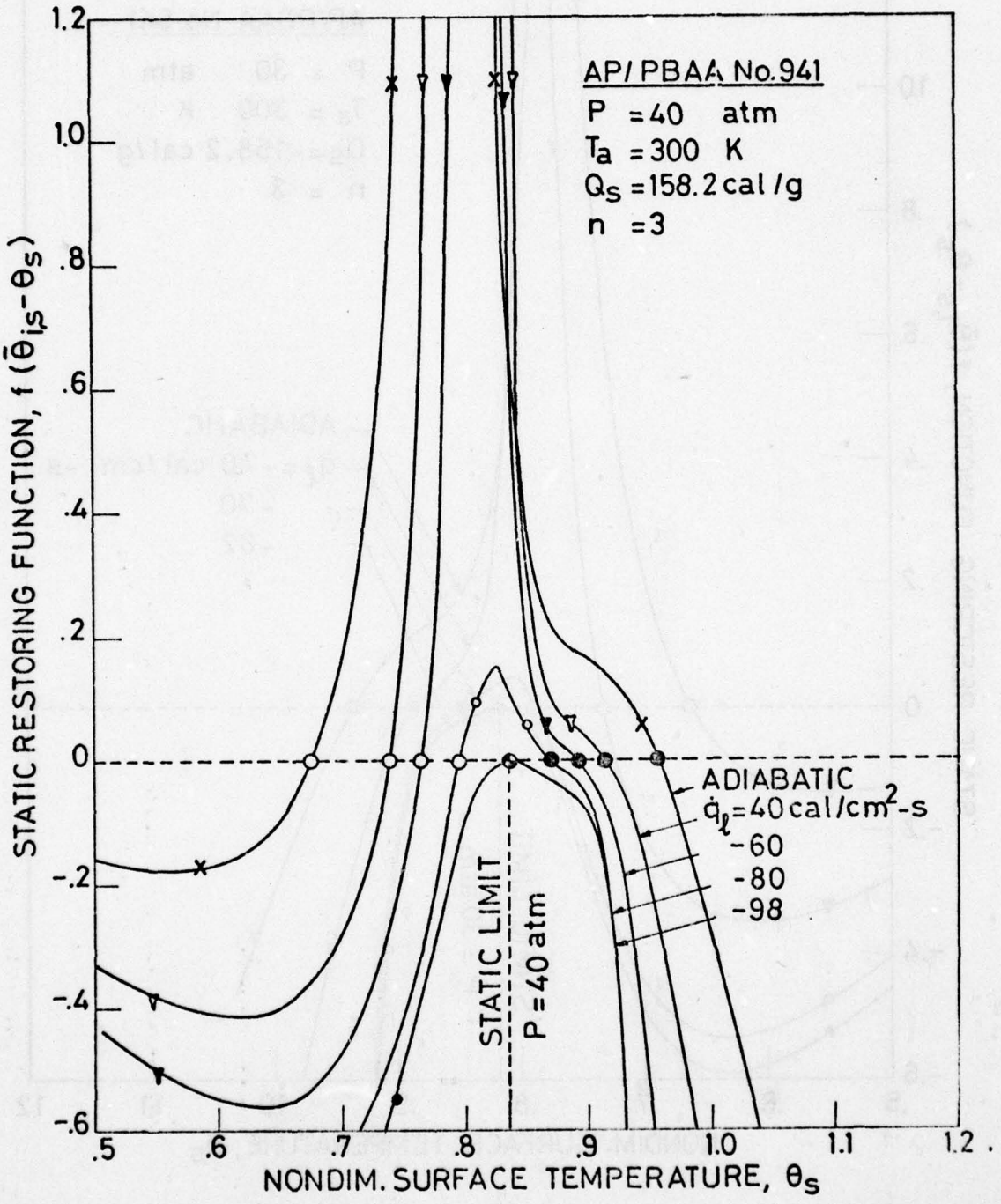
AP/ PBAA No.941
P = 40 atm
T_a = 300 K
Q_s = 158.2 cal/g
n = 3
STATIC RESTORING FUNCTION, $f(\bar{\theta}_{is}-\theta_s)$
NONDIM. SURFACE TEMPERATURE, θ_s
ADIABATIC
$\dot{q}_\ell$ = 40 cal/cm^2-s
-60
-80
-98
STATIC LIMIT
P = 40 atm
1.2
1.0
.8
.6
.4
.2
0
-.2
-.4
-.6
.5
.6
.7
.8
.9
1.0
1.1
1.2

FIG. 32

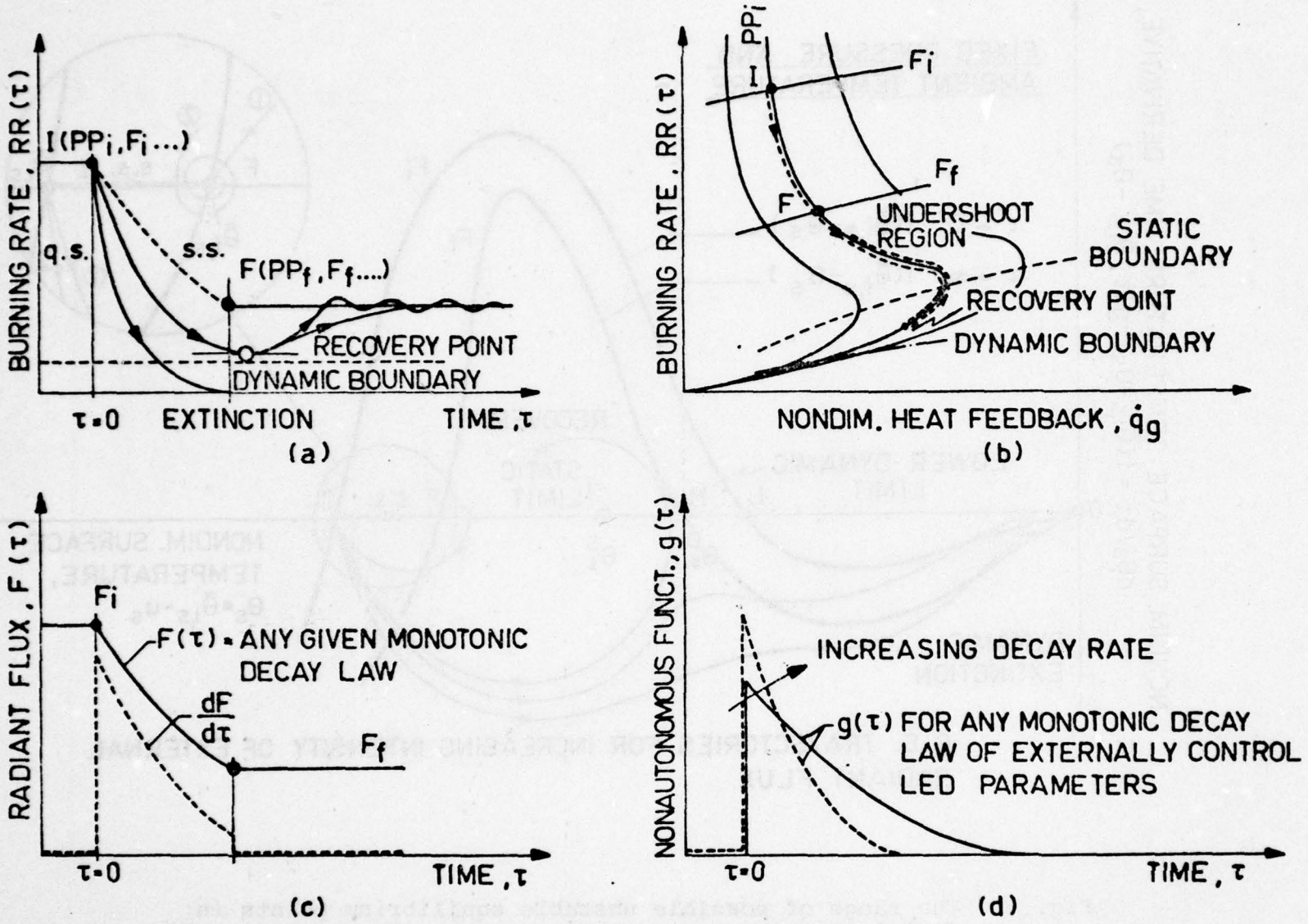

Fig. 33a Representative time histories of burning rate during deradiation showing possible occurrence of dynamic extinction.

Fig. 33b Corresponding trajectories in burning rate vs heat feedback plane.

Fig. 33c Nomenclature used for deradiation transients.

Fig. 33d Nature of nonautonomous function considered in this study.

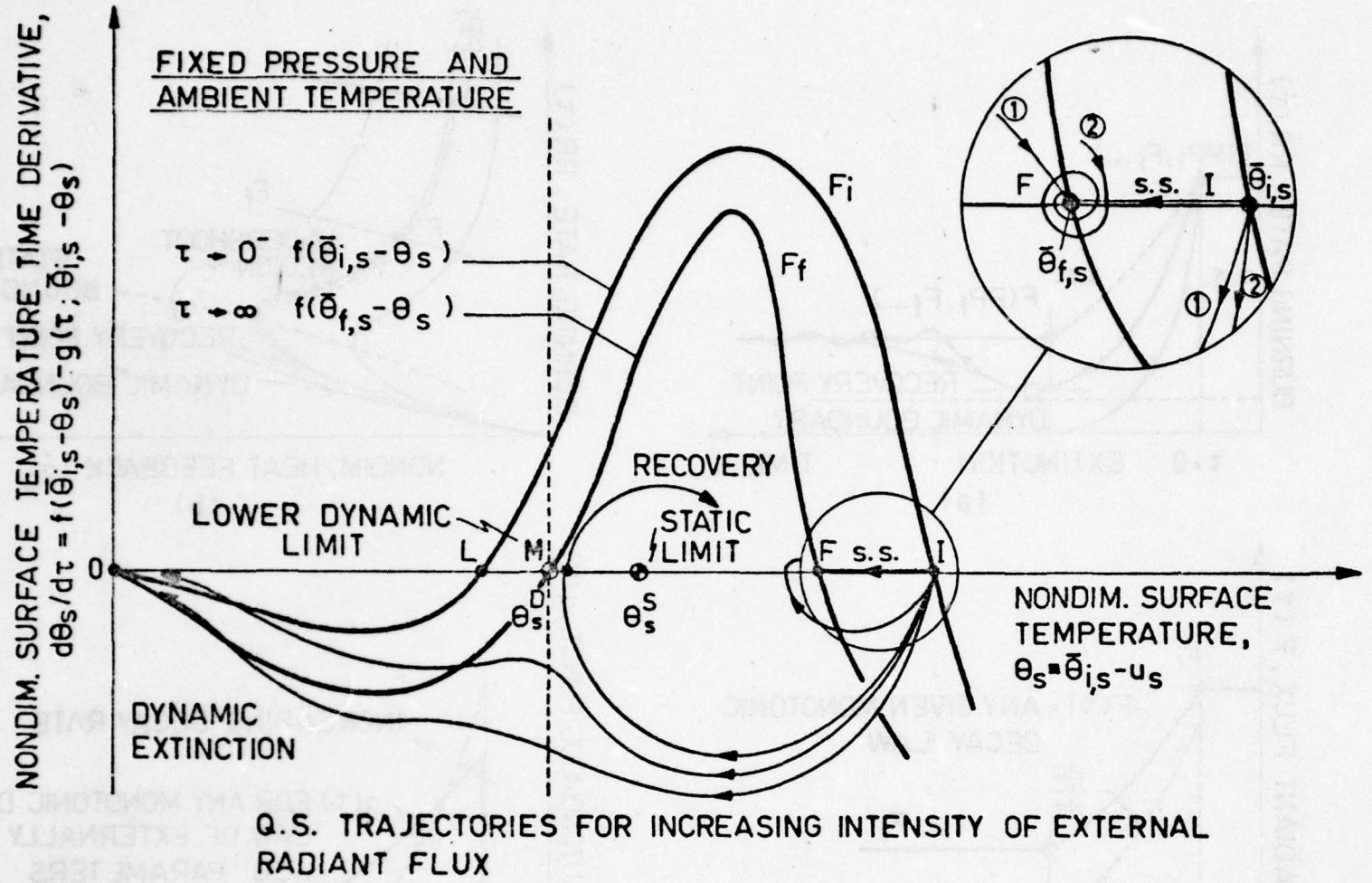

Q.S. TRAJECTORIES FOR INCREASING INTENSITY OF EXTERNAL RADIANT FLUX

Fig. 34 The range of possible unstable equilibrium points in dynamic burning regime is limited by the no-return point M (the unstable root associated to the static restoring function for $\tau \to \infty$).

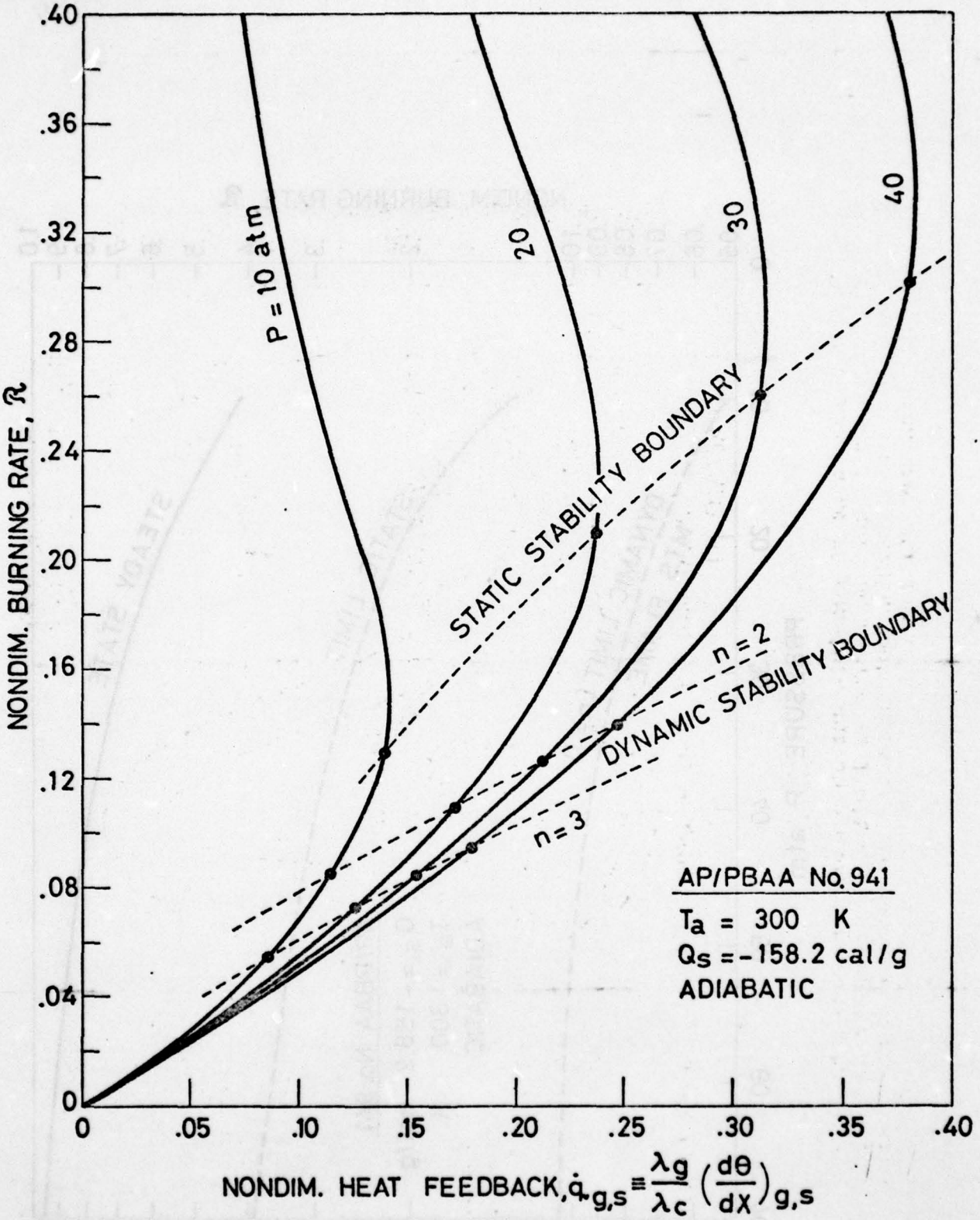
.40
.36
.32
.28
.24
.20
.16
.12
.08
.04
0
NONDIM. BURNING RATE, R
P = 10 atm
20
30
40
STATIC STABILITY BOUNDARY
DYNAMIC STABILITY BOUNDARY
n = 2
n = 3
AP/PBAA No. 941
T_a = 300 K
Q_s = -158.2 cal/g
ADIABATIC
0
.05
.10
.15
.20
.25
.30
.35
.40
NONDIM. HEAT FEEDBACK, $\dot{q}_{g,s} \equiv \frac{\lambda_g}{\lambda_c}\left(\frac{d\theta}{dX}\right)_{g,s}$

FIG. 35

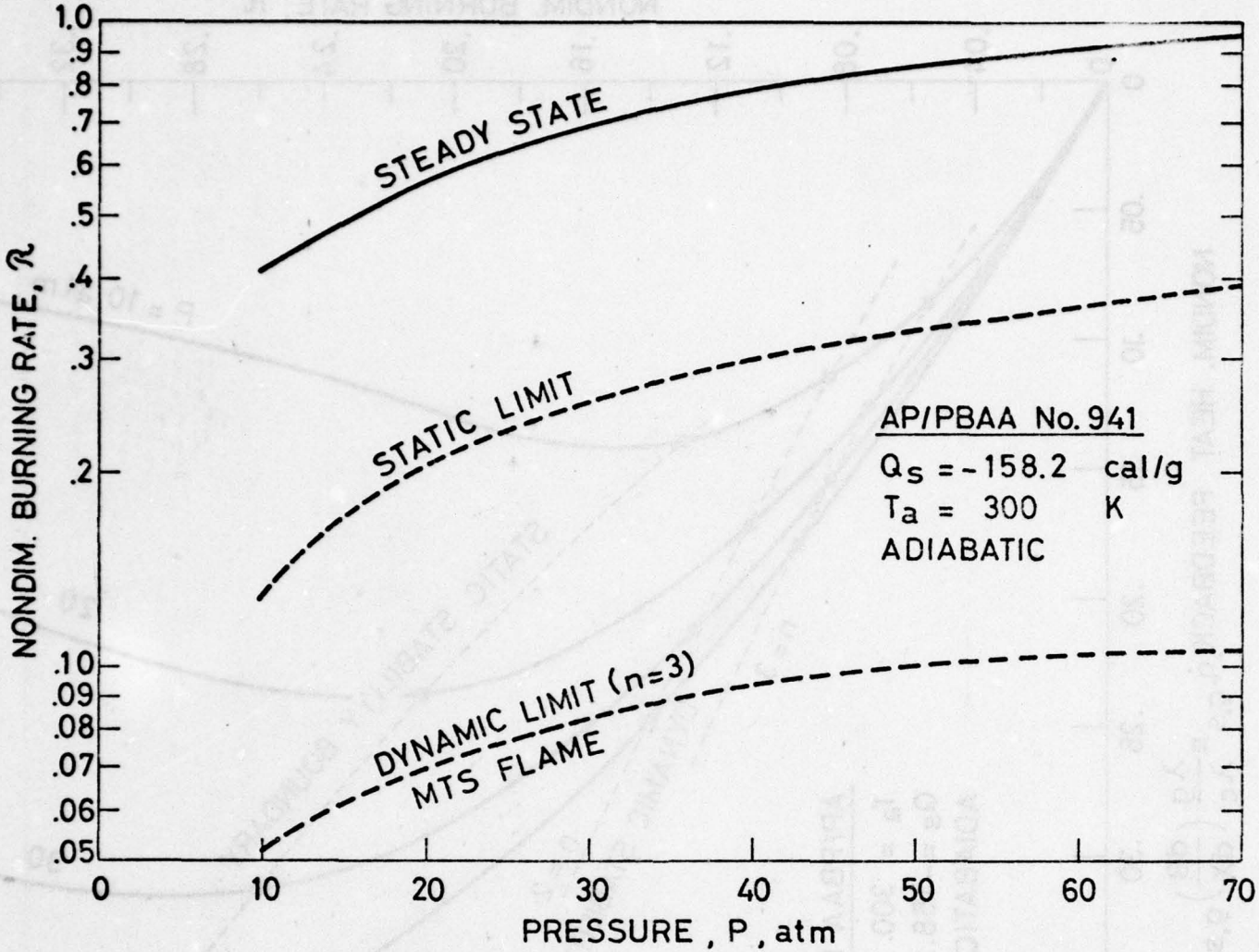
NONDIM. BURNING RATE, R
1.0
.9
.8
.7
.6
.5
.4
.3
.2
.10
.09
.08
.07
.06
.05
STEADY STATE
STATIC LIMIT
DYNAMIC LIMIT (n=3)
MTS FLAME
AP/PBAA No. 941
Q_s = -158.2 cal/g
T_a = 300 K
ADIABATIC
0
10
20
30
40
50
60
70
PRESSURE , P , atm

FIG. 36

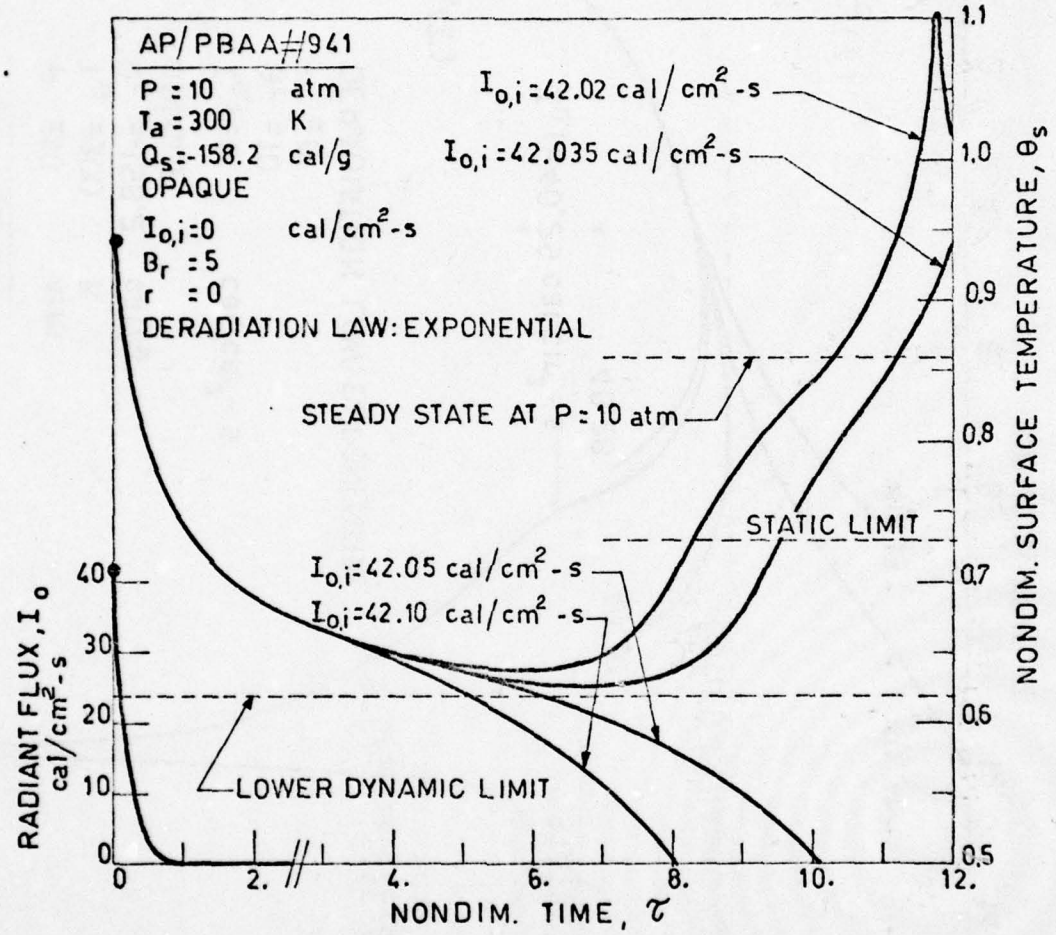
AP/PBAA#941
P = 10 atm
T_a = 300 K
Q_s = -158.2 cal/g
OPAQUE
$I_{0,i}$ = 0 cal/cm²-s
B_r = 5
r = 0
DERADIATION LAW: EXPONENTIAL
$I_{0,i}$ = 42.02 cal/cm²-s
$I_{0,i}$ = 42.035 cal/cm²-s
STEADY STATE AT P = 10 atm
STATIC LIMIT
$I_{0,i}$ = 42.05 cal/cm²-s
$I_{0,i}$ = 42.10 cal/cm²-s
LOWER DYNAMIC LIMIT
RADIANT FLUX, I_0 cal/cm²-s
NONDIM. SURFACE TEMPERATURE, θ_s
NONDIM. TIME, τ
0
10
20
30
40
0.5
0.6
0.7
0.8
0.9
1.0
1.1
2.
4.
6.
8.
10.
12.

FIG. 37

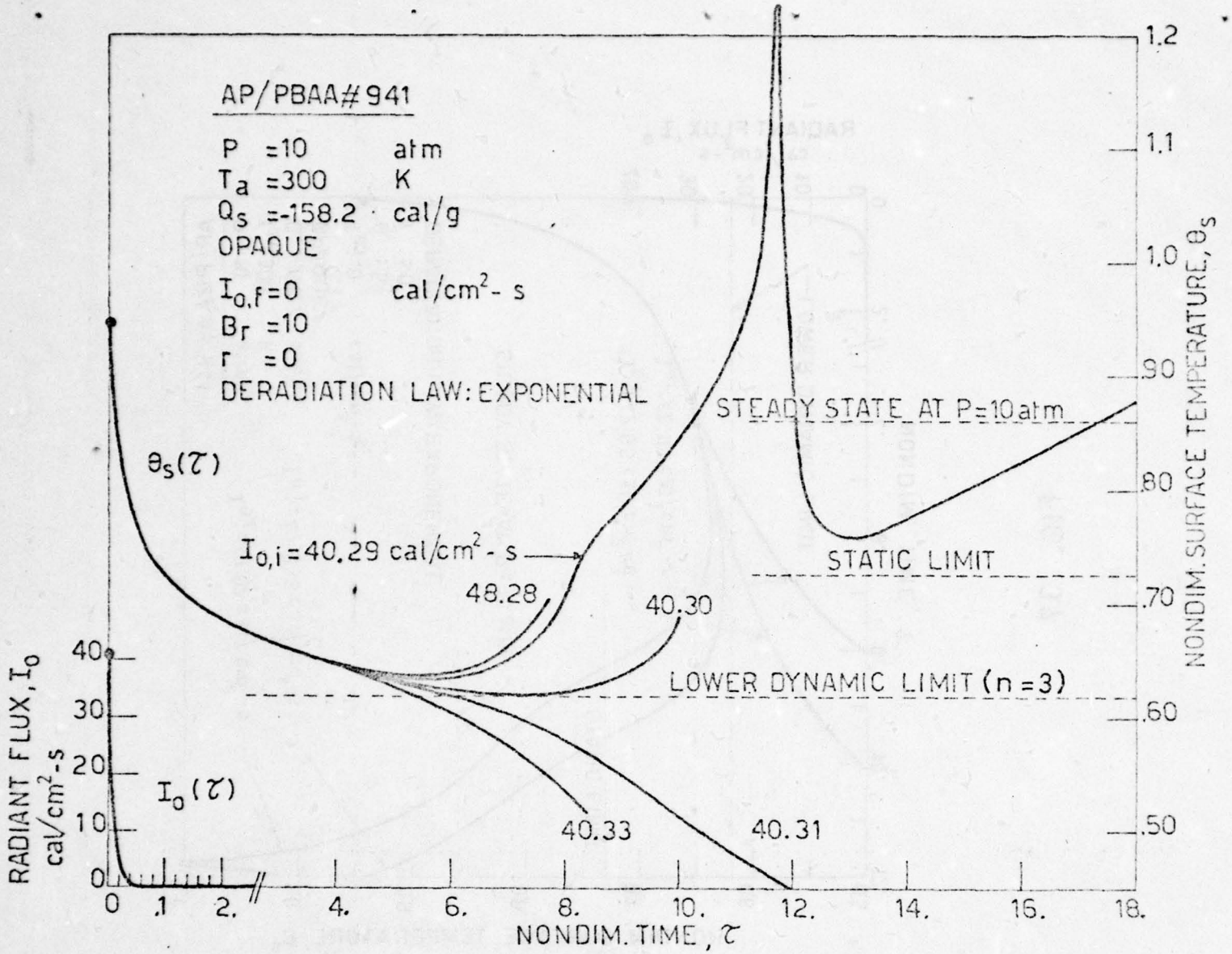
AP/PBAA#941
P =10 atm
T_a =300 K
Q_s =-158.2 cal/g
OPAQUE
$I_{0,f}$=0 cal/cm²- s
B_r =10
r =0
DERADIATION LAW: EXPONENTIAL
$\theta_s(\tau)$
$I_{0,i}$=40.29 cal/cm²- s
48.28
40.30
40.33
40.31
$I_0(\tau)$
STEADY STATE AT P=10 atm
STATIC LIMIT
LOWER DYNAMIC LIMIT (n=3)
RADIANT FLUX, I_0 cal/cm²-s
NONDIM. SURFACE TEMPERATURE, θ_s
NONDIM. TIME, τ
0
10
20
30
40
.50
.60
.70
.80
.90
1.0
1.1
1.2
0
.1
2.
4.
6.
8.
10.
12.
14.
16.
18.

FIG. 38

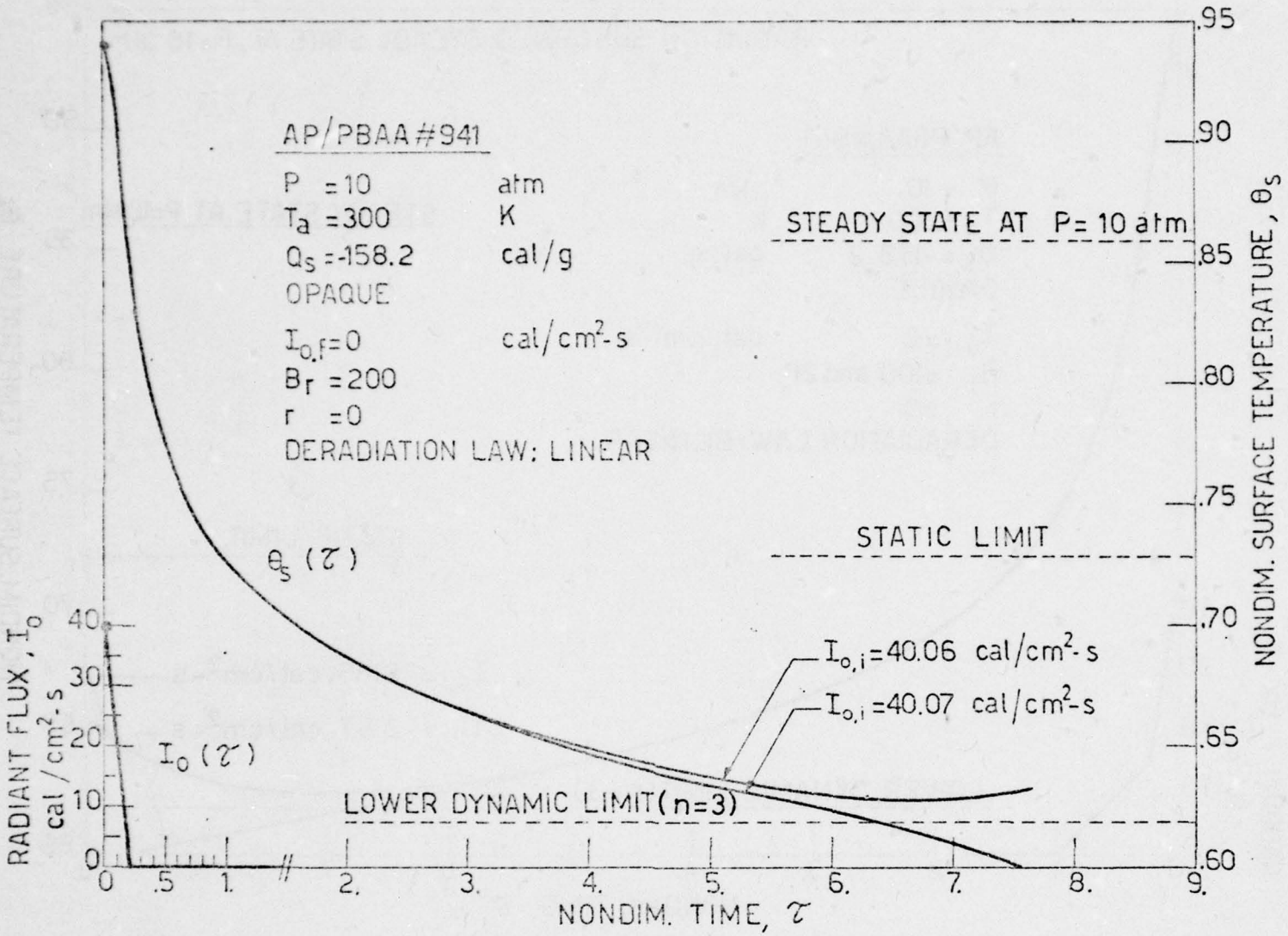
AP/PBAA#941
P =10 atm
T_a =300 K
Q_s =-158.2 cal/g
OPAQUE
$I_{o,f}$=0 cal/cm²-s
B_r =200
r =0
DERADIATION LAW: LINEAR
STEADY STATE AT P= 10 atm
STATIC LIMIT
LOWER DYNAMIC LIMIT(n=3)
$\theta_s(\tau)$
$I_o(\tau)$
$I_{o,i}$=40.06 cal/cm²-s
$I_{o,i}$=40.07 cal/cm²-s
RADIANT FLUX, I_o cal/cm²-s
NONDIM. SURFACE TEMPERATURE, θ_s
NONDIM. TIME, τ
0
10
20
30
40
.60
.65
.70
.75
.80
.85
.90
.95
0
.5
1.
2.
3.
4.
5.
6.
7.
8.
9.

FIG. 39

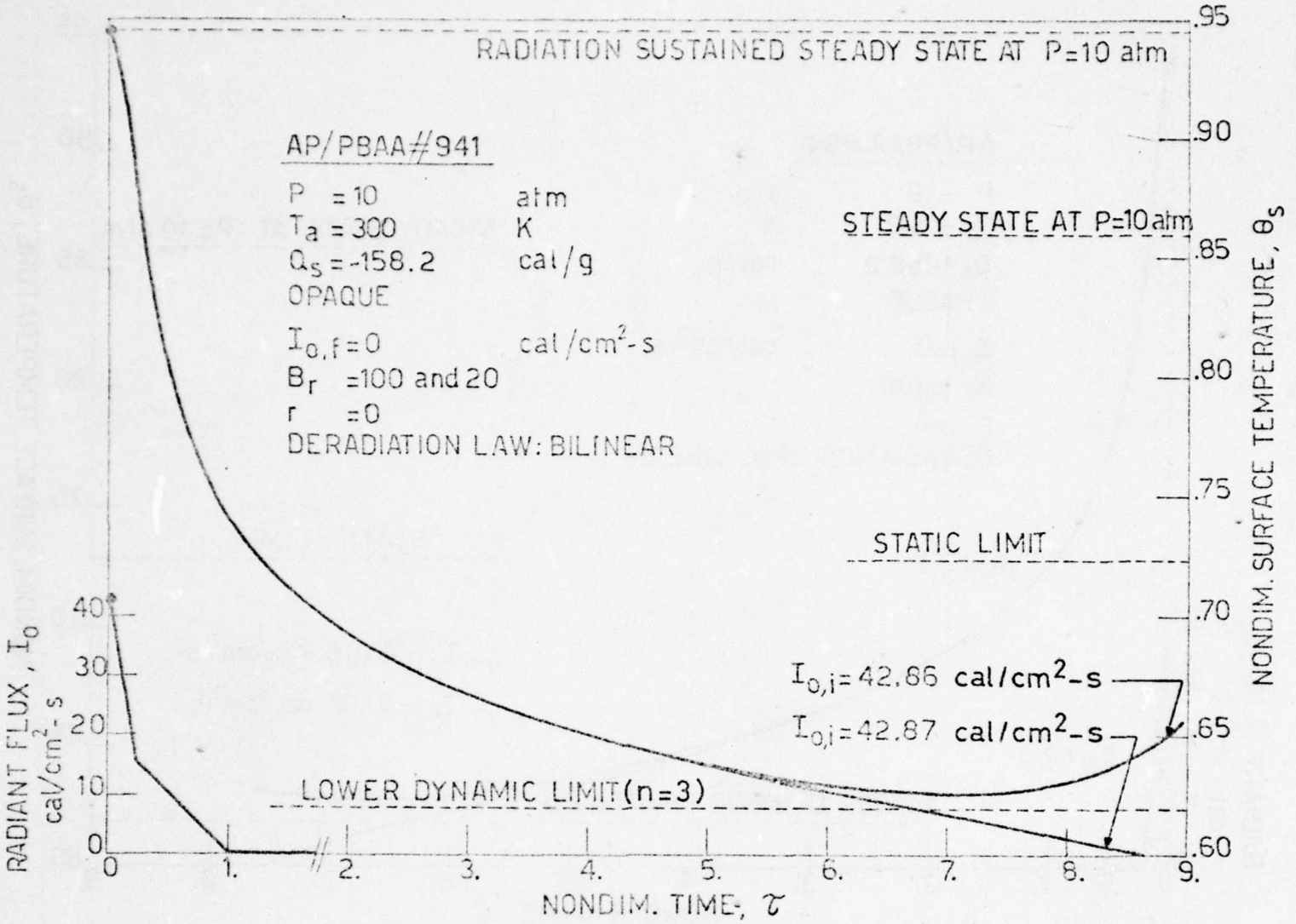
RADIATION SUSTAINED STEADY STATE AT P=10 atm
AP/PBAA#941
P = 10 atm
T_a = 300 K
Q_s = -158.2 cal/g
OPAQUE
$I_{0,f}$ = 0 cal/cm²-s
B_r = 100 and 20
r = 0
DERADIATION LAW: BILINEAR
STEADY STATE AT P=10 atm
STATIC LIMIT
$I_{0,i}$ = 42.66 cal/cm²-s
$I_{0,i}$ = 42.87 cal/cm²-s
LOWER DYNAMIC LIMIT (n=3)
RADIANT FLUX, I_0 cal/cm²-s
NONDIM. SURFACE TEMPERATURE, θ_s
NONDIM. TIME, τ
0
10
20
30
40
.60
.65
.70
.75
.80
.85
.90
.95
0
1.
2.
3.
4.
5.
6.
7.
8.
9.

FIG. 40

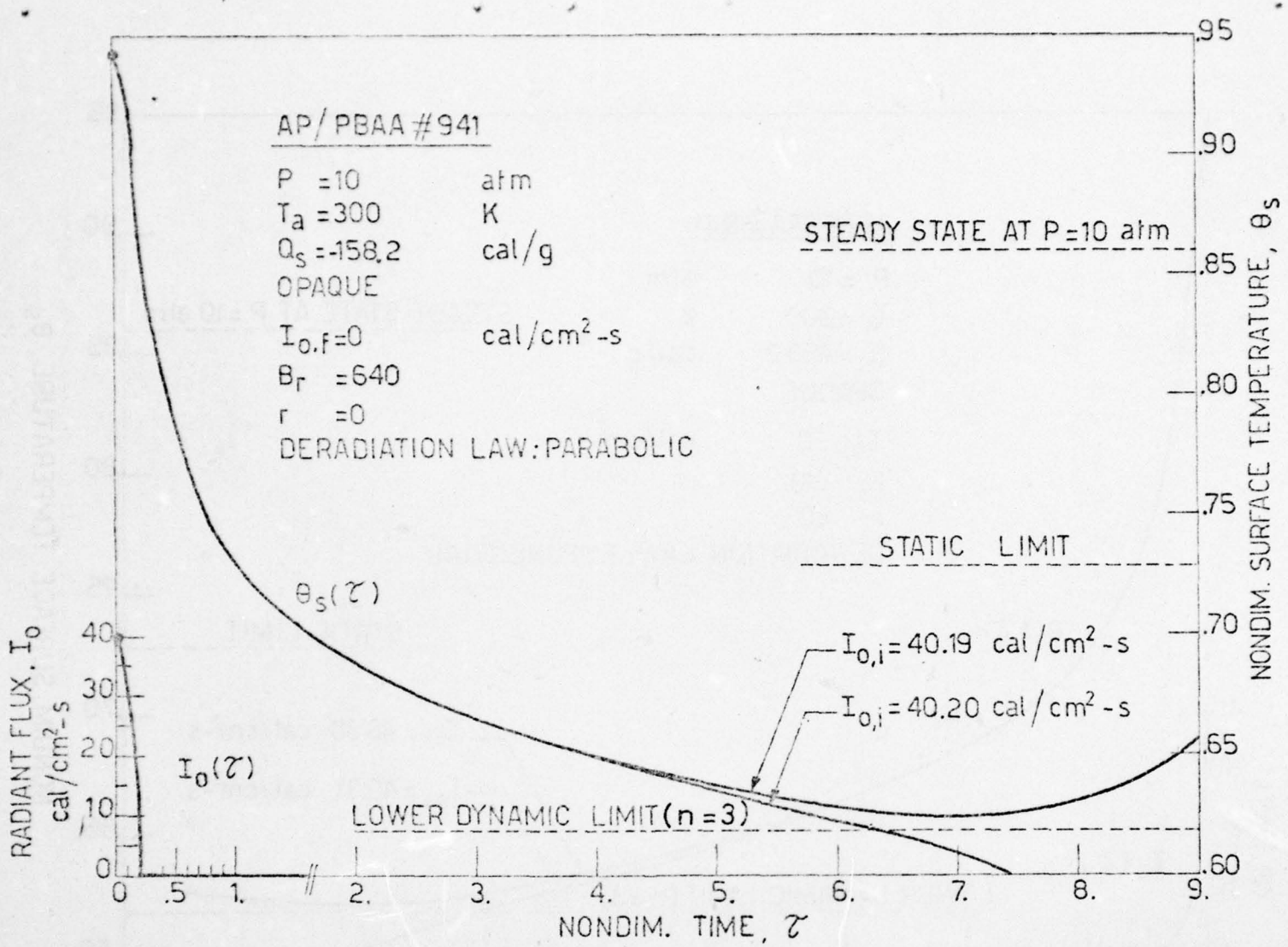
AP/PBAA #941
P =10 atm
T_a =300 K
Q_s =-158.2 cal/g
OPAQUE
$I_{o,f}$=0 cal/cm²-s
B_r =640
r =0
DERADIATION LAW: PARABOLIC
STEADY STATE AT P=10 atm
STATIC LIMIT
LOWER DYNAMIC LIMIT (n=3)
$\theta_s(\tau)$
$I_o(\tau)$
$I_{o,i}$=40.19 cal/cm²-s
$I_{o,i}$=40.20 cal/cm²-s
RADIANT FLUX, I_o cal/cm²-s
NONDIM. SURFACE TEMPERATURE, θ_s
NONDIM. TIME, τ
0
10
20
30
40
.5
1.
2.
3.
4.
5.
6.
7.
8.
9.
.60
.65
.70
.75
.80
.85
.90
.95

FIG. 41

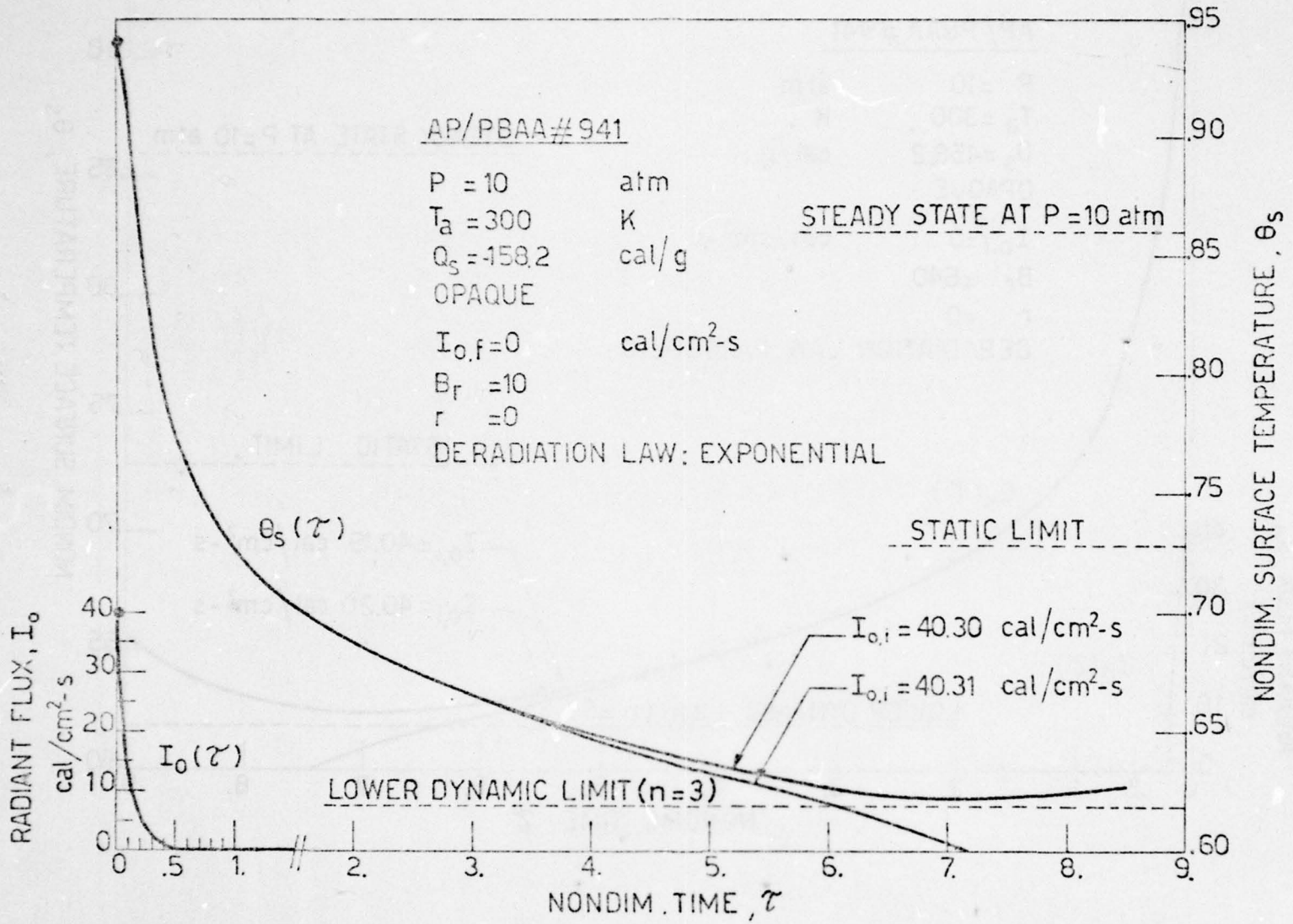
AP/PBAA#941
P = 10 atm
T_a = 300 K
Q_s = 158.2 cal/g
OPAQUE
$I_{o,f}$ = 0 cal/cm²-s
B_r = 10
r = 0
DERADIATION LAW: EXPONENTIAL
STEADY STATE AT P = 10 atm
STATIC LIMIT
LOWER DYNAMIC LIMIT (n = 3)
$\theta_s(\tau)$
$I_o(\tau)$
$I_{o,i}$ = 40.30 cal/cm²-s
$I_{o,i}$ = 40.31 cal/cm²-s
RADIANT FLUX, I_o cal/cm²-s
NONDIM. SURFACE TEMPERATURE, θ_s
NONDIM. TIME, τ
0
10
20
30
40
.60
.65
.70
.75
.80
.85
.90
.95
0
.5
1.
2.
3.
4.
5.
6.
7.
8.
9.

FIG. 42

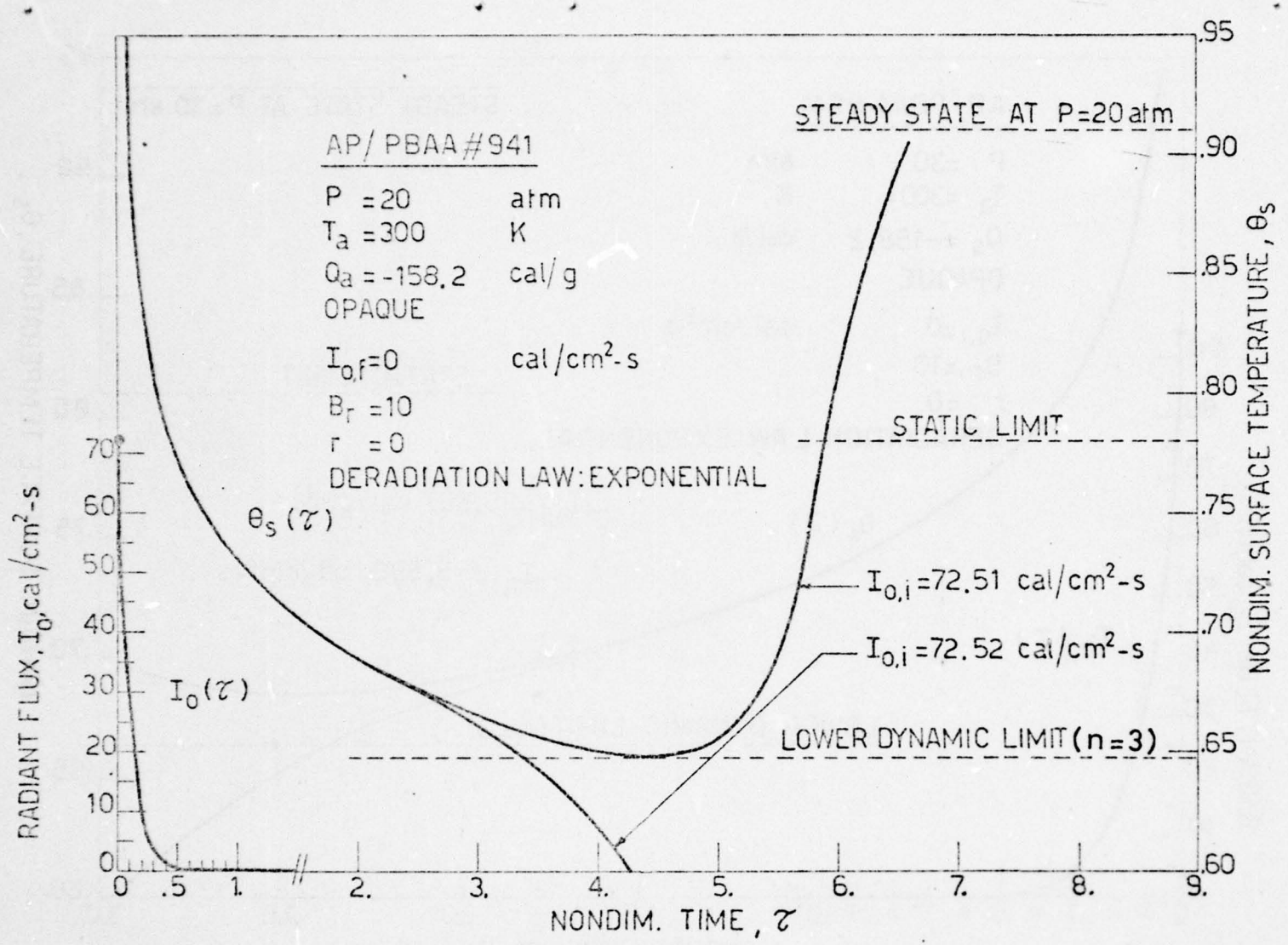
AP/ PBAA #941
P = 20 atm
T_a = 300 K
Q_a = -158.2 cal/g
OPAQUE
$I_{0,f}$ = 0 cal/cm²-s
B_r = 10
r = 0
DERADIATION LAW: EXPONENTIAL
STEADY STATE AT P=20 atm
STATIC LIMIT
LOWER DYNAMIC LIMIT (n=3)
$\theta_s(\tau)$
$I_0(\tau)$
$I_{0,i}$ = 72.51 cal/cm²-s
$I_{0,i}$ = 72.52 cal/cm²-s
RADIANT FLUX, I_0, cal/cm²-s
NONDIM. SURFACE TEMPERATURE, θ_s
NONDIM. TIME, τ
0
10
20
30
40
50
60
70
.60
.65
.70
.75
.80
.85
.90
.95
0
.5
1.
2.
3.
4.
5.
6.
7.
8.
9.

FIG. 43

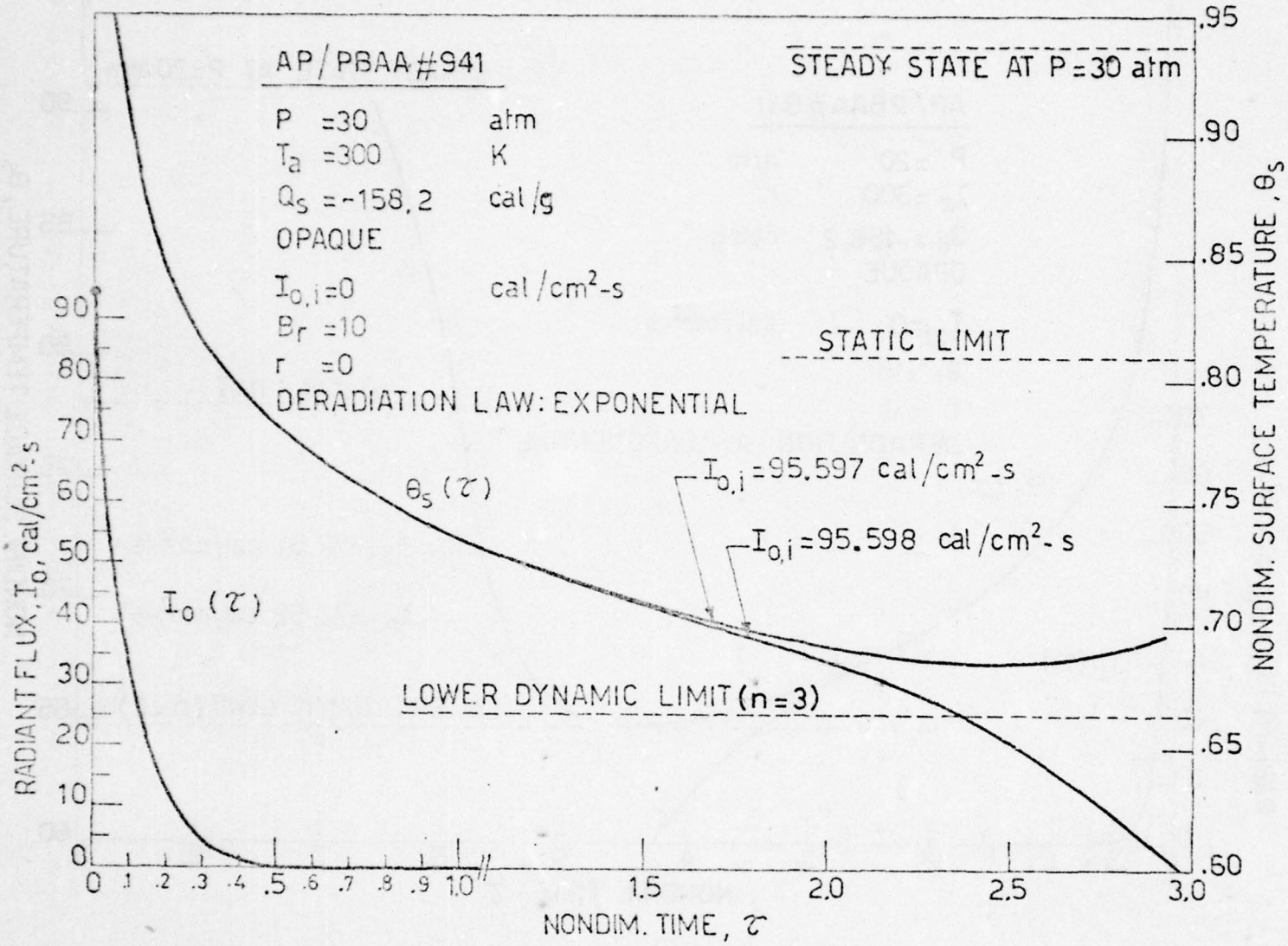
AP/PBAA#941
P =30 atm
T_a =300 K
Q_s =-158.2 cal/g
OPAQUE
$I_{0,i}$=0 cal/cm²-s
B_r =10
r =0
DERADIATION LAW: EXPONENTIAL
STEADY STATE AT P=30 atm
STATIC LIMIT
LOWER DYNAMIC LIMIT (n=3)
$\theta_s(\tau)$
$I_0(\tau)$
$I_{0,i}$=95.597 cal/cm²-s
$I_{0,i}$=95.598 cal/cm²-s
RADIANT FLUX, I_0, cal/cm²-s
NONDIM. SURFACE TEMPERATURE, θ_s
NONDIM. TIME, τ
0 10 20 30 40 50 60 70 80 90
.60 .65 .70 .75 .80 .85 .90 .95
0 .1 .2 .3 .4 .5 .6 .7 .8 .9 1.0 1.5 2.0 2.5 3.0

FIG. 44

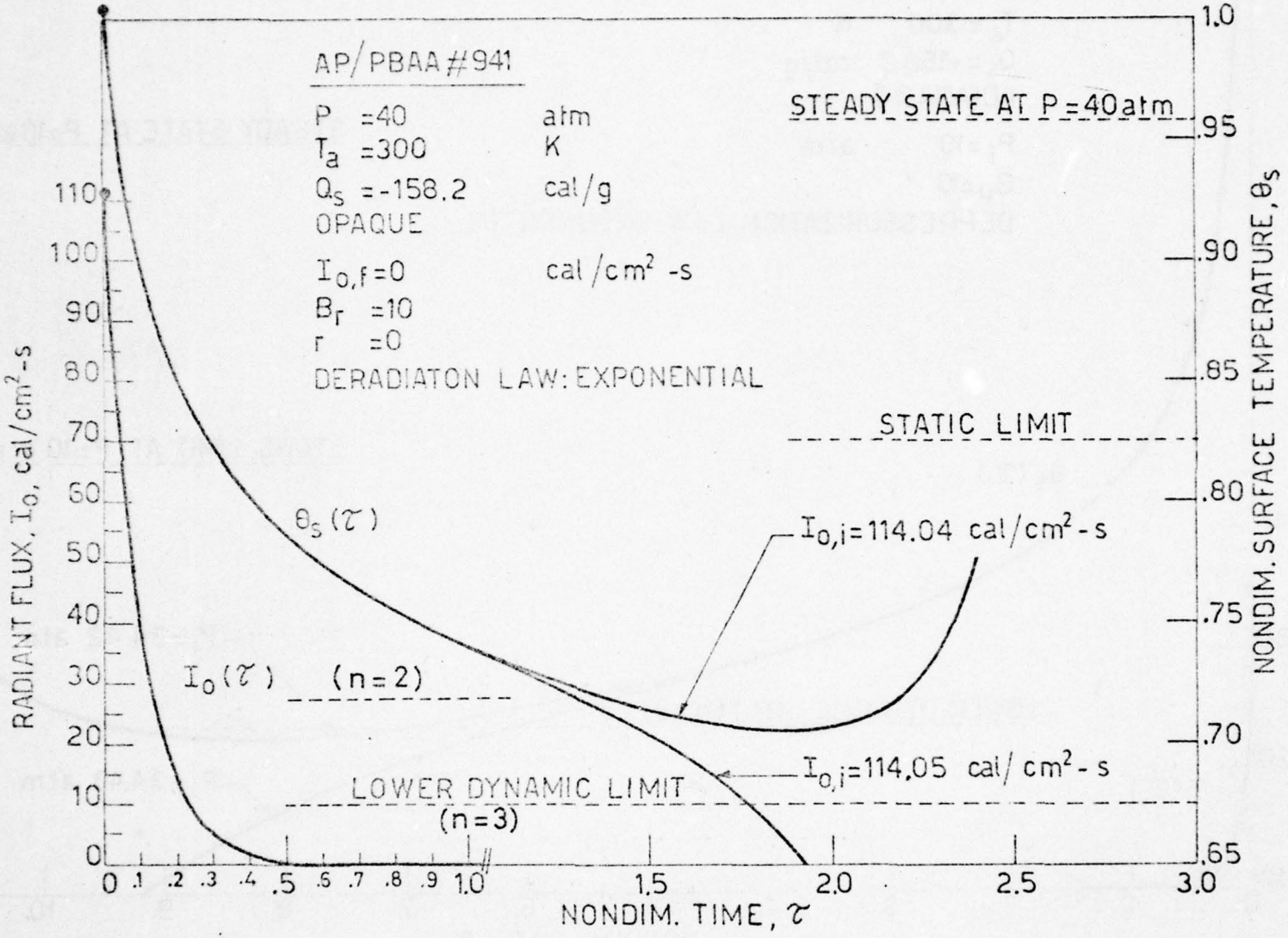
AP/PBAA #941
P =40 atm
T_a =300 K
Q_s =-158.2 cal/g
OPAQUE
$I_{o,f}$=0 cal/cm² -s
B_r =10
r =0
DERADIATON LAW: EXPONENTIAL
STEADY STATE AT P=40atm
STATIC LIMIT
$\theta_s(\tau)$
$I_{o,i}$=114.04 cal/cm² -s
$I_o(\tau)$ (n=2)
$I_{o,i}$=114.05 cal/cm² -s
LOWER DYNAMIC LIMIT
(n=3)
RADIANT FLUX, I_o, cal/cm²-s
NONDIM. SURFACE TEMPERATURE, θ_s
NONDIM. TIME, τ
0 10 20 30 40 50 60 70 80 90 100 110
.65 .70 .75 .80 .85 .90 .95 1.0
0 .1 .2 .3 .4 .5 .6 .7 .8 .9 1.0 1.5 2.0 2.5 3.0

FIG. 45

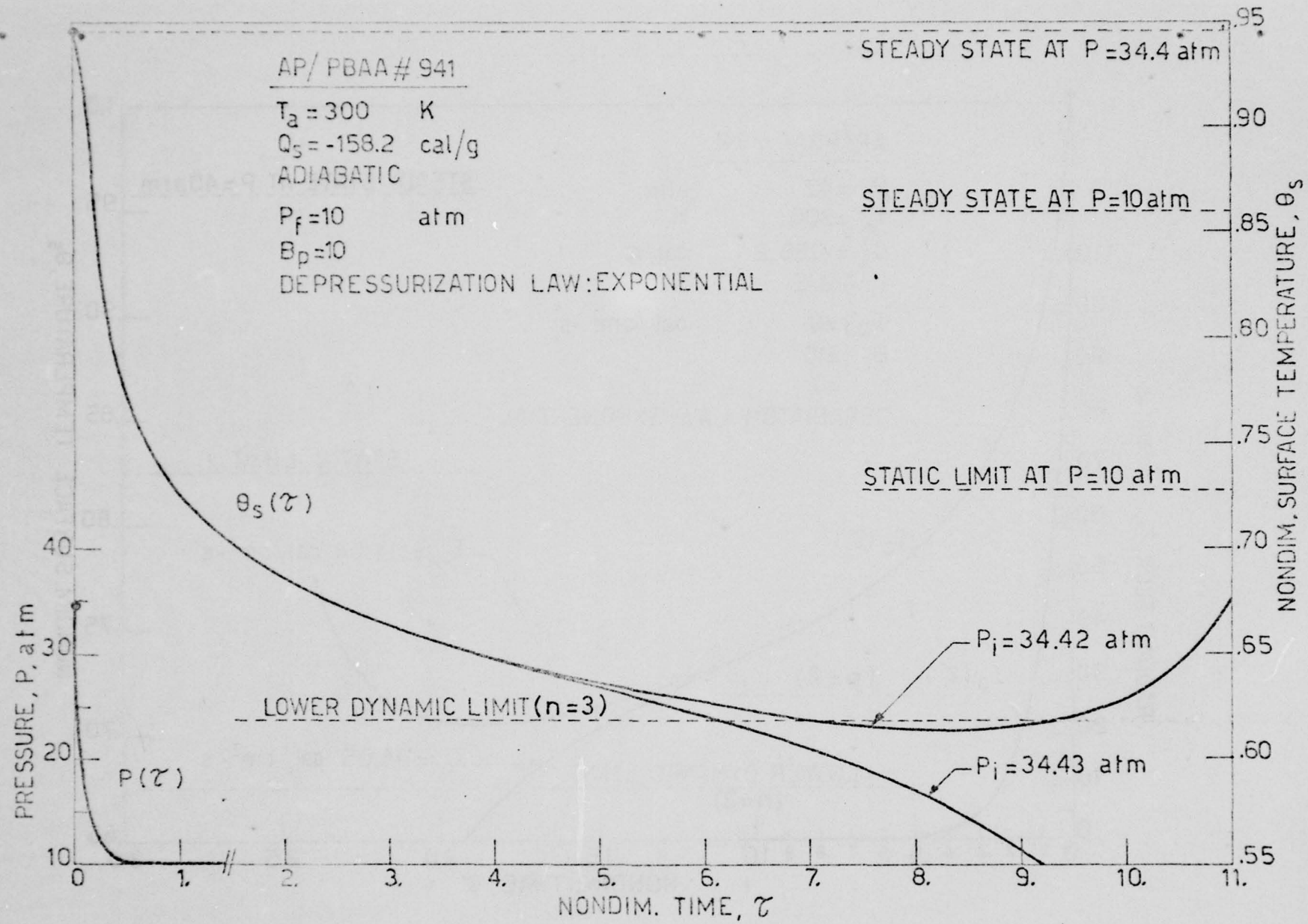
AP/ PBAA # 941
T_a = 300 K
Q_s = -158.2 cal/g
ADIABATIC
P_f = 10 atm
B_p = 10
DEPRESSURIZATION LAW: EXPONENTIAL
STEADY STATE AT P = 34.4 atm
STEADY STATE AT P = 10 atm
STATIC LIMIT AT P = 10 atm
LOWER DYNAMIC LIMIT (n = 3)
$\theta_s(\tau)$
$P(\tau)$
P_i = 34.42 atm
P_i = 34.43 atm
PRESSURE, P, atm
NONDIM. SURFACE TEMPERATURE, θ_s
NONDIM. TIME, τ
40
30
20
10
.95
.90
.85
.80
.75
.70
.65
.60
.55
0
1.
2.
3.
4.
5.
6.
7.
8.
9.
10.
11.

FIG. 46

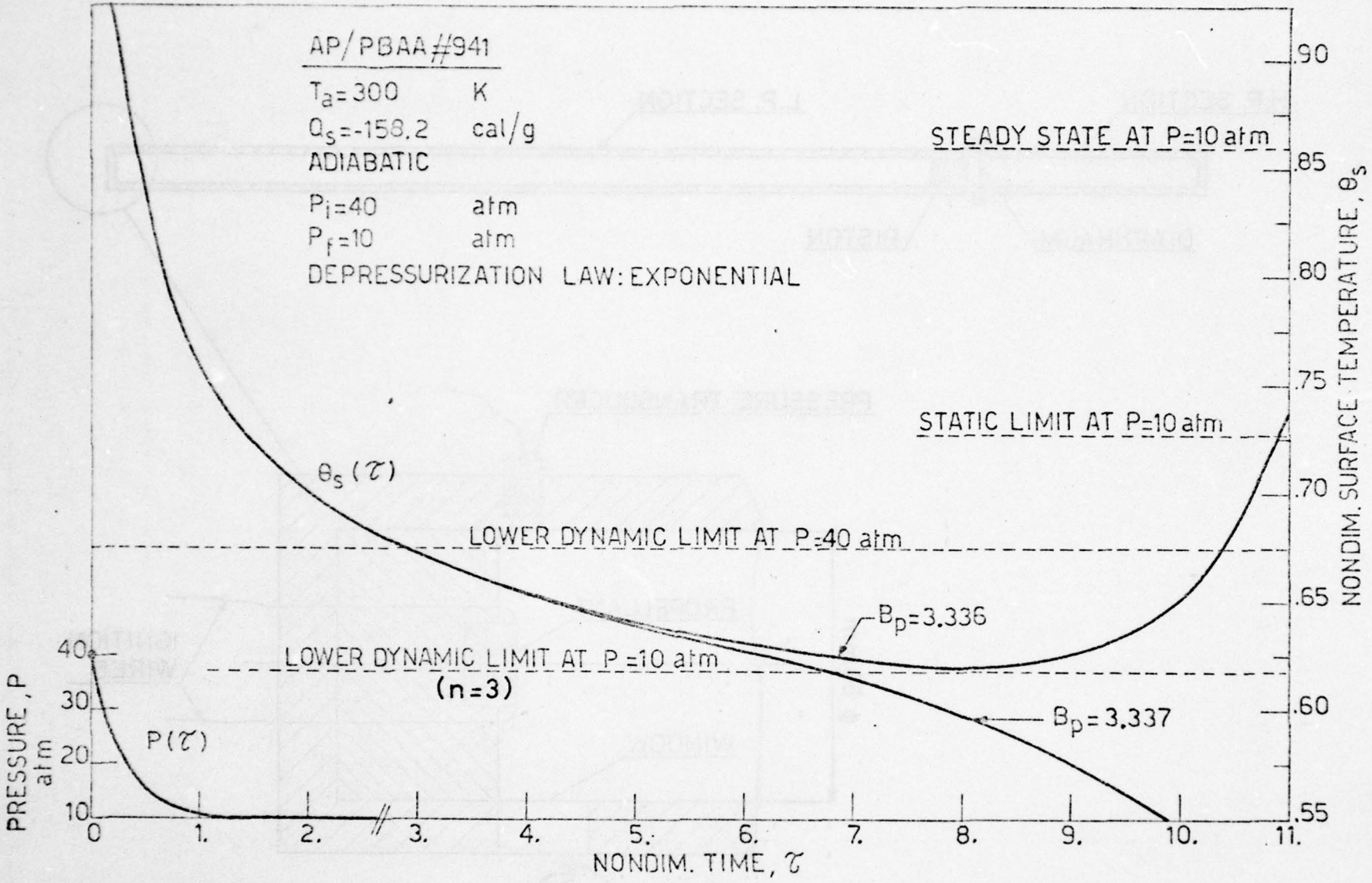
AP/PBAA#941
T_a=300 K
Q_s=-158.2 cal/g
ADIABATIC
P_i=40 atm
P_f=10 atm
DEPRESSURIZATION LAW: EXPONENTIAL
STEADY STATE AT P=10 atm
STATIC LIMIT AT P=10 atm
$\theta_s(\tau)$
LOWER DYNAMIC LIMIT AT P=40 atm
B_p=3.336
LOWER DYNAMIC LIMIT AT P=10 atm
(n=3)
B_p=3.337
P(τ)
PRESSURE, P atm
NONDIM. SURFACE TEMPERATURE, θ_s
NONDIM. TIME, τ
40
30
20
10
0
1.
2.
3.
4.
5.
6.
7.
8.
9.
10.
11.
.90
.85
.80
.75
.70
.65
.60
.55

FIG. 47

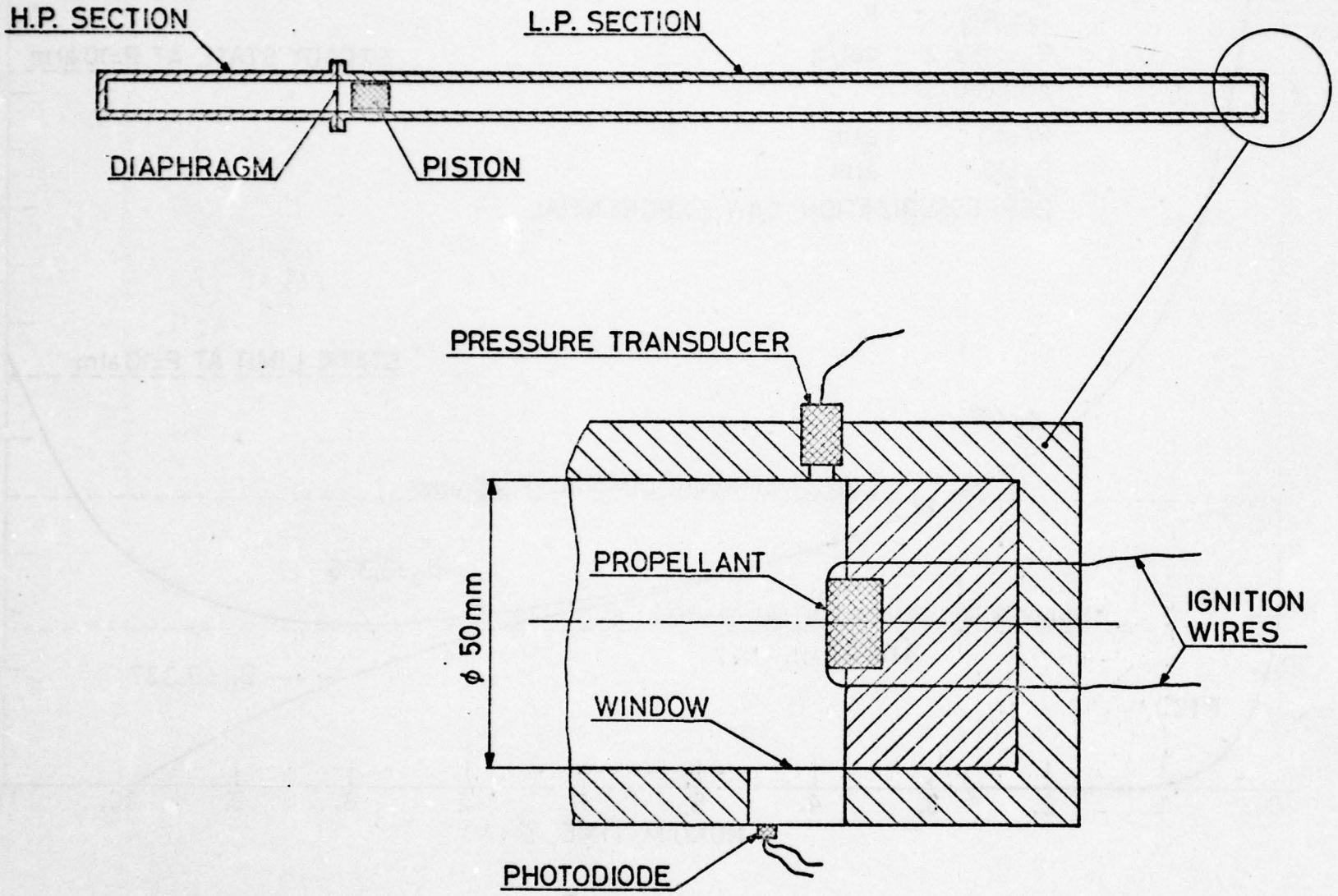
H.P. SECTION
L.P. SECTION
DIAPHRAGM
PISTON
PRESSURE TRANSDUCER
PROPELLANT
IGNITION WIRES
ϕ 50mm
WINDOW
PHOTODIODE

FIG. 48

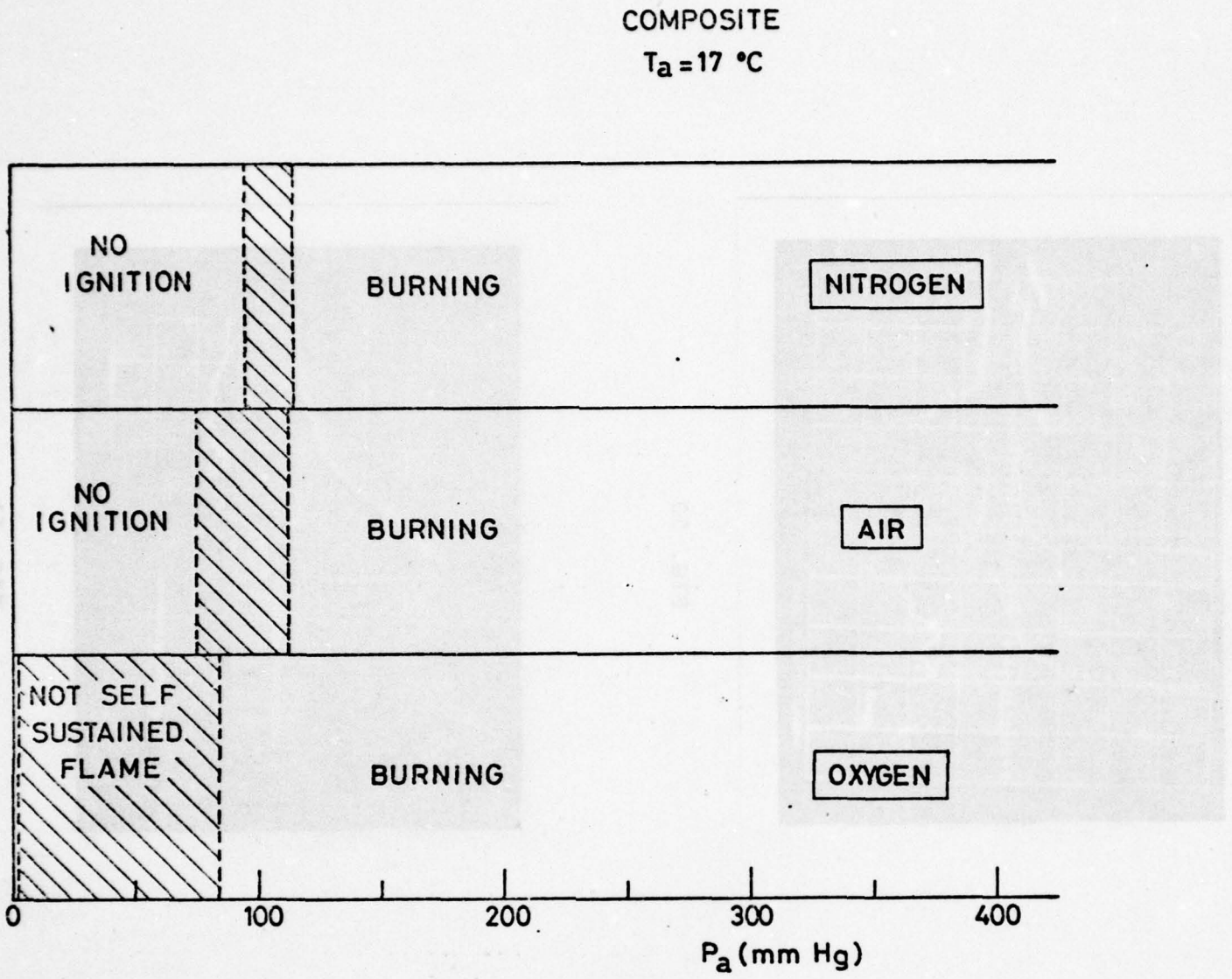
COMPOSITE
$T_a = 17$ °C
NO IGNITION
BURNING
NITROGEN
NO IGNITION
BURNING
AIR
NOT SELF SUSTAINED FLAME
BURNING
OXYGEN
0
100
200
300
400
P_a (mm Hg)

FIG. 49

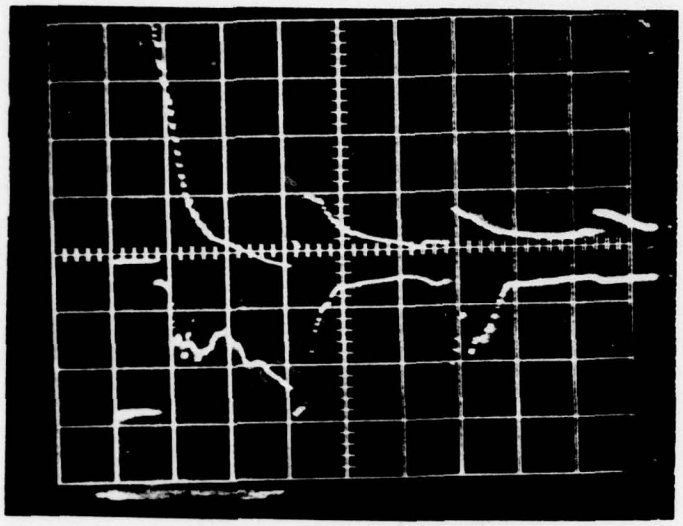

FIG. 50

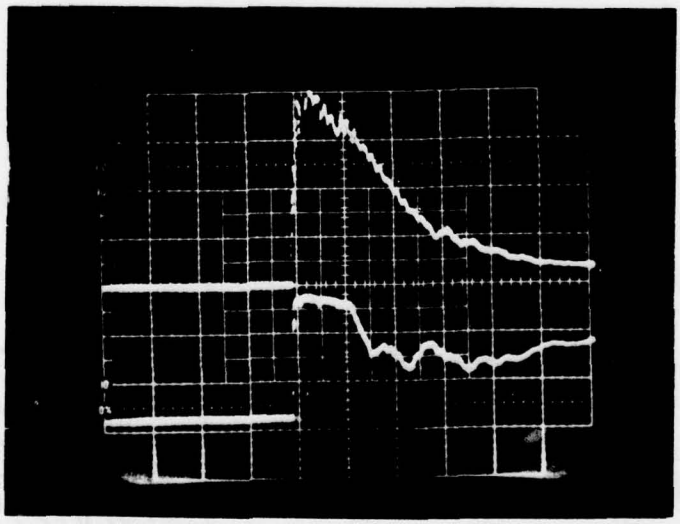

FIG. 51

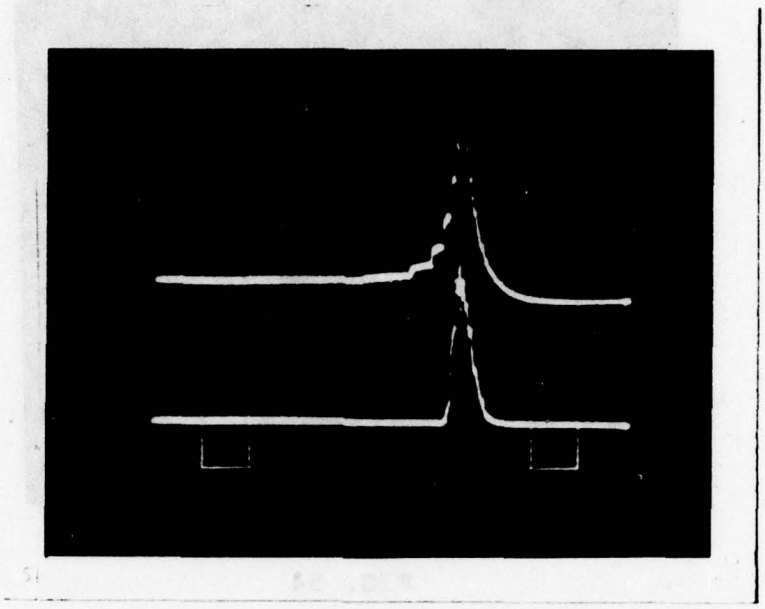

FIG. 52

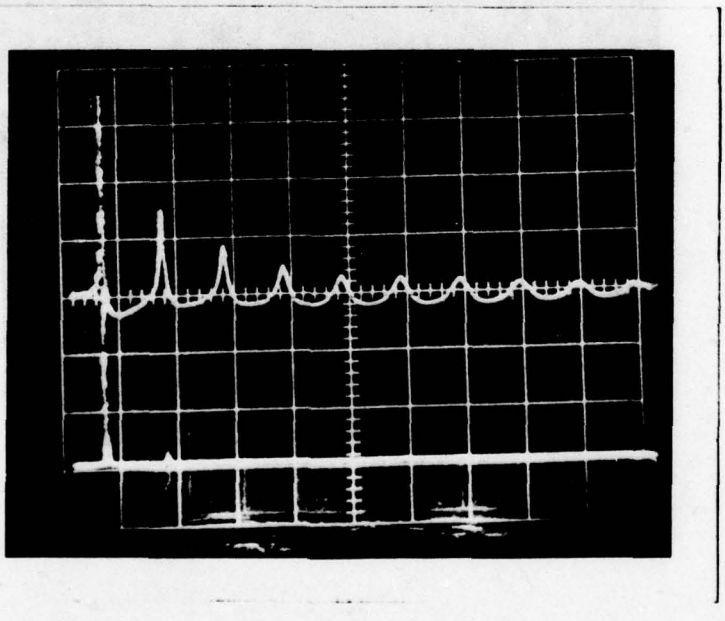

FIG. 53

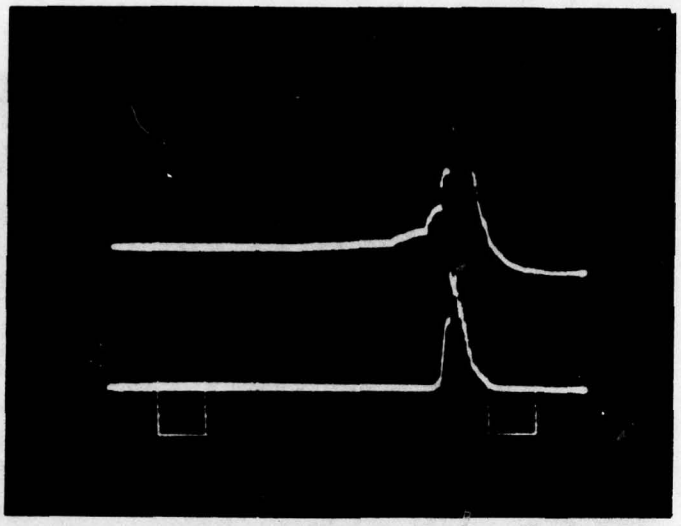

FIG. 54

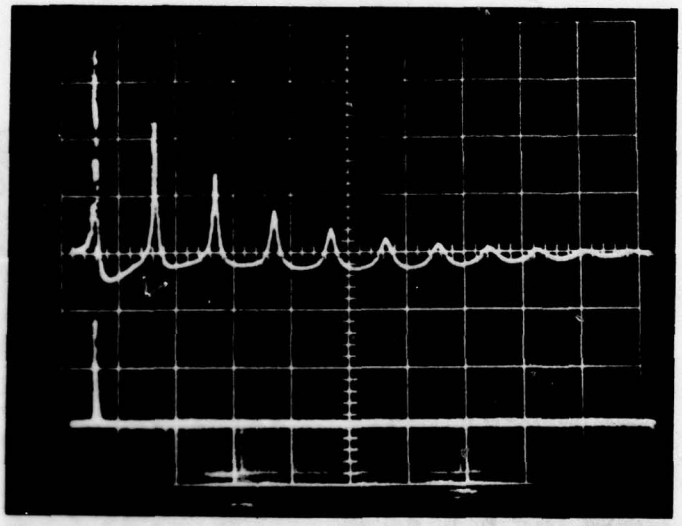

FIG. 55

CHAPTER 3

APPLICATION OF THE LASER DOPPLER VELOCI METRY TO THE FLAME STRUCTURE OF SOLID PROPELLANTS

Sec. 3.1 - INTRODUCTION

The LDV technique is intended to measure the velocity profiles in the gaseous region near the burning surface of a solid propellant. The main reason of this choice is the fact that the usual intrusive experimental techniques are of little help in a high temperature reactive medium with large thermal gradients. By other standard techniques the flame temperature, the burning rate and the condensed phase thermal profile can also be determined. This would allow to cross-check the LDV results in the gas phase zone.

A steady state strand burner, with two symmetrical and opposite optical windows, was specifically designed for LDV experiments. The operating pressure range is 1 to 15 atm. A computerized data acquisition and processing system was also realized. The facility has been applied to a steadily burning solid propellant, with the purpose of exploring the possibility of future applications to unsteady situations.

Several tests of preliminary nature were performed using double-base (DB) (both catalized and noncatalized) and ammonium perclorate (AP) based composite solid propellants. The differential mode of operation was used for the LDV instrument, with observation in the forward direction. The particles present in the plume of the burning solid propellant were used as scattering centers. Reasonably good results of the LDV measurements were obtained in the steady burning of composite propellants; in principle, useful information could be obtained in unsteady situations as well. Some problems remain to be solved and more data are needed in order to cross-check the LDV results and to clarify the uncertainties so far encountered.

Sec. 3.2 - LASER DOPPLER VELOCIMETRY

The basic principle involved in Laser Doppler Velocimetry (LDV) is the Doppler frequency shift of a monochromatic and coherent light beam scattered by micrometric particles suspended in a moving medium.

The Doppler frequency shift in normally resolved by heterodyning the scattered light with a reference beam on the surface of a photodetector (reference beam LDV). Alternatively, scattered waves coming from two incident beams can be heterodyned (differential LDV). The resulting light intensity and, hence, the photocurrent will be modulated at the Doppler frequency (Refs. 1-3).

$$f_D = 2\,U \sin(\beta/2)/\lambda \tag{3.2.1}$$

where U is the particle velocity component in the direction of the bisector of the illuminating cross-beams; $k = 2\pi/\lambda$ is the wave vector; λ is the wave-length of the laser beam and β is the angle between the two cross-beams (see Fig. 1).

LDV technique allows a direct measurement of velocity components (through the measurement of the Doppler frequency by an electronic signal processor) with a very sharp space resolution ($\simeq 0.1$ mm^3) and without disturbing the flow. This is an important feature in reactive media. However, a sufficiently large number of scattering particles ($\geq 10^8$ M^{-3}) is required to obtain continous velocity information.

The performance of an LDV system strongly depends on the size distribution and concentration of the particles scattering light into the photodetector. Particle concentration has to be high to obtain good time resolution of the velocity variation, while particle sizes have to be very small to follow spatial velocity gradients. The capability of particles to follow the gas flow can be roughly estimated from the Bassett's general equation (Refs. 4 and 5). In unsteady flows the LDV chain of instruments must be treated as a transducer for which the transfer function is determined by the dynamics of tracer particles.

Parallel measurements of particle size and density are of the greatest importance in experiments where flow seeding with particles of known size is not feasible or it cannot be assumed "a priori" that ambient particles are adeguately following the fluid flow, LDV systems can provide informations on particle size from the correlation of particle diameter with the shape of the LDV signal.

Sec. 3.3 - MIE SCATTERING

It was shown (Refs. 6-9) that the single particle Doppler signal can be accurately predicted on the basis of the Mie scattering theory. The general expression of the Doppler photocurrent, produced by a single particle crossing the geometric center of the probe volume, is given by

$$(3.3.1) \qquad i(t) = \frac{\eta I_0}{k} \left\{ P(\vartheta,\varphi) + D(\vartheta,\varphi) \cos\left[\omega_D t - \Psi(\vartheta,\varphi)\right] \right\}$$

where η is the detector sensitivity, $\omega_D = 2\pi f_D$, and the two incident beams are assumed to have equal intensities $I_{01} = I_{02} = I_0$. The term P represents the "pedestal" amplitude of the current (Fig. 2), while D represents the Doppler amplitude and Ψ determines the phase of the scattered intensity. P, D and Ψ are integral quantities, integrated over the collecting solid angle, Ω, of the receiving optics. They depend an the direction of detection (ϑ, φ), i.e. the axis of the collecting aperture, and are defined in terms of the complex amplitude functions given by the Mie theory (Refs. 10 - 12).

The quantities P, D and Ψ depend only on the scattering properties and size of the particle (for a fixed LDV geometry), whereas the photocurrent is a time-varying function of the particle position in the probe volume. Indeed, a moving fringe pattern is seen by the detector due to two beam interference and particle motion.

The fringe contrast or visibility is defined by

$$(3.3.2) \qquad V = D/P$$

The exact dependence of V on particle diameter, d, can be numerically obtained through P and D evaluated by a computer code (Ref. 9) based on Mie scattering formula. Visibility is an important parameter because its computed values can be easily compared with experimental ones.

Experimental results reported in the literature showed the possibility of parallel measurements of individual particle velocity and size (Refs. 7, 8, 9 and 13). Applications include particle size measurements from calibrated monodisperse aerosols, polydisperse fuel sprays in combustion and dusts in the atmosphere. Comparisons with other particle sizing methods indicate that, within the bounds of experimental error, the use of the visibility function yields particle size distribution measurements which agree with the results obtained by other methods.

Unfortunately, the visibility signal cannot be related to particle size over a wide range by a monotonic function (see Fig.3). Therefore, some kind of correlation of particle visibility with signal magnitude or pedestal, P, is also necessary. Moreover, the visibility is a sensitive function of the index of refraction of particles. If this parameter is unknown, some other technique has to be used. For example the measurements of the ratio of the light scattered from individual particles at

two or more finite angles. Combined results of the two techniques have been proved useful in making "in situ" measurements of particle diameters.

Sec. 3.4 - EXPERIMENTAL SET-UP

The LDV measurements were performed in a steady state strand burner, with two symmetrical and opposite optical windows, specifically designed for this purpose. In the final version of the experimental set-up (see Fig. 4), two thick lenses were mounted directly on the burner. Advantages of this configuration are simplicity and the possibility of utilising all of the small window aperture that is available.

The differential LDV mode was chosen because of its higher signal to noise characteristics at moderate particle concentrations. Moreover, this type of LDV system is the best suited for individual realization velocimetry and parallel particle size analysis. It is not difficult to realize the situation in which the Doppler signal, that is available for processing, is produced by no more than one particle in the probe volume at a time. In fact, it is possible to adjust the probe volume dimensions, both in diameter and in length, by selecting the proper cross-beam angle β and the magnification of the light collecting system. Typical values relative to our experiments are given in Table 1. The main advantage of the differential LDV is that it is quite simple to align and is not sensitive to small vibrations. Also, the Doppler frequency is independent of the detection angle and a large collection aperture can be used without a spread of Doppler frequency.

The LDV system comprises a 5 mW He-Ne laser and a beam splitter with variable beam separation, which allows continuous variation of the cross-beam angle. The two incident parallel laser beams were directed toward the lens L_1, in such a way that one laser beam was centered on the lens axis. This beam is not diverted from its horizontal direction, but focused on the focal point (on the axis of the strand burner). The second beam is impinging on the lens L_1 at a distance h from the axis, and is deflected and focused in the same focal point. The crossing region defines the probe volume of the LDV system and the velocity component in the vertical direction can be measured. With the geometry of Fig. 4 the measured velocity component is not exactly the axial one; however the difference, of the order of $\sin(\beta/2)$, is not significant for small β.

LDV experiments were performed by using as scattering centers the particles present in the plume of the burning solid propellant sample. No external seeding was used in order to avoid any disturbance of the combustion processes. Preliminary experiments showed that, generally, sufficiently high particle rates are found in the region near the burning surface.

The experimental conditions are now schematically described. Initially, the rod of solid propellant, centered on the axis of the burner, shuts out the two incident laser beams.

When the rod burns, its surface goes down and at the instant t_o the horizontal beam is allowed to pass. After a delay Δt, the second beam is also passing and the scattered light with Doppler informations is received by the photomultiplier. A triggering signal, coming out from the photodiode (P.D.) intercepting the horizontal beam, precisely defines the instant t_o. From this the axial position of the LDV probe volume, with respect to the burning surface, can be inferred by comparison of the time delay and the propellant burning rate. The strand burner is also equipped for simultaneous measurements of the propellant burning rate and the instantaneous pressure (Ref. 14).

The receiving optics of the LDV system comprises: the lens L_2, fixed on the burner window, that collects the radiation scattered in the forward direction; the lens L_3 that is movable and focuses the scattered light on a 0.3 mm pinhole in front of a photomultiplier. This is equipped with an interferential optical filter, centered at 632.8 $\pm$ 1.0 nm (the laser wave-length), in order to reject flame emission.

The photomultiplier signal is processed by an electronic counter processor (DISA mod. 55L90) that allows working with variable particle concentrations and does not have dropout problems. Moreover, it has a large dynamic range and no slewrate limitations; it accepts individual signals and determine the correct Doppler frequency, hence, the particle velocity. Proper use of this instrument would require rejection of multiple particle signals, because of random phase fluctuations which will lead to incorrect velocity measurements (Ref. 15). This requirement can be generally satisfied by proper reduction of the probe volume dimensions.

Sec. 3.5 - EXPERIMENTAL RESULTS

A typical individual Doppler signal, after amplification and band-pass filtering, is shown in Fig. 5. Many of these signals were recovered in order to optimize the optical system and to define the effective probe volume dimension, by comparing the observed and the computed fringe number.

With the experimental conditions summarized in Tab. 1 and the solid propellants used, we observed that generally no more than one particle at once was present in the probe volume. If the pass-band filtered Doppler signal, relative to each particle, satisfies a number of validation conditions (in terms of amplitude level and signal to noise ratio), the counter processor measures the Doppler frequency by means of a zero-crossing method. The output is velocity information that is retained until another particle gives a validated signal.

During preliminary experiments, the velocity time history was monitored by a storage oscilloscope (Tektronix, mod.466), after digital to analog conversion of the output of the Doppler counter processor . Typical results obtained with a noncatalyzed double-base (a,b) and an AP based composite propellants (c, d) are reported in Fig. 6. The upper trace is the continuous recording of the photodiode output; the lower trace is the velocity recording in which each point corresponds to a single particle measurement. Oscilloscope records are triggered by the photodiode signal and have the same time base. It can be noted that large variations with sharp gradients characterise the velocity of the DB propellant in conjunction with irregular fluctuations in the particle rate (i.e. the number of points/div. in velocity traces). At exactly the same experimental conditions, higher particle rates and more regular velocity traces were found with the AP propellant.

The time resolution of the LDV measurements depends on the particle rate, $\dot{n}$, hence on the particle concentration N, the mean particle axial velocity $\bar{U}$ and the probe volume cross-section S:

$$\dot{n} = \alpha N \bar{U} S \qquad (3.5.1)$$

where α is an efficiency factor taking into account the validation rate of particle signals from the counter processor. In our experiments with double-base propellants the time history of $\dot{n}$ was measured by a multiscaler. Many tests were made during preliminary velocity measurements and the mean values of $\dot{n}$ for different optical and electronic configurations of the LDV were determined in order to match the optical system to the mean particle concentration. Large fluctuations in $\dot{n}$ were found from 0 to a maximum value of about 1 KHz that will correspond to a particle concentration of about 2×10^8 m^{-3}.

With these experimental conditions the LDV cannot provide a continuous record of the gas velocity. Moreover, since the particles cross randomly the probe volume, they provide a randomly sampled time series of the fluctuating velocity. Time resolution can be limited by this characteristic. This is an important feature for unsteady situations and rapidly fluctuating flows. As far as a steady state situation is concerned, the particle rate is more than adequate to velocity measurements by LDV. Present results are limited to this case.

Data reduction was performed by a minicomputer (WANG, mod. 2200). The computer interface, which reads the velocity data supplied by the counter processor, was activated by a triggering pulse derived by the photodiode signal. Once the data relative to one test (about 2,000 velocity measurements) have been acquired into memory, they are transferred to a tape for permanent storage. To date, with the minicomputer at our disposal, the maximum data acquisition rate is of about 2 KHz. Analysis programs have been developed for the LDV measurements and are described in Ref. 16. An example of the results obtained with this computerized system is shown in Fig. 7. Points represent the mean velocity evaluated in a fixed period of time (= 12.5 ms) over about 10-20 particles. The total time base covers more than 1 s, corresponding to the burning of about 5 mm of the solid propellant sample. This velocity curve refers to the same experimental test of Fig. 6 d.

Sec. 3.6 - CONCLUSIONS AND FUTURE WORK

Data collected up to now suggest the possibility of resonable measurements of particle velocity in the gaseous region above the burning surface. So far, only tests in a steady state situation at pressures up to 6 atm were performed, but futher progress is being made. The possibility of instantaneous measurements of gas velocity versus time is strictly dependent on scattering particle concentration and particle size distribution. Generally, particle concentration is not uniform in time and depends on the solid propellant type; particle size distribution is, up to now, an unknown parameter and will be of fundamental importance to determine it in order to be sure that particles follow the gas flow.

The minimum time resolution that can be obtained depends on the mean particle velocity ($\simeq$ 15 m/s), the probe volume dimension in the axial direction (=0.15 mm) and the particle rate. If the typical transit time for a particle to cross the probe volume is of about 10 μs, the maximum particle rate could be 100 KHz, still satisfying the condition of single particle scattering. This theoretical result is well above the observed one and, in our situation, is quite impossible to define a fixed time resolution because of the large fluctuations of particle rate.

Several tens of runs with the LDV technique show more complicated profiles than expected. Although results are not always reproducible, we may affirm that the velocity behaviour presents wide irregular fluctuations in the case of the DB propellants (Fig. 6 a and b) and a surprising minimum after about 200 ms in some tests with the AP propellant (Fig. 7). In all runs a large velocity dispersion (up to 20%) was observed around the mean value; this is difficult to explain on the basis of fluidynamics considerations. Comparison with shadograph pictures at similar test conditions suggest a quasi-monodimensional laminar gas flow.

The discrepancy with the presumed steady state laminar flame conditions could be due to a polydisperse particle size distribution and the consequent difficulty for larger particles or agglomerates to follow accurately the gas flow. Indeed, the measured mean velocities, for both the DB and AP propellant, seem to be below (about 30%) the values obtained by the measured burning rate of the condensed phase and the estimated flame temperature, assuming a quasi-steady state mass balance. In addition, overlapping effects are due to somewhat time-varying pressure during the burning of the solid propellant.

The precision of the LDV instrument itself could be questioned, in this difficult application, but comparative tests with cold flows in the same burner and the analysis of a large number of Doppler signals during burning conditions con-

firmed the reliability of LDV measurements with experimental errors in the bounds of + 5%.

In conclusion, a polydisperse particle size distribution could be the major source of the wide spread in the measured instantaneous velocities. Indeed, the particle size evaluation by means of electron microscope analysis seems to confirm this hypothesis, showing a large number of particle diameter well above 10 μm. However the particle capture could cause agglomeration and clustering. The same phenomena may also occur while particles are traveling and reacting in the gaseous stream and this could explain the behaviour of Fig. 7.

To resolve this problem, a research program is starting with the purpose of a systematic analysis of particle size. The first attempt will be performed by measuring relative scattered light intensities at different scattered angles and comparing with theoretical values computed on the basis of the Mie theory. Qualitative informations could be obtained, but is should be noted that this technique is only applicable to particle diameters in the range of 0.5 μm to 5 μm (Ref.17). Particle sizing by visibility measurements will be used to measure diameters in the range 5 μm to 50 μm. The second tecnique has been proven practical in making in situ measurements of particle diameters simultaneously with measurements of velocity and particle concentration (Ref.13). The ideal situation will be characterised by the possibility of parallel measurement of size and velocity for each individual particle. This is possible, in principle, but requires a more sophisticated and expensive electronic instrumentation.

REFERENCES

1) Durst, F., Melling, A., and Whitelaw, J.H., "Principles and Practice of Laser Doppler Anemometry", Academic Press, 1976.

2) Durrani, T.S., and Greated, C.A., "Laser Systems in Flow Measurement", Plenum Press, 1977.

3) Watrasiewicz, B.M., and Rudd, M.J., "Laser Doppler Measurements", Butterworths, 1976.

4) Soo, S.L.,"The Physics of Fluids", 18,2, 1975.

5) Melling, A., and Whitelaw, J.H., Proceedings of the LDA Symposium, pp. 382-402, Copenhagen, 1975.

6) Adrian, R.J., and Orloff, K.L., Applied Optics, 16,3,1977.

7) Adrian, R.J., and Earley, W.L., Proceedings of the Minnesota Symposium on laser anemomtry, pp. 426-454, Minneapolis, Minnesota, 1976.

8) Chu, W.P., and Robinson, D.M., Applied Optics, 16,3, pp. 619-626, 1977.

9) Coghe, A., and Ghezzi, U.,"LDA signal processing",Dynamic Flow Conference, Marseille, 1978.

10) Kerker, M., "The Scattering of Light", Academic Press, 1969.

11) Born, M., and Wolf, E., "Principles of Optics", Pergamon Press, 1975.

12) Van de Hulst, C.H., "Light Scattering by Small Particles", J. Wiley, 1957.

13) Farmer, W.M.,"Measurement of particle size and concentrations using LDV techniques", Dynamic Flow Conference, Baltimore, 1978.

14) De Luca, L., and Zanotti, C.,"Measurement of steady solid propellant burning rate and data processing", XXXII Congresso ATI, Roma 1977.

15) George, W.K., Proceedings of the LDA Symposium, pp. 20-63, Copenhagen, 1975.

16) Coghe, A., Sensalari, G.L., and Volpi, A. C.N.P.M. NT/RT No. 305, Politecnico di Milano, 1978.

17) Bacholo, W.D., Particle field measurements in coal-fired systems, Dynamic Flow Conference, Baltimore, 1978.

TABLE 1

Laser wavelength	632.8 nm
Cross angle	4.70^{o}
Fringe spacing	7.7 μm
Probe vol. dimension	3 x 0.15 x 0.15 mm^3
Fringe number	20
Collecting solid angle	4^{o}
Magnification of the collecting optics	2

Optical features of the LDV experimental set-up used in this work.

LIST OF FIGURES

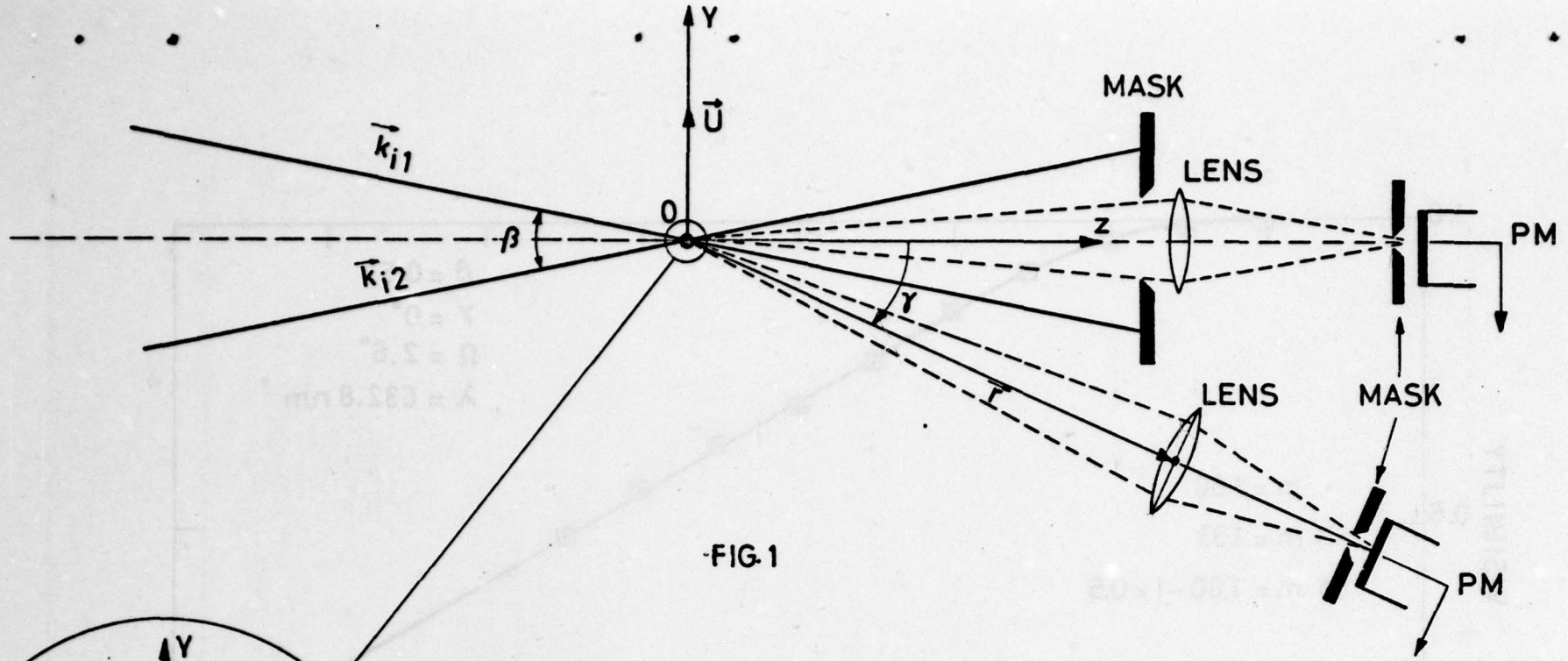
Y
$\vec{U}$
$\vec{k}_{i1}$
$\vec{k}_{i2}$
β
0
z
MASK
LENS
PM
γ
r
LENS
MASK
PM

FIG. 1

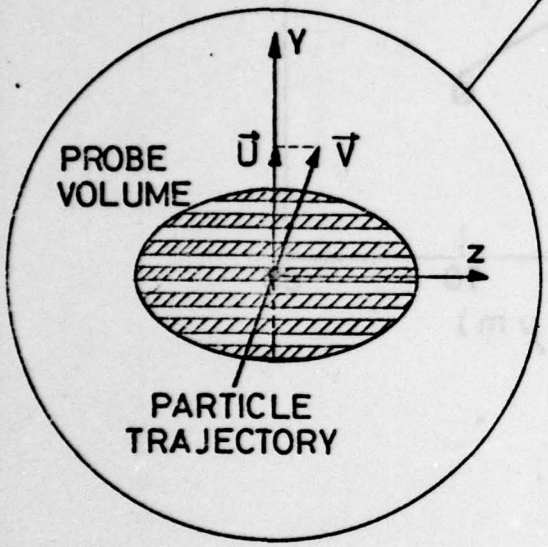
Y
PROBE VOLUME
$\vec{U}$
$\vec{V}$
z
PARTICLE TRAJECTORY

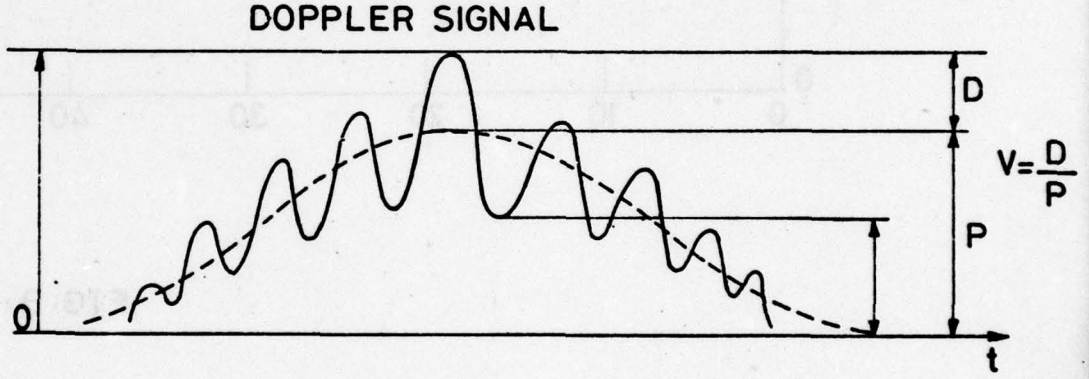
DOPPLER SIGNAL
D
P
$V=\frac{D}{P}$
0
t

FIG. 2

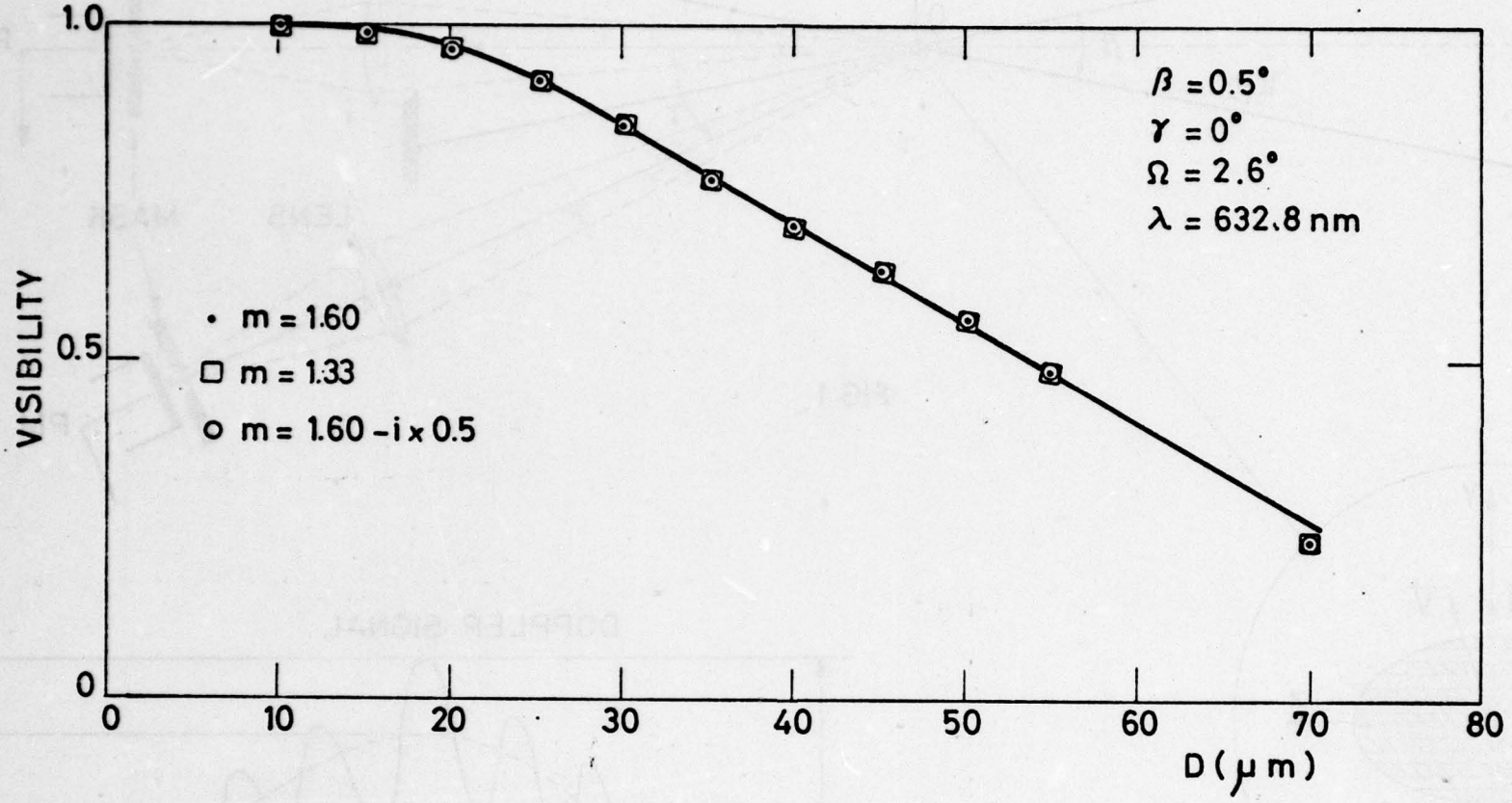
1.0
0.5
0
VISIBILITY
β = 0.5°
γ = 0°
Ω = 2.6°
λ = 632.8 nm
• m = 1.60
□ m = 1.33
○ m = 1.60 - i x 0.5
0
10
20
30
40
50
60
70
80
D (μm)

FIG. 3

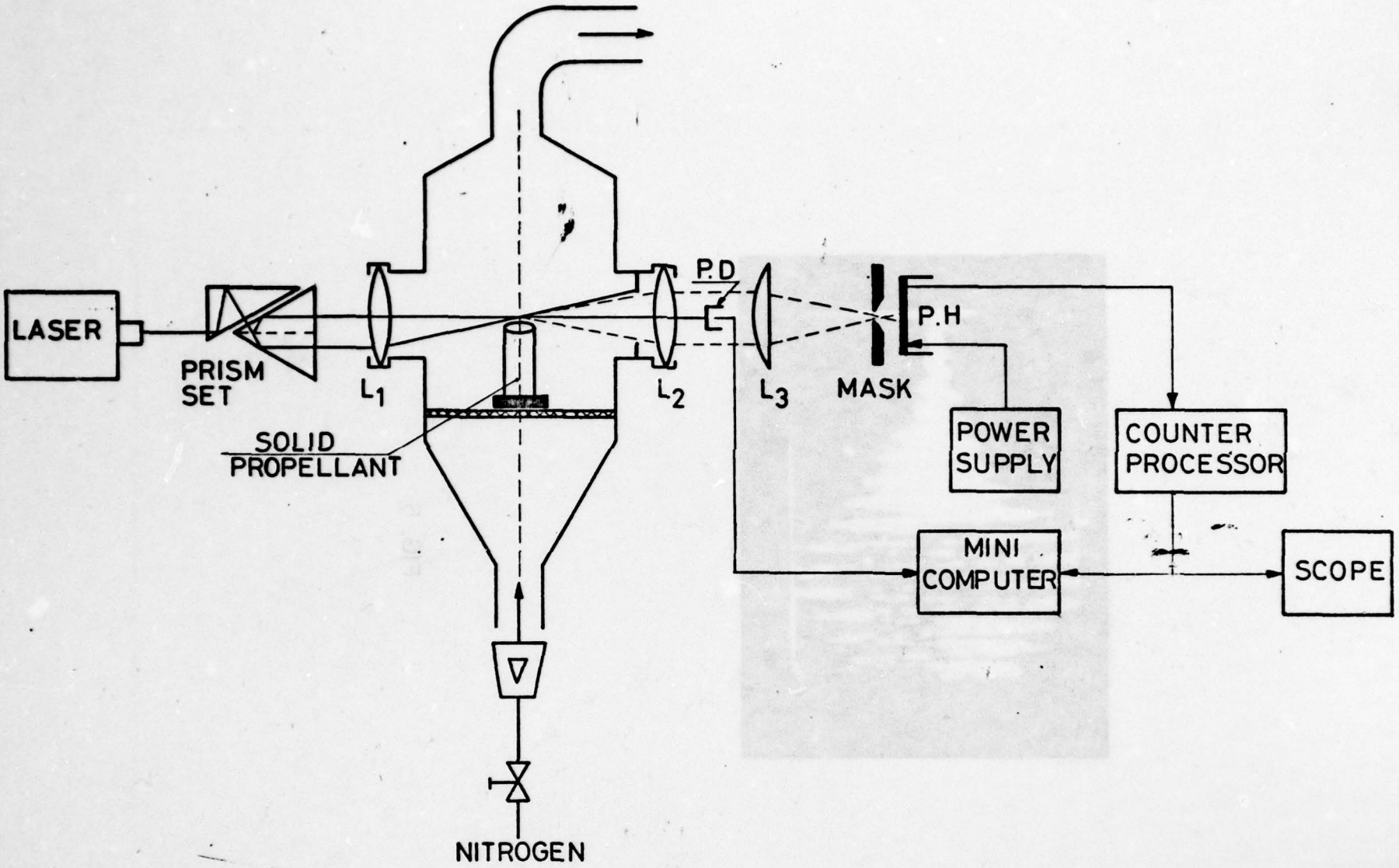
LASER
PRISM SET
L1
L2
L3
P.D
P.H
MASK
SOLID PROPELLANT
POWER SUPPLY
COUNTER PROCESSOR
MINI COMPUTER
SCOPE
NITROGEN

FIG. 4

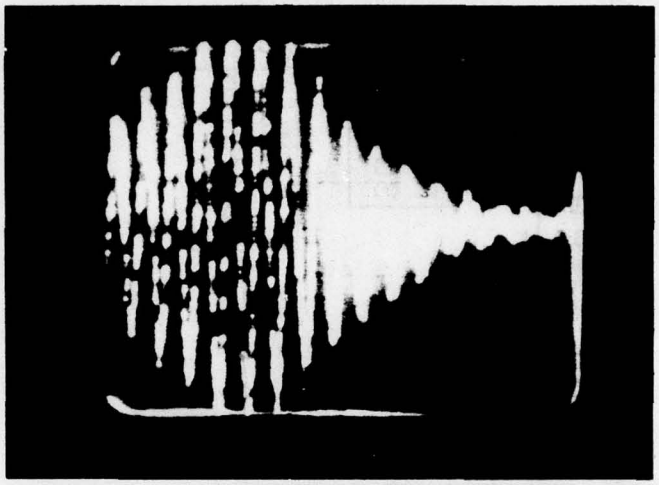

FIG. 5

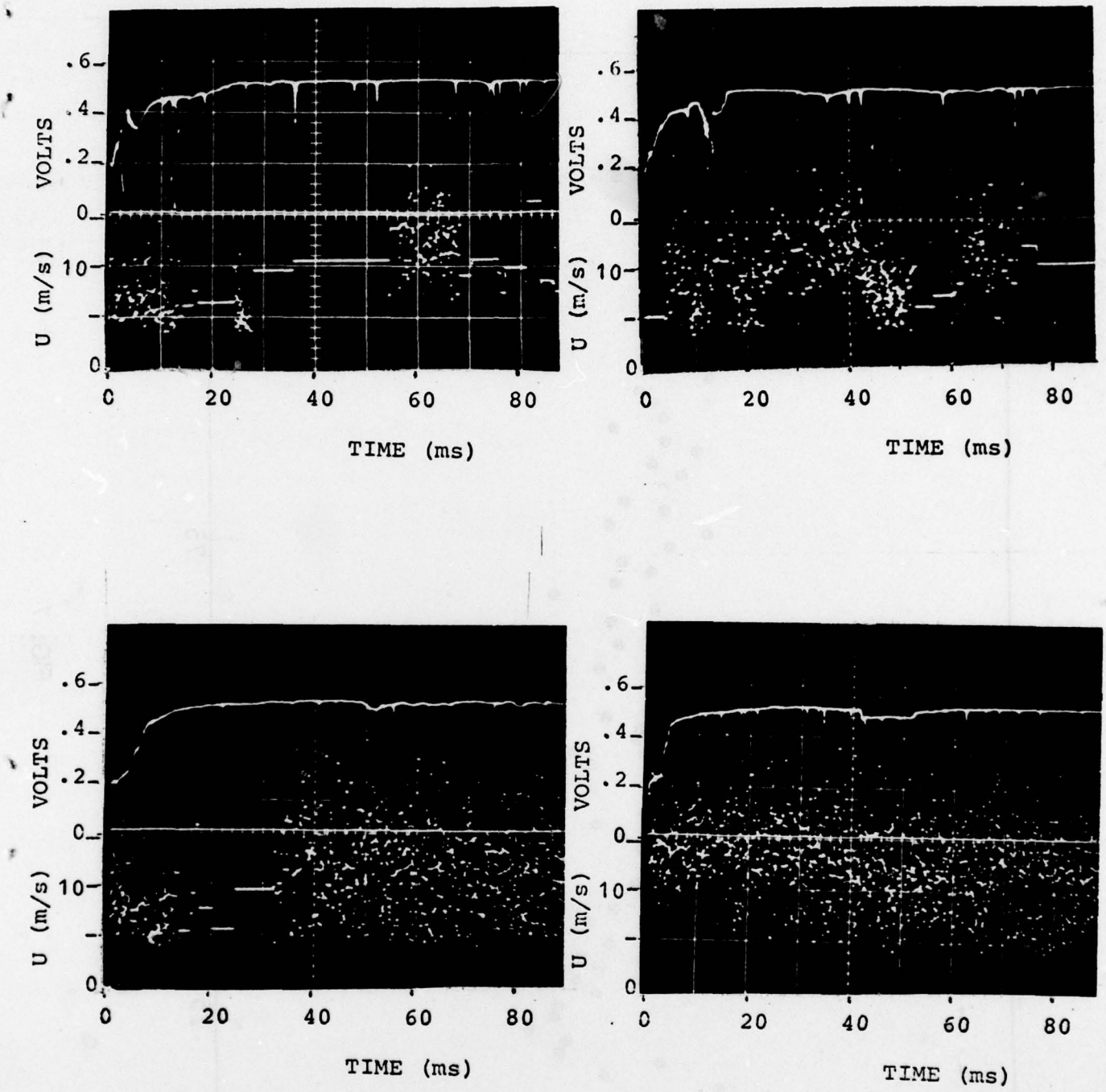

FIG. 6

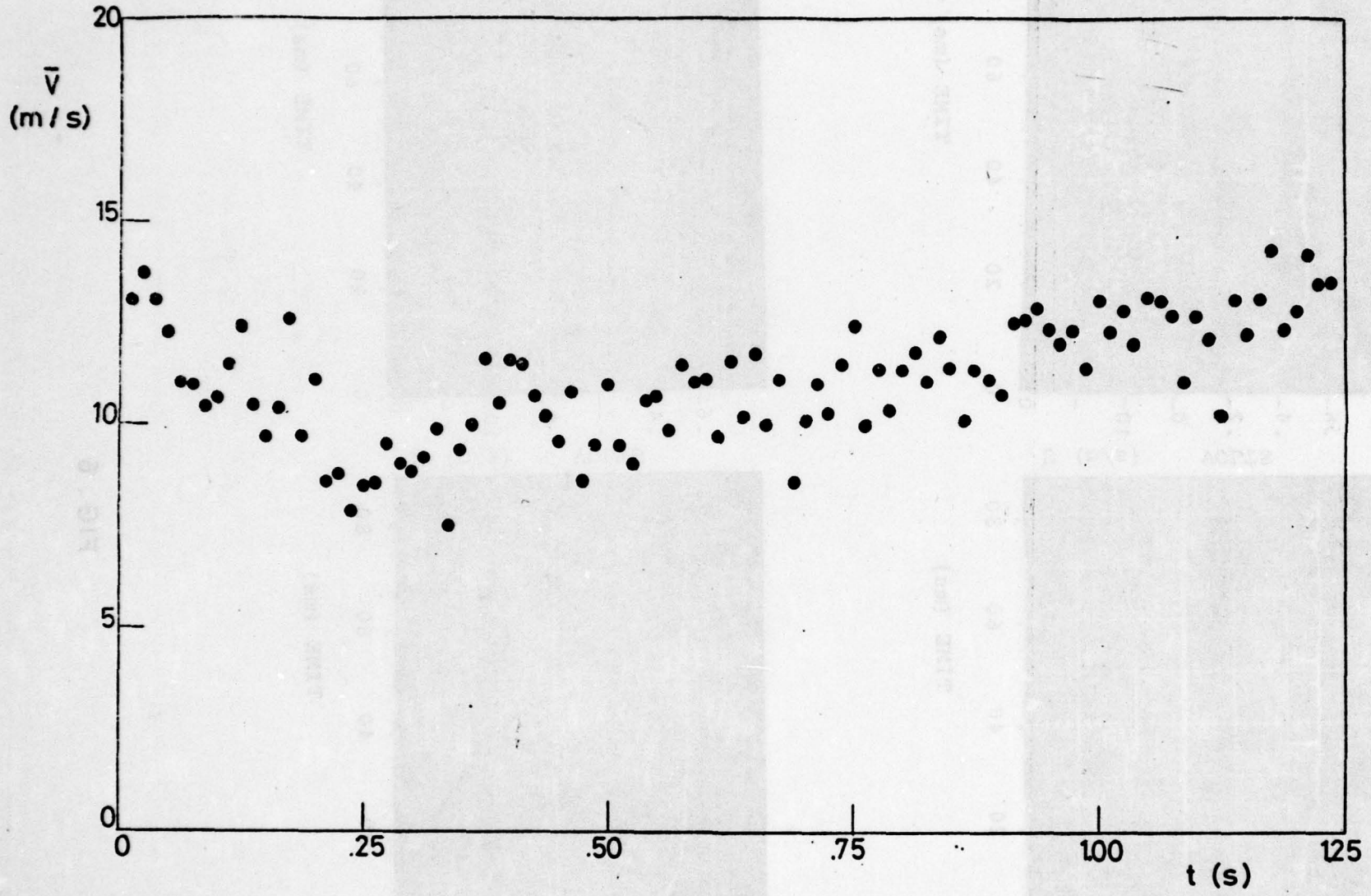

FIG. 7

CHAPTER 4

CONCLUSIONS AND FUTURE WORK

Sec. 4.1 - CONCLUSIONS

Sec. 4.2 - FUTURE WORK.

Sec. 4.1 - CONCLUSIONS

A nonlinear stability analysis of solid propellant burning was carried out, within the framework of a thermal theory and for quasi-steady gas phase, allowing for finite size disturbances. This required an integral method in reducing the partial differential equation for the condensed phase heat feedback to an approximate ordinary differential equation. It is shown that a nonlinear algebraic function, called restoring function, can be defined that contains all basic properties of equilibrium and stability of burning solid propellants. This function does not depend on time, but only on the nature of the solid propellant (including its flame) and the operating conditions (pressure, ambient temperature, and energy exchange with surroundings). Analysis of the nonlinear algebraic restoring function reveals that two well defined burning regimes exist, each limited by stability boundaries: the static and the dynamic regimes. Of these two, the region of dynamic burning is wider, in that under dynamic conditions a propellant may pass through a region which is statically unstable but dynamically stable.

The static regime can be observed experimentally and therefore can be studied also in the framework of Zeldovich approach. Static stability boundaries are defined as the lines of separation between regions where stable steady state solutions are allowed and regions where only unstable or no steady solutions are found. For usual propellants, only a lower (burning rate of the order of 0.1 cm/s or less) static stability boundary is found. For propellants with large surface heat release, lower and upper (burning rate of the order of 1 cm/s or more) static stability boundaries are found. Between these two static stability boundaries, the stable steady solution is either stationary or self-sustained oscillating. Several methods are suggested as to the determination of the static stability boundaries.

The dynamic regime cannot be observed experimentally in a stationary mode and can only be studied in the framework of a flame model. The lower dynamic stability boundary is defined as that ultimate burning condition beyond which extinction necessarily follows during a burning transient. The upper dynamic stability boundary implies vigorous accelerations of the combustion wave, possibly followed by dynamic extinction. For usual propellants only the former is found; for propellants with large surface heat release the latter is also found.

It is shown that the lower dynamic stability boundary holds true both for deradiation and depressurization, for opaque as well as transparent condensed phase, for fast deceleration of the combustion wave (e.g., by depressurization) as well as for fast acceleration (e.g., by pressurization) if an excessively large burning rate overshoot is attained. The lower dynamic stability boundary was determined as an asymptotic (in time) boundary for monotonically decreasing external

controlling parameters. If no change in time of the external controlling parameters occurs, the propellant is only subjected to random intrinsic disturbances and the static stability analysis apply. Moreover, if the effect of the time change of the external controlling parameters (nonautonomous function) is negligible compared to the restoring function, the lower dynamic stability boundary holds true for any time (even finite) and for any external law (even non monotonic or increasing).

MTS, KTSS nonlinearized and KTSS linearized unsteady flame models were implemented in this study. While KTSS linearized is of no value for burning rate less than about 90% of the steady state value, very reasonable and similar results are displayed by MTS and KTSS nonlinearized. However, MTS flame model is considered superior since it accounts also for chemical kinetics (but it requires two constants to be evaluated).

The order of the polynomial chosen to approximate the disturbance thermal profile in the condensed phase does not affect qualitatively the shape of the restoring function. A cubic law was found to give accurate predictions for pressures up to about 30 atm; a quadratic law seems more appropriate for larger pressures.

The validity of this nonlinear stability theory was verified by computer simulated transients. In general, excellent agreement was found between the analytical predictions and the numerical results obtained by integration of the governing partial differential equation. Numerical values are given only for a particular, ammonium percholorate based, composite propellant. It is felt, however, that all analyses were conducted from a broad point of view and, therefore, the conceptual findings may be extended to other types of solid propellants, provided a proper flame model is employed.

In conclusion, nonlinear propellant burning instability can be immediately defined from the knowledge of the associated restoring function. This a property strictly dependent on the nature of the propellant and the operating conditions.

Experimental work is in progress. Three different solid propellants are being characterized: an ammonium perchlorate based composite, a catalyzed double - base, and a noncatalyzed double - base. Steady state burning rates were measured in a strand burner; thermal profiles in the condensed phase and radiative emissions are being detected; high speed movies are being taken. Depressurization and pressurizations tests are being conducted respectively in a specifically designed strand burner and in a properly modified shock tube. Laser doppler anemometry is being applied to burning propellants in order to be able to measure the gas velocity in the plume of the sample.

Sec. 4.2 - FUTURE WORK

Other unsteady flame models will be investigated, in particular the Kooker-Zinn model proposed in 1974. Results similar to those obtained with the KTSS linearized flame model are expected. Further improvements of the analytical technique used to reduce the governing partial differential equation into an approximately equivalent ordinary differential equation will be sought. Extension of the proposed stability theory to the ignition problem will be continued; attempts made so far were inconclusive. Extension of both, stability theory and computer simulated tests, in the high pressure range (above 40 atm) and in the low pressure range (below 5 atm) will be done. Very likely, the subatmospheric pressure range will require a careful choice of the flame model, including its steady state aspects. Studies on the self - sustained oscillating regime will be pursued.

Experimentally, data on combustion vs extinction will be furnished both from a specially designed strand burner and a properly modified shock tube. This should allow at least a qualitative comparison between predicted and experimentally observed dynamic stability boundaries. Better data are expected from the laser doppler velocimetry apparatus.